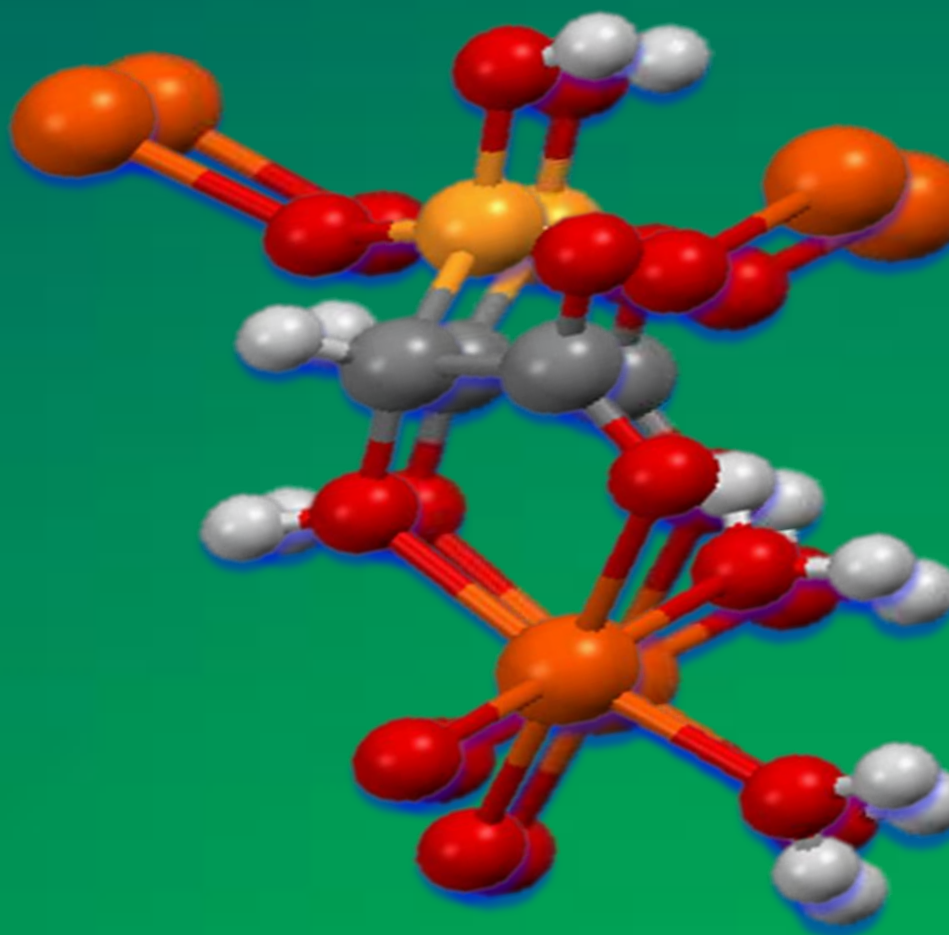# Multifunctional metal phosphonate frameworks for proton conductivity and photocatalysis

European PhD Thesis

Antonia Montserrat Bazaga García
Málaga, 2015

UNIVERSIDAD
DE MÁLAGA

Facultad de Ciencias

Departamento de Química Inorgánica, Cristalografía y Mineralogía

TESIS DOCTORAL

"MULTIFUNCTIONAL METAL PHOSPHONATE FRAMEWORKS FOR PROTON CONDUCTIVITY AND PHOTOCATALYSIS"

Antonia Montserrat Bazaga García

Málaga, 2015

MULTIFUNCTIONAL METAL PHOSPHONATE FRAMEWORKS FOR PROTON CONDUCTIVITY AND PHOTOCATALYSIS

Memoria presentada por la Ingeniera Química Dª Antonia Montserrat Bazaga García para optar al grado de Doctora en Ciencias con mención de **"Doctorado Europeo"** por la Universidad de Málaga

Fdo: Antonia Montserrat Bazaga García

Los Directores:

Fdo:

Dr. Aurelio Cabeza Díaz
Profesor Titular de la Universidad
de Málaga

Fdo:

Dr. Pascual Olivera Pastor
Profesor Titular de la Universidad
de Málaga

Fdo:

Dr. Miguel Ángel García Aranda
Catedrático de la Universidad de Málaga

Dr. Aurelio Cabeza Díaz, Profesor Titular de Química Inorgánica, **Dr. Pascual Olivera Pastor**, Profesor Titular de Química Inorgánica y **Dr. Miguel Ángel García Aranda**, Catedrático de Química Inorgánica, todos pertenecientes al Departamento de Química Inorgánica, Cristalografía y Mineralogía de la Facultad de Ciencias de la Universidad de Málaga.

CERTIFICAN:

Que la presente memoria titulada "Multifunctional metal phosphonate framewoks for proton conductivity and photocatalysis", ha sido realizado bajo nuestra dirección en el Departamento de Química Inorgánica, Cristalografía y Mineralogía de la Universidad de Málaga por la Ingeniera Química Dª. Antonia Montserrat Bazaga García. Este trabajo reúne, a nuestro juicio, contenido científico suficiente y las condiciones necesarias para ser presentado y defendido ante el tribunal correspondiente para optar al grado de Doctora. Los resultados de este trabajo han sido publicados en revistas internacionales de medio/alto índice de impacto, lo que avala la presentación de la tesis en formato de compendio de publicaciones, no habiendo sido ninguna de ellas utilizadas en tesis anteriores.

Málaga, a 29 de Junio de 2015

Fdo:

Dr. Aurelio Cabeza Díaz
Profesor Titular de la Universidad
de Málaga

Fdo:

Dr. Pascual Olivera Pastor
Profesor Titular de la Universidad
de Málaga

Fdo:

Dr. Miguel Ángel García Aranda
Catedrático de la Universidad de Málaga

Publicaciones y
Divulgación Científica

UNIVERSIDAD
DE MÁLAGA

Dr. Pedro Jesús Maireles Torres, Catedrático de la Universidad de Málaga y Director del Departamento de Química Inorgánica, Cristalografía y Mineralogía de la Facultad de Ciencias de la Universidad de Málaga.

INFORMA:

Que la presente memoria realizada por Dª Antonia Montserrat Bazaga García, titulada: "Multifunctional metal phosphonate framewoks for proton conductivity and photocatalysis", ha sido realizada bajo la dirección del profesor Dr. Aurelio Cabeza Díaz, el profesor Dr. Pascual Olivera Pastor y el Catedrático Dr. Miguel Ángel García Aranda en el Departamento de Química Inorgánica, Cristalografía y Mineralogía de la Facultad de Ciencias de la Universidad de Málaga. Este trabajo constituye la Memoria de Tesis Doctoral de la interesada, cuya presentación autorizo.

Málaga, a 29 de Junio de 2015

Fdo:

Dr. Pedro Jesús Maireles Torres
Catedrático de la Universidad de Málaga

AGRADECIMIENTOS

Llegado este momento, es un poco difícil resumir en unas pocas líneas los nombres de profesores y compañeros con los que he podido compartir tantos buenos momentos a lo largo de todos estos años.

En primer lugar, agradecer a mis directores de tesis, Dr. *Aurelio Cabeza Díaz*, Dr. *Pascual Olivera Pastor* y Dr. *Miguel Ángel García Aranda*, la oportunidad ofrecida, todo el tiempo dedicado y conocimiento transmitido, sin los cuales, no habría podido realizar esta tesis. Agradecer especialmente a *Pascual*, por acordarse de mí para formar parte del grupo de investigación, y a *Aurelio* por dedicarme tantas horas a mejorar mis conocimientos de los fosfonatos metálicos dentro de ese gran mundo que son los MOFs.

En segundo lugar, quiero agradecer la ayuda económica recibida a través de la Beca de Formación del Personal Investigador *BES-2011-044563* del Ministerio de Ciencia e Innovación de España.

Quiero dedicarle una parte de los agradecimientos al Dr. *Enrique Ramírez Losilla*, sin su ayuda y paciencia yo no habría podido realizar gran parte de los estudios de impedancia que forman parte de la tesis que aquí presento. Agradecerle tanto como me ha enseñado y lo que sé que ha callado, así como que me mostrase el mundo de los conductores protónicos

Agradecer también a la Dr^a. *Rosario M. Pérez Colodrero*, por haber sido "mi profe" con las síntesis y los ajustes de Rietveld. Por todas esas horas poniendo síntesis sin parar y esos buenos momentos vividos en los viajes a ALBA. Así como a *Laura*, por animarme y ayudarme en el manejo de los equipos de difracción, y siempre con una sonrisa.

Quiero agradecer al resto de profesores del departamento, por toda vuestra ayuda a lo largo de todos estos años. Especialmente a *Maribel*, *Ramón*, *Pepa* y *Laureano* por esas horas de prácticas inolvidables. También agradecer a *David* por ayudarme con los equipos de impedancia y enseñarme una nueva palabra "truño". Así como agradecer al profesor *Miguel Hernández*, por permitirme utilizar el equipo de medida del TOC *(mi rojillo)*.

También quiero expresar mi agradecimiento al *Prof. Norbert Stock* por aceptarme en su amplio equipo y por todo lo aprendido durante mi estancia en la Universidad Christian-Albrechts de Kiel (Alemania), y mostrarme la forma alemana de festejar una lectura de tesis.

A todos mis compañeros de despacho/english room, por tantos buenos momentos compartidos dentro y fuera de esas cuatro paredes. A *Lucía* y *Mercedes* por cuidar de nosotros con tan maravillosos platos cocinados (son mis MasterChef malagueñas). A *Mª José* (habichuelita I y II), *Ana*, *Marta*, *Gema*, *Diana*, *José, José Compaña*, y *María del Mar* por vuestra amistad y esas partidas de bolos en las que no conseguí ganar nunca. A los compañeros de

catálisis, *Juanmi, Juan*, *Enrique*, *Cristina*, *Mª José* . . . por esos momentos compartidos tanto en el despacho como en los laboratorios.

Y por último y con permiso de todos, los agradecimientos más grandes van destinados a las tres personas que siempre han estado a mi lado, en los buenos y malos momentos, por vuestro cariño y por estar ahí animándome a seguir siempre hacia delante. Papi, mami y Ana, gracias, muchísimas gracias.

A mis padres y hermana

CONTENTS

Publicaciones y
Divulgación Científica

ma

UNIVERSIDAD
DE MÁLAGA

Publicaciones y
Divulgación Científica

ma
UNIVERSIDAD
DE MÁLAGA

CHAPTER 1
INTRODUCTION

1.   INTRODUCTION.

1.1. COORDINATION POLYMERS, COORDINATION NETWORKS AND METAL-ORGANIC FRAMEWORKS.

Coordination polymers (CPs) and metal–organic frameworks (MOFs) are recognized to be among the most prolific research areas of inorganic chemistry and crystal engineering in the last 20 years *(Batten et al., 2012).* However, fast growing of the field and the diversity in scientific basis of the researchers involved have brought about a puzzling terminology and unclear definitions for this class of compounds. Thus, the IUPAC division of Inorganic Chemistry initiated the project on Coordination polymers and metal–organic frameworks: terminology and nomenclature guidelines.

According to the IUPAC 2013 Recommendations *(Batten et al., 2013)* the following definitions were endorsed:

- *Coordination Polymer (CP)*: "A coordination compound with repeating coordination entities extending in 1, 2 or 3 dimensions."

- *Coordination Network (CN)*: "A coordination compound extending, through repeating coordination entities, in 1 dimension, but with cross-links between two or more individual chains, loops or spiro-links, or a coordination compound extending through repeating coordination entities in 2 or 3 dimensions."

- *Metal-Organic Framework (MOF)*: "A Metal-Organic Framework is a Coordination Network with organic ligands containing potential voids." Metal–organic frameworks are thus considered a subclass of

coordination network solids, which in turn is a subclass of coordination polymer, see Figure 1.1.

In addition, the use of topology descriptors has been strongly encouraged for naming the solids *(Öhrström, 2015).*
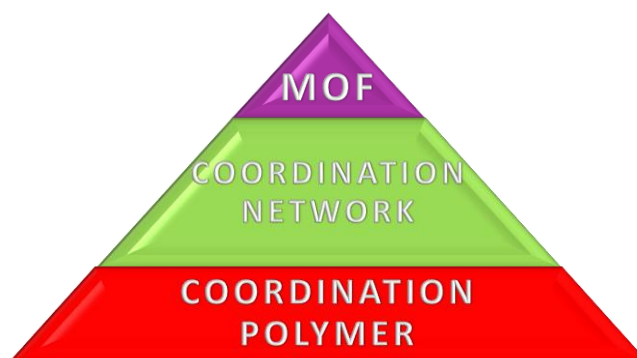
Figure 1.1. From coordination polymers class to metal organic frameworks (MOF) subclass.

It follows, from the above definitions, that the term CPs encompasses a great diversity of chemical structures, many of which possess attractive properties for potential applications in different fields. The main interest of these materials lies in the possibility of tailoring chemical and physical properties through synthetic and structural studies, which allows establishing straightforward relationships between structure and properties. This valuable knowledge may then be used to design materials for specific purposes. *(Sanchez et al., 2005; Wang et al., 2014a; Li and Xu, 2013)*

1.1.1. METAL ORGANIC FRAMEWORKS (MOFs).

MOFs are Coordination Networks formed by metal ions or metal clusters connected via organic ligands *(Kitagawa et al., 2004; Férey, 2008 and Furukawa et al., 2013).* These compounds are crystalline materials, with proven porosity in many cases. Generally, the organic units (known as linkers or bridging-ligands) are di-, tri- or tetradentate organic ligands *(Yaghi et al., 1995 and Férey, 2008)* such as carboxylates or other organic anions as phosphonate, sulfonate, and heterocyclic compounds *(Lu et al., 2014).*

MOFs have proved to give versatile performances in different research fields since, in the early 90's, Robson *(Abrahams et al., 1994)* and Moore *(Wu et al., 1992)* pointed out the possibility of using polydentate ligands coordinated to metals for the design of frameworks with specific geometries *(Rosseinsky, 2004).* This is due to the fact that they can be made porous, have large surface areas and tunable pore sizes and topologies.

The permanent porosity is a feature especially desired for MOFs because from it derives most of its applications. They can present isolated cavities, one-dimensional channels, two-dimensional space and interconnected channels. They usually have homogeneous microporosity with pores of different shapes and well defined structure. Compared to 1st generation of porous materials, whose structure collapses by removing molecules lodged in their cavities, MOFs tend to have robust structures, stable and constant porosity (2nd generation of porous composite), or flexible and dynamic porous frameworks responsive to external stimuli (3rd generation of porous materials) *(Fletcher et al., 2005; Kitagawa et al., 2004; Horike, et al., 2009).* Due to these features, Porous Coordination Polymers (PCPs) can be

categorized into robust and flexible classes on the basis of the structural transformation ability *(Bureekaew et al., 2008)*:

a) <u>*Robust PCPs*</u> do not show any structural transformations upon applying external stimuli, e.g. guest molecule, heat, or magnetic or electric field. High porosity and high surface area, together with permanent pore size and pore shape, are the key properties of robust MOFs for gas storage application.

b) <u>*Flexible PCPs*</u> respond to external stimuli by reversible structural transformation (rotation of bridging ligands, shape-responsive fitting or Interdigitate and interpenetrate). Generally, guest molecules act as the stimuli for the transformation of flexible MOFs, and the guest-induced distortion phenomena can be classified into the following categories:

   i. *Guest induced crystal-to-amorphous transformation.* After the removal of guest molecules, these MOFs collapse and become amorphous. However, crystallinity is regained under restoring the initial conditions.

   ii. *Guest induced crystal-to-crystal transformation.* Frameworks of MOFs in this category are transformed to other networks with the retention of crystallinity, after the removal or exchange of guest molecules.

The structural versatility and porosity are the main characteristics of MOFs, which give rise to their most important properties and applications. Thus, structural versatility is of great importance for gas

purification and separation (*Schröder, 2010; Farruseng, 2011; Li et al., 2012)*, as well as for the storage of gases such as H_2 *(Suh et al., 2012)*, CO_2 and CH_4 *(Jiang and Xu, 2011; Sumida et al., 2012)*. In addition, the presence in the framework of lanthanides or transition metals has allowed extending the use of MOFs as catalysts *(Schröder, 2010; Farruseng, 2011; Gu et al., 2014).* It is also worth mentioning the applications related to other physical properties such as: magnetism *(Mondal et al., 2014; Lago et al., 2013*), electronic sensors *(Liu et al., 2014; Kreno et al., 2012; Manos et al., 2012; Wang et al., 2014b)*, etc. A great deal of attention has been given to proton conductivity, more specifically to the possible role of MOFs materials as electrolytes in fuel cells *(Li and Xu, 2013; Ramaswamy et al., 2014).* Recently, MOFs have also been recognized as promising materials for liquid-phase adsorption of various hazardous compounds from aqueous media *(Wang et al., 2014a; Hasan and Jhung, 2015).*

1.1.2. METAL PHOSPHONATES.

In metal phosphonates, the ligands can be described as derivatives of the phosphate ion, PO_4^{3-}, in which a P-O bond has been replaced by a P-R bond. R is an organic group that can be either, aliphatic or aromatic, and may have other function groups such as carboxylates, sulfonates, hydroxyl, amino, etc., *(Alberti et al., 1992a and 1992b; Burwell and Thompson, 1991; Dines and DiGiacomo, 1981)*. The $-PO_3^{2-}$ moiety bonded to the metal is the inorganic fraction of the material and it allows the formation of an inorganic lattice that links to the R group, which provides the characteristic properties of the organic fraction.

Due to thermal and chemical stability of the M-O-P bonds and the capacity of these ligands to bond with a large number of mono-, di-, tri-, tetra-, penta- and hexavalent metals, phosphonic groups are very interesting as building blocks for the design of new coordination network-constituted materials. Moreover, the synthetic chemistry of phosphonates is well developed, so phosphonic acids can be obtained with the desired characteristics by meaning of simple and well-known reactions. Under the mild synthesis conditions employed, the function of the organic molecule remains in the final product, which allows obtaining new materials with a great structural diversity and properties as a result of the interplay of their components *(Forster and Cheetham, 2003)*. Furthermore, the synthesis of metal phosphonate materials can be carried out via a number of different routes that do not necessarily give products with the same structure, which means a greater potential of structural diversity in the resulting products *(Demadis et al., 2009c)*.

In addition to the metals and phosphonic acids used as precursors in the preparation of these materials, the synthesis conditions are also of great importance. Structural and chemical properties of metal phosphonates are variable depending on many synthetic parameters such as phosphonate source, metal source, metal/P ratio, solvent, concentration, pH, and reaction temperature *(Maeda, 2004)*.

Molecular complexes, linear structures (1D), layered (2D) and three-dimensional (3D), both extended and open structures (open-framework) have been obtained. The predominant layer nature was explained by the tendency to segregate a metal oxide network from the organic linkers *(Clearfield, 1998; Rao and Vidyasagar, 2005)*. The interest in metal phosphonates is due to the large number of applications that can be developed and which have been recently reviewed in the books "Metal Phosphonate Chemistry: from synthesis to applications"

(Clearfield and Demadis, 2012) and "Tailored Organic-Inorganic Materials" *(Brunet et al., 2015).*

1.1.2.1. MULTIFUNCTIONAL METAL PHOSPHONATES.

The integration of the inorganic phosphonate (CPO_3^{2-}) group and numerous rigid or flexible organic functional moieties within the same composite would, therefore, be expected to result in a variety of organic–inorganic architectures with adjustable properties *(Li et al., 2007b).* Along this line, the use of bifunctional or multifunctional anionic units, such as diphosphonates, aminophosphonates or phosphonocarboxylates has led to a number of materials with microporous or open-framework structures *(Li et al., 2008).* Nevertheless, in some cases, the functional groups participate in the coordination to metal ions by using part or all of their binding sites at the cost of their functionalities *(Cao et al., 2005).*

The introduction of porosity into the metal phosphonates has been a major synthetic target. Although no general method has been found *(Kaempfe and Stock, 2008; Wang et al., 2011)*, the use of multifunctional phosphonic acids has led to a rich variety of open framework structures *(Maeda, 2004; Zhang et al., 2008; Clearfield and Demadis, 2012).*

The next sections will show the role of different functional groups in configuration of metal phosphonate frameworks. To do that, metal phosphonates containing additional groups attached to the phosphonate moiety, such as carboxylate, amine, etc., are classified

according to the number of phosphonate groups present and organized by increasing complexity.

1.1.2.2. METAL CARBOXYPHOSPHONATES AND AMINOPHOSPHONATES.

Phosphonic acids with additional carboxylic functional groups, such as $HOOC–R–PO_3H_2$, $HOOC–RN–(CH_2PO_3H_2)_2$ or $HOOC–RNHCH_2PO_3H_2$ (R represents an organic group), have been selected as ligands for the synthesis of open-framework and/or porous materials because these linkers can adopt various coordination modes under different reaction conditions *(Zhang et al., 2009).*

The chelating ability of the carboxylic and phosphonic groups respect to the metal may be conveniently modified. Thereby, syntheses at low pH values may yield the carboxylic group protonated meanwhile at higher pH values, both groups may be deprotonated and bonded to the metal. Furthermore, the variation of this parameter may favor the incorporation of hydroxyl groups and even the alteration of the metal/organic molar ratio in the resulting compounds. Rational design of the synthesis of metal carboxyphosphonates is, however, not an easy task because of a large number of experimental factors that must be precisely controlled: temperature, pH of the starting mixture, concentration, metal/acid molar ratio, reaction time, presence, if required, of organic templates, etc. Once, a crystalline compound is formed, the length of the organic chain is another key parameter to define the structural framework.

The carboxyethylphosphonate ions act as bridging as well as chelating ligands, but the chelation mode may differ depending on the number of carbon atoms in the ligand. The structural variety of these

metal carboxyphosphonates ranges from 1D networks to 3D open-frameworks, the most common architectures being, however, layered and pillared layered structures. The diverse synthesis methodologies employed, structures and main applications of metal carboxyphosphonates have been reviewed *(Cabeza and Aranda, 2012)*.

Among the numerous carboxyphosphonic acids the racemic ligands *R,S*-2-hydroxyphophonoacetic acid [$H_2O_3PCH(OH)CO_2H$] (HPAA) is prominent *(Dong et al., 2007)*, because it is a simple low molecular weight acid bearing three different coordination groups (-OH, -COOH and -PO_3H_2). This acid is also chemically stable, inexpensive and safe to use, with demonstrated applications as corrosion inhibitor *(Demadis et al., 2008)*. Moreover, the presence of a chiral carbon in its backbone opens the possibility to synthesize no centrosymmetric metal-organic coordination polymers for possible nonlinear optical applications *(Fu et al., 2005b)*.

Generally, reactions of hydrated metal salts with HPAA, at low pH and room temperature yield low dimensionality solids, whereas hydrothermal reactions result in 2D *(Fu et al., 2005b)* or 3D frameworks *(Colodrero et al., 2010 and Demadis et al., 2010a and 2010b)*.

One-dimensional (1D), two-dimensional (2D), and three-dimensional (3D), materials containing the HPAA ligand have been reported *(Demadis et al., 2010a; Li et al., 2007a; Zhang et al., 2007; Sun et al., 2006 and 2007; Zhu et al., 2009)*. In the basic building unit of 1D solids, [$M(II)(HO_3PCH(OH)CO_2)(H_2O)_2 \cdot 2H_2O$] (M=Mg, Co, and Zn) *(Colodrero et al., 2010)*, the M^{2+} cations are located in a distorted octahedral environment formed by two chelating bidentate HPAA^{2-} ligands, an monodentate carboxylate, a hydroxyl group, and two water

molecules. These results in infinite zigzag chains which run parallel to the *a*-axis (Figure 1.2).
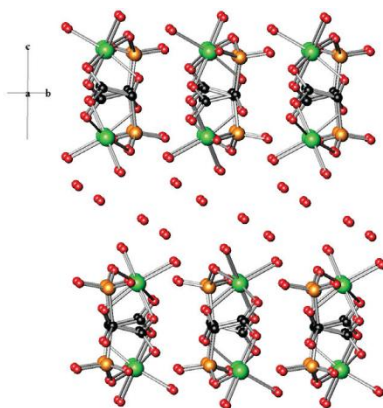

Figure 1.2. 1D chain arrangement (viewed down *a*-axis) of [M{HO$_3$PCH(OH)CO$_2$}(H$_2$O)$_2$]·2H$_2$O (M=Mg, Co, Zn). Adapted from reference *(Colodrero et al., 2010).*

On the other hand, hydrothermal reactions at 140-180 ºC usually lead to higher dimensionality compounds. For instance, the isostructural series [M(II)(HO$_3$PCH(OH)CO$_2$)(H$_2$O)$_2$] (M(II)=Mn, Fe, Co, and Zn), with layered structure *(Fu et al. 2005a)*. The crystal structures of these solids are built by corner-shared [MO$_6$] octahedra and [CPO$_3$] tetrahedra wriggled chains, which are interlaced by carboxylate and hydroxyl groups into a wavelike layer structure.

In Fe(HO$_3$PCH(OH)COO)·2H$_2$O (FeHPAA), the asymmetric unit includes one Fe^{2+} cation, one doubly deprotonated HPAA^{2-} anion, and two coordinated water molecules (see Figure 1.3.a). The doubly deprotonated HPAA^{2-} anion is chelated to the Fe^{2+} ion through one carboxylate oxygen atom and one hydroxyl oxygen atom with a very small bond angle. Each Fe^{2+} ion links three HPAA^{2-} anions and two water molecules through Fe-O covalent bonds. On the other hand, the

HPAA^{2-} anion connects three iron atoms, the carboxylate together with hydroxyl groups chelating one Fe^{2+} ion and the phosphonate group linking the other two Fe^{2+} centers. In addition, interaction through hydrogen bonds gives rise to a three dimensional arrangement of layers (see Figure 1.3b) *(Fu et al. 2005a)*.

(a)   **(b)**
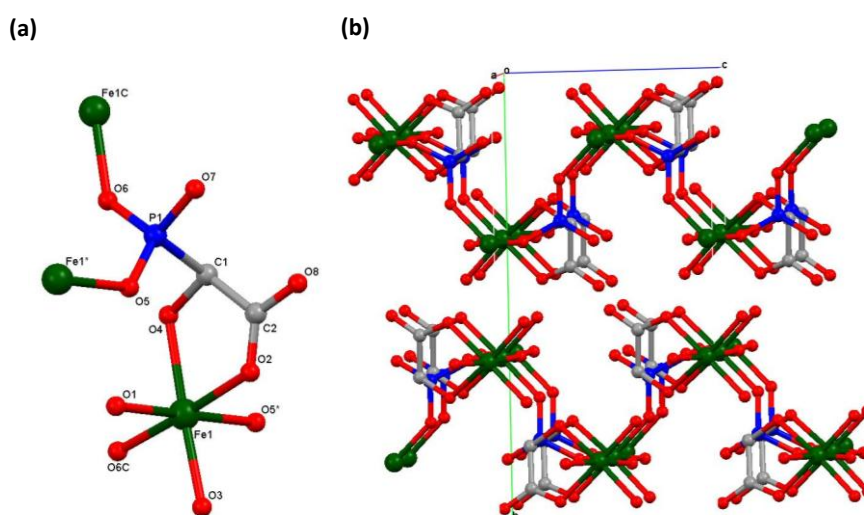
Figure 1.3. Crystal structure views of [Fe{HO$_3$PCH(OH)CO$_2$}(H$_2$O)$_2$] showing (a) the metal to ligand coordination mode; (b) crystal packing showing the layers along the a axis. Adapted from reference (*Fu et al., 2005a).*

Different calcium derivatives have been reported by using variable synthesis conditions [Ca$_3$(O$_3$PCHOHCO$_2$)$_2$·14H$_2$O (0D), Ca(HO$_3$PCHOHCO$_2$)·3H$_2$O (2D), Ca$_5$(O$_3$PCHOHCO$_2$)$_2$(HO$_3$P-CHOHCO$_2$)$_2$·6H$_2$O (3D), CaLi(O$_3$PCHOHCO$_2$) (3D) and Ca$_2$Na(O$_3$PCHOHCO$_2$) (HO$_3$PCHOHCO$_2$)·1.5H$_2$O (2D)] *(Colodrero et al., 2011)*. The compounds 2D, Ca(HO$_3$PCHOHCO$_2$)·3H$_2$O, and 3D, Ca$_5$(O$_3$PCHOHCO$_2$)$_2$(HO$_3$P-CHOHCO$_2$)$_2$.6H$_2$O, are formed by interaction of anionic monomeric species with cationic trimeric bricks, that result from protonation of the molecular cluster depicted in Figure

1.4. In addition, denser modified networks are formed by the presence of small alkali cations, Li$^+$ and Na$^+$ in the structure.
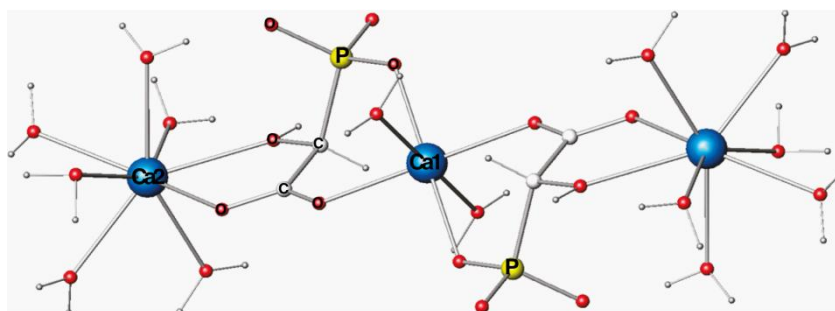

Figure 1.4. Ball-stick representation of Ca$_3$(O$_3$PCH(OH)COO)$_2$·14H$_2$O trimer, showing the five- and six-membered rings. Reprinted with permission from (Colodrero et al., *Cryst. Growth Des.*, **2011**, *11*, 1713–1722). Copyright (**2011**) American Chemical Society.

Zn^{2+}, Co^{2+} and Ba^{2+} derivatives having complex networks were obtained by extending the system M^{2+}/HPAA to mixed solutions containing both, secondary ligands and two different metal salts *(Fu et al., 2011)*. The appearance of new coordination modes reveals a high adaptability of this ligand in different frameworks, what offers great chances of tuning material properties.

A number of M'(I)M(II)HPAA frameworks have also been reported. In them, additional organic or inorganic metal ions, present in the reaction media, are also incorporated to the frameworks for charge balance, giving 3D bimetallic structures. It is noteworthy to mention the large diversity in structural architectures found for these bimetallic compounds. Some examples of these compounds are [(NH$_4$)Zn{O$_3$PCH(OH)CO$_2$}] *(Fu et al., 2005b)* or [Na$_2$Cd$_2${O$_3$PCH(OH)CO$_2$}$_2$(H$_2$O)$_3$]·2H$_2$O *(Sun et al., 2007)* where the hydrated Na$^+$ ions, instead of H$^+$, are used to compensate the negatively charged layers.

Colodrero et al., 2012c reported a family of functional 3D Ln-HPAA solids (Ln: La, Ce, Pr, Sm, Eu, Gd, Tb, and Dy) prepared by slow crystallization at ambient conditions, which means that large metal ions favor higher dimensionality with this ligand. This simple procedure is in clear contrast with other preparations using smaller metal ions, that usually requires hydrothermal or solvothermal conditions *(Stock and Biswas, 2012).* Two polymorph series of Ln-HPAA compounds, with formula $Ln_3(H_{0.75}O_3PCHOHCOO)_4 \cdot xH_2O$ (x=15−16), were synthesized. Three-dimensional open frameworks resulted from the linkage of similar organo-inorganic layers, in the *ac*-plane, by central lanthanide ions, which yield trimeric units also found in other metal-HPAA compounds (Figure 1.5). Ln-HPAA networks enclose water-filled 1D channels and undergo remarkable crystalline-to-amorphous-to-crystalline transformations upon dehydration and rehydration cycles *(Colodrero et al., 2012c).* Both polymorphic forms showed proton conductivity at room temperature, with a gadolinium polymorph being highest proton conductor, while a europium derivative exhibited the best photo-luminescent properties, which are strongly dependent on dehydration-rehydration processes *(Colodrero et al., 2012c).*
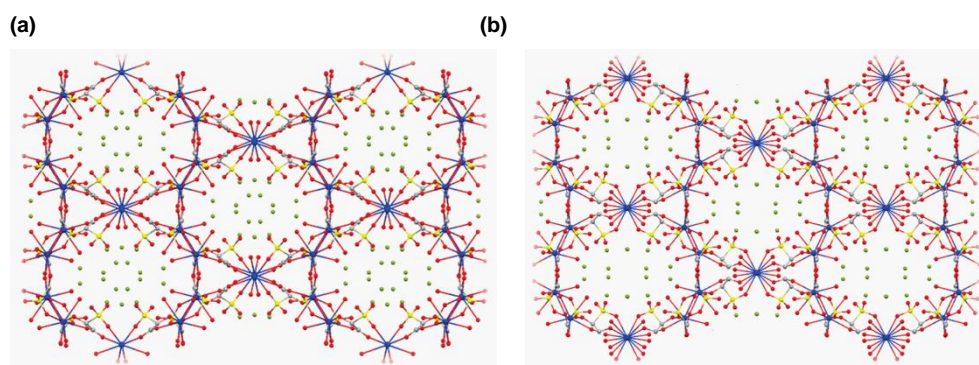
(a)   **(b)**

Figure 1.5. *c*-axis view *b*-axis horizontal of the crystal structures for $Ln_3(H_{0.75}O_3PCHOHCOO)_4 \cdot xH_2O$ hybrids showing the 1D channels along the *c*-axis filled with

lattice waters for (a) $Gd_3(H_{0.75}O_3PCHOHCOO)_4 \cdot 16H_2O$ GdHPA-II (series-II) and (b) $Ce_3(H_{0.75}O_3PCHOHCOO)_4 \cdot 15H_2O$ CeHPA-I (series-I). The lattice water molecules occupying the channels are highlighted in green. Reprinted with permission from (Colodrero et al., *Chem. Mater*, **2012**, *24*, 3780-3792). Copyright (**2012**) American Chemical Society.

Li et al. obtained 2D layered and 3D pillared-layered zinc compounds based on 5-(phosphonomethyl)-isophthalic acid, 1,3-$((HO_2C)_2C_6H_5CH_2PO_3H_2$) (5-pmipH$_4$) by hydrothermal reaction. This ligand has a flexible phosphonate group at the fifth position of the isophthalic acid. *(Li et al., 2015)*.

Amino derivatives of phosphonate ligands provide additional connectivity to metal ions. So, the amino group in aminophosphonates materials can play two roles: be only protonated or directly coordinated to metal ions, acting as a donor site *(Cao et al, 2005)*. Furthermore, the presence of nitrogen donors provides other coordination capabilities.

N-(phosphonomethyl)iminodiacetic acid, $(HO_2CCH_2)_2N$-$CH_2PO_3H_2$ (H$_4$PMIDA) is a clear exponent of the variability in coordination modes under different reaction conditions. The structures of the corresponding aminophosphonates depend on the extent of deprotonation of the ligand as well as on the nature of the metal ions. Under acidic conditions, only the phosphonic group is coordinated to the metal ions and -COO$^-$ groups and N are only involved in hydrogen bonding. Consequently, the compounds tend to display low dimensionality. However, when the solution is less acidic the chelation coordination mode is adopted and the metal ions have an affinity for the nitrogen atom as is displayed in Figure 1.6. So, high-symmetry 3D structures result of combining large coordination numbers of metal ions and high connectivity of the ligand. *(Cabeza et al., 2015).*
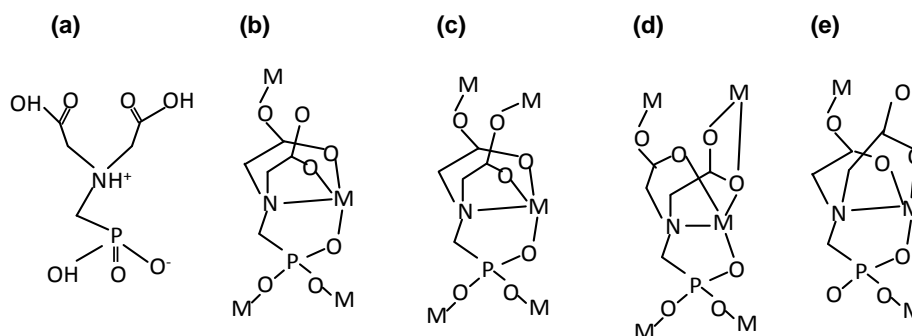
(a)   **(b)**   **(c)**   **(d)**   **(e)**

Figure 1.6. (a) Ligand (HO$_2$CCH$_2$)$_2$NCH$_2$PO$_3$H$_2$ (H$_4$PMIDA) and the various coordination modes in 2D [Co(II) (b) and Zn (II) (c)] and 3D [Pb(II) (d) and Ln(III) (e)] networks. Adapted from reference (Cabeza et al., in *Tailored Organic-Inorganic Materials*, 2015, Chapter 4).

1.1.2.3. METAL POLYPHOSPHONATES.

Obtaining phosphonate-based open structures has been the leitmotiv of using flexible or rigid polyphosphonic acids that contain phosphonate moieties in divergent positions *(Gagnon et al., 2012; Clearfield and Demadis, 2012)*.

The combination of organo-diphosphonate ligands (H$_2$O$_3$P-R-PO$_3$H$_2$) with metal ions was expected to lead to three-dimensional structures with open frameworks and unique properties. Not only do these ligands form materials with progressively longer organic chains to expand the pore size or contain organic functional groups exposed to guest molecules within the pores, but they are also desirable in their pillared framework with clearly different organic and inorganic parts. Investigations of di-, tri-, and tetravalent metal phosphonates for several decades have yielded a wide structural diversity with interesting properties *(Clearfield and Demadis, 2012; Ramaswamy et al., 2014; Brunet et al., 2015)*.

Attfield et al. (2010 and 2012) have investigated the structural consequences of systematically increasing the length of the organic

alkylene group within a diphosphonic acid on the resulting structure of group 13 metal alkylenediphosphonates (aluminium and gallium). Thus, the series $Al_2[O_3PC_nH_{2n}PO_3](H_2O)_2F_2$ (n= 2-6) all of them contain identical inorganic components with isostructural corrugated inorganic Al-O-P layers whose stacking arrangement, either AAAAAA or ABABAB, depend upon the configuration and number of carbon atoms in the alkyl chains which are linking the inorganic layers *(Harvey et al., 2004a)*. In terms of structure design, it was apparent that pillared materials are formed when the alkylene chain length is greater than a methylene group and the separation of layers by these pillars increases in direct relation to the length of the organic linker. Also, as the alkylene chain increases the full condensation of all the P-O bonds of each -PO_3 group in the resulting materials appears less likely (see Figure 1.7), *(Attfield et al., 2010)*.
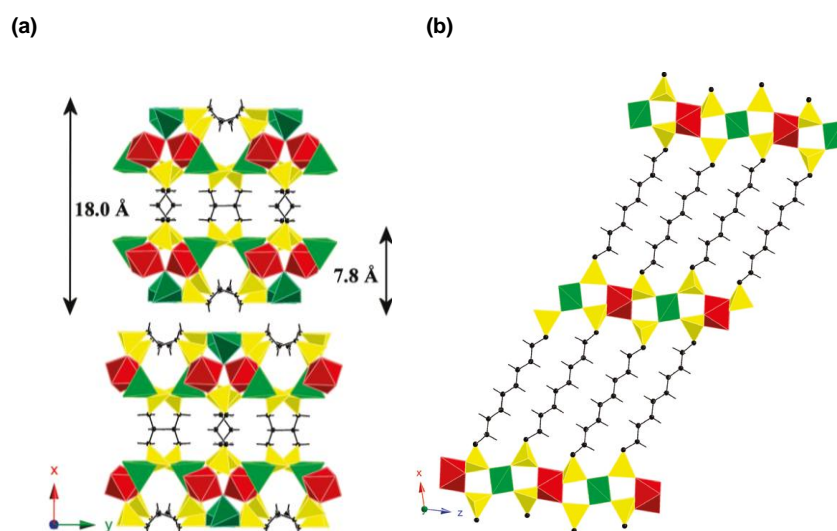
Figure 1.7. (a) A polyhedral/ball-and-stick representation of $Ga(HO)(O_3PC_3H_6PO_3)_2$ and (b) $Ga(HO_3PC_{10}H_{20}PO_3)$ viewed along the *c* axis and *b* axis, respectively. Reprinted with permission from (Attfield et al., *Inorg. Chem.*, 2010, *49*, 2656-2666). Copyright (2010) American Chemical Society.

A plethora of compounds of variable dimensionality has been reported with ligands containing amino bis-methylenphosphonic groups and the general formula: R-N(CH2PO3H2)2, with R = n-alkyl, carboxyalkyl, carboxyphenyl,…). Di- and tetravalent metal derivatives of R-N(CH$_2$PO$_3$H$_2$)$_2$ phosphonic acids show similar layered structures in which the organic pendants are located between the inorganic sheets with a herringbone interdigitated arrangement. This feature is often dependent on the steric hindrance, the length of the organic moieties attached to the amino diphosphonic group, and the hydrophobic/hydrophilic interactions that occur among them *(Clearfield and Demadis, 2012; Taddei et al., 2013)*.

Microporous three dimensional networks resulted when N,N'-piperazinebis(methylenephosphonic acid) (H$_2$O$_3$P-CH$_2$-NC$_4$H$_8$N-CH$_2$PO$_3$H$_2$) and its methyl analogue N,N'-2-methylpiperazinebis(methylenephosphonic acid) were reacted with divalent (Mn^{2+}, Fe^{2+}, Co^{2+}, Ni^{2+}) [M$_2$(H$_2$O)$_2$(O$_3$PCH$_2$N(C$_4$H$_8$)-NCH$_2$PO$_3$)·xH$_2$O, STA-12] (see Figure 1.8), *(Miller et al., 2008)* and [M$_2$(H$_2$O)$_2$(O$_3$PCH$_2$N(C$_4$H$_8$)$_2$NCH$_2$PO$_3$)·xH$_2$O, STA-16] (see Figure 1.9), *(Wharmby et al., 2011)*, trivalent (Al^{3+}, Ln^{3+}) [M(OH)(O$_3$PCH$_2$NHC$_4$H$_8$NH-CH$_2$PO$_3$)·nH$_2$O, MIL-91] *(Wharmby and Wright, 2012)* or tetravalent (Ti^{4+}) [TiO(O$_3$P-CH$_2$NHC$_4$H$_8$NHCH$_2$PO$_3$)·4.5H$_2$O, MIL-91(Ti)] metal ions.

(a)   **(b)**

Figure 1.8. (a) The diphosphonic acid used in the synthesis of STA-12. (b) Structure of hydrated (Ni)STA-12. Reprinted with permission from (Miller et al., *J. Am. Chem. Soc*, **2008**, *130*, 15967-15981). Copyright (**2008**) American Chemical Society.

(a)   **(b)**

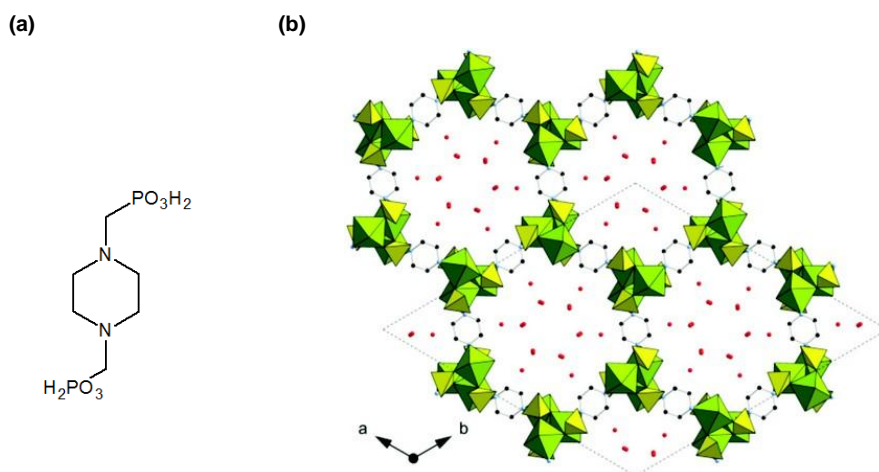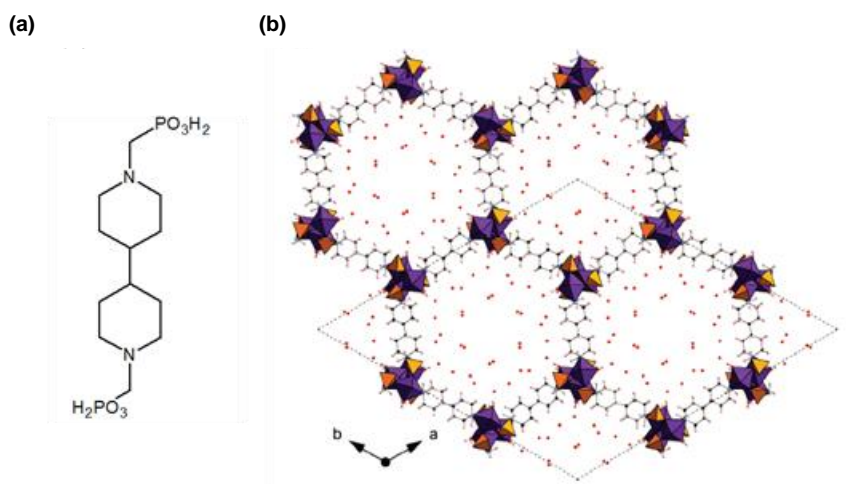**Figure 1.9.** (a) The diphosphonic acid used in the synthesis of STA-16. (b) Structure of hydrated (Co)STA-16. Reprinted with permission from (Wharmby et al., *J. Am. Chem. Soc*, **2011**, *133*, 1266-1269). Copyright (**2011**) American Chemical Society.

Crystallization with these types of ligands tends to give 3D frameworks rather than layered structures. The networks are

composed of inorganic chains running in one direction and cross-linked by the piperazine moieties. These bisphosphonate MOFs show permanent porosity, large breathing effects upon reversible adsorption and desorption of water, coordinatively unsaturated metal sites upon loss of coordinated water, and cation exchange capacity *(Wharmby and Wright, 2012)*. Interestingly, the Co-based STA-12 material $[Co_2(H_2O)_2(O_3PCH_2N(C_4H_8)NCH_2PO_3)\cdot xH_2O$ STA-12(Co)] also exhibits good catalytic properties for the aerobic epoxidation of olefins *(Beier et al., 2012)* as compared to the Co-doped zeolite catalysts, typically used for this reaction.

An alternative approach to forming pores in metal phosphonates is to employ a large, multidirectional ligand that would completely disfavor the formation of a layered inorganic motif. An example, is the 1,3,5-benzenetriphosphonic acid $[C_6H_3(PO_3H_2)_3, H_6BTP]$, analogous to trimesic acid present in many MOFs, and where the trigonal substitution should disfavor a simple layered motif. A study on Zn^{2+} derivatives of this ligand $Zn_3[C_6H_3(PO_3)_3](H_2O)_2\cdot 2H_2O$, (Zn-BTP, PCMOF-3), resulted in a layered network where the interlayer region was lined with phosphonate oxygen atoms and Zn-ligated water molecules *(Taylor et al., 2010)*, and two Zn-BTP derivatives with 3-D frameworks are $Zn_{2.5}(H)_{0.4-0.5}(C_6H_3O_9P_3)(H_2O)_{1.9-2}(NH_4)_{0.5-0.6}$ and $Zn_{2.5}(H)_{0.75}(C_6H_3O_9P_3)(H_2O)_2(CH_3NH_3)_{0.25}$. These materials show isostructural frameworks built from inorganic-organic layers linked by ZnO_4 tetrahedra. The negative charge of the framework is compensated by NH_4^+ or $CH_3NH_3^+$ ions located together with free water molecules in the internal cavities. In addition, NH_4^+ can be exchanged for lithium ions and reversible dehydration-rehydration takes place through intermediate structural changes *(Kinnibrugh, et al., 2013)*. However, the reaction of 1,3,5-benzenetrimethilenephosphonic acid

[$C_6H_3(CH_2PO_3H_2)_3$, H_6BMT] ligand with lanthanum salt, using a microwave-assisted synthesis leads to different compounds. 1D and nonporous 3D lanthanide derivatives are also known *(Vilela et al., 2012 and 2013a)*.

One of the most common aminophosphonic acid is the amino-*tris*-(methylenephosphonic acid), $N(CH_2PO_3H_2)_3$ (H_6AMP), which is mainly used to prevent scale formation in water systems due to its excellent chelating ability *(Clearfield and Demadis, 2012)*. This phosphonic acid has been investigated with a large variety of metal ions, from monovalent *(Martínez-Tapia et al., 2000)* to trivalent, such as Al^{3+} *(Cabeza et al., 2001)* and Ln^{3+} *(Cunha-Silva et al., 2007; Silva et al., 2011)*. Generally, the H_6AMP ligand reacts with divalent ions displacing two protons to form compounds with the stoichiometry M(II)-[$HN(CH_2PO_3H)_3$]·$3H_2O$. Even when combinations of several metals were used, the same structure was obtained *(Cabeza et al., 1999; Cabeza et al., 2002; Sharma et al., 2001; Mao et al., 2002b; Demadis and Katarachia, 2004; Demadis et al., 2005; Demadis et al., 2006a)*.

Reactions of H_6AMP with trivalent metal ions result in a nonporous 3D framework, $Al[N(CH_2PO_3H)_3]$·H_2O *(Cabeza et al., 2001)* or in 2D networks, [($LnN(CH_2PO_3H)_3$).$1.5H_2O$, $Ln(H_3AMP)$)·$1.5H_2O$ (Ln = La, Pr, Nd, Sm and Eu)] *(Cunha-Silva et al., 2007; Silva et al., 2011)*. The crystal structure of $La(H_3AMP)$ is formed by LaO_9 polyhedra, where the La^{3+} center is coordinated to seven phosphonate groups arising from four AMP^{3-} anionic ligands. Moreover, this compound behaves as an effective heterogeneous catalyst and its Eu- and Tb-doped derivatives show photoluminescent properties *(Silva et al., 2011)*. A different connectivity was observed for [$Pr(H_3AMP)$]$_3$·$1.5H_2O$, where the layers are composed of 1D chains formed by edge-shared

Ln^{3+} polyhedra interconnected via a phosphonate group *(Silva et al., 2011).*

Tetraphosphonates possessing the aminomethylenephosphonate (-N-CH$_2$-PO$_3$H$_2$) group deserve special attention by their great versatility to prompt a variety of topologies. In addition, some polyphosphonates with layered structures have the phosphonic groups within the layers. Normally, the polyphosphonates tend to have a high structural variability influenced by the flexibility and the high number of connecting oxygen atoms. Although rigidity in the organic ligand may be a necessary condition in order to induce permanent porosity and robustness for better pore size control.

Two examples of rigid ligands are the 1,4-*bis*(aminomethyl)benzene-*N,N'*-*bis*(methylenephophonic) acid [(H$_2$O$_3$PCH$_2$)$_2$-N-CH$_2$C$_6$H$_4$CH$_2$-N-(CH$_2$PO$_3$H)$_2$] (*p*-H$_8$L) and 1,3-*bis*(aminomethyl)benzene-*N,N'*-*bis*(methylenephophonic) acid (*m*-H$_8$L). 1D structure have been obtained when x stand for para-position of the diaminetetraphosphonate groups and metal Mg, Mn, Co, Ni and Zn cations *(Stock et al., 2004b).* By contrast, a pillared layered networks result when the ligand is *m*-C$_{12}$H$_{18}$O$_{12}$N$_2$P$_4$ *(Feyand et al., 2013).*

Another rigid tetraphophonic ligand, but without amino groups, is 1,2,4,5-tetrakisphosphonomethylbenzene [(H$_2$O$_3$PCH$_2$)$_4$C$_6$H$_2$]. The combination of this ligand with cadmium or copper salts results in 3D open-frameworks. In these networks, dimers of [Cd$_2$O$_{10}$] or [Cu$_2$O$_8$] are connected through the tetraphosphonate ions [(HO$_3$PCH$_2$)$_4$C$_6$H$_2$]$^{4-}$ *(Stock et al., 2005; Kaempfe et al., 2008). However, the* lanthanum derivative, [La(HO$_3$PCH$_2$)$_4$(O$_3$PCH$_2$)C$_6$H$_2$(H$_2$O)$_4$] (PCMOF-5), exhibits

1D channels within a modified pillared-layered framework containing diprotic phosphonic acid groups *(Taylor et al., 2013)*.

Flexible tetraphosphonic acids with aminobismethylenephosphonic groups $[(H_2O_3PCH_2)_2N\text{-}R\text{-}N(CH_2PO_3H_2)_2]$ $[R=(CH_2)_2$, H_8EDTMP; $(CH_2)_4$, H_8TDTMP; $(CH_2)_6$, H_8HDTMP; $(CH_2)_8$, H_8ODTMP; etc.] not only give rise to a rich structural variability but also outstanding properties, such as luminescence *(Costantino et al., 2010)*, ion-exchange capacity *(Vivani et al, 2006)*, ionic conduction properties *(Costantino et al., 2012)* as well as scale/corrosion inhibition *(Demadis et al., 2009b)*.

Compounds M(II)-$[(HO_3PCH_2)_2N\text{-}(CH_2)_2\text{-}N(CH_2PO_3H_2)_2$, M(II)-$H_6EDTMP\cdot3H_2O$ [M(II)=Ca and Sr] are 1D coordination polymers with H_6EDTMP^{2-} acting as both chelating and bridging ligand. Some of these derivatives show catalytic activity in dye photo-degradation *(Ma and Yuan, 2011)*.

A family of isostructural and 3D structure with general formula $M^{II}\text{-}H_6TDTMP$ was reported from the reaction of the acid $(H_2O_3PCH_2)_2N\text{-}(CH_2)_4\text{-}N(CH_2PO_3H_2)_2$, H_8TDTMP with divalent transition metals in a high-throughput system *(Stock and Bein, 2004; Stock et al., 2004a and 2004b)*. Gd-H_5TDTMP shows luminescent properties, with the Gd^{3+} ion being coordinated by eight oxygen atoms from five different phosphonate groups of five different ligands. The compound exhibits a broad blue fluorescent emission band at 441nm *(Ying et al., 2006)*. Others, such as Ga-H_5TDTMP, show significant ability to suppress metastatic tumors *(Su et al., 2005)*. On the other hand, Vivani et al., (2006), prepared the layered Zr-$H_6TDTMP\cdot4H_2O$ solid, in which the phosphonic groups were placed inside the layers, contributing to the formation of organo- inorganic sheets *(Vivani et al., 2006)*.

Based on the hexamethylenediamine tetrakis-(methylenephosphonic acid) (H_8DTMP), Colodrero et al. (2009) described a family of calcium tetraphosphonates, $Ca[(HO_3PCH_2)_2NH(CH_2)_6NH(CH_2PO_3H)_2]\cdot 2H_2O$ [CaH_6DTMP]. The layered structure of CaH_6DTMP is composed of a six-coordinated Ca^{2+} centers exclusively surrounded by phosphonate oxygen atoms from the H_6DTMP^{2-} ligand, embedded within the layers, to give infinite chains along the *a* axis, with one crystallographically independent lattice water molecule between the hybrid layers *(Colodrero et al., 2009)*. Moreover, CaH_6DTMP exhibited a reversible "breathing effect", accommodating a large number of guest molecules (up to 10 NH_3/H_2O) (Figure 1.10). This intercalation process allowed isolating three new compounds: $Ca(H_6DTMP)\cdot 6H_2O\cdot 4NH_3$, $Ca(H_6DTMP)\cdot 1.5H_2O\cdot 1.5NH_3$ and $CaH_6DTMP)\cdot 5NH_3$. Demadis et al. (2006b) reported a Zn^{2+} derivative with the same ligand, $Zn(H_6DTMP)\cdot H_2O$. In this case, the network exhibited a different arrangement although chains of MO_6 polyhedra were also found.

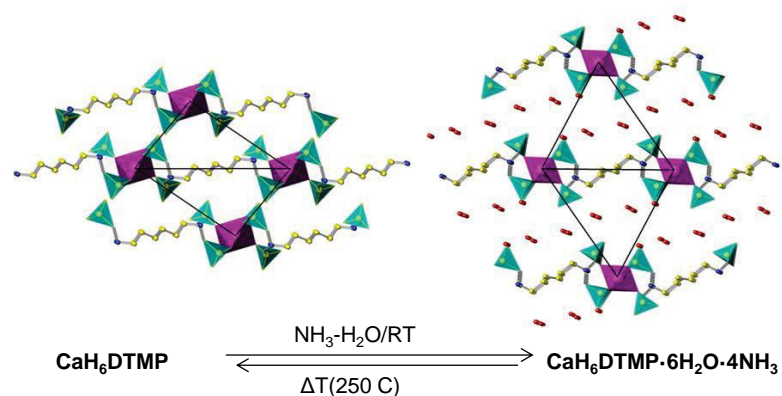**CaH_6DTMP** $\xrightleftharpoons[\Delta T(250\ C)]{NH_3-H_2O/RT}$ **CaH_6DTMP·6H_2O·4NH_3**

Figure 1.10. Crystal structures of CaH_6DTMP the showing the structural changes during the adsorption/desorption processes. Reprinted with permission from (Colodrero et al., *Chem.Eur. J.* **2009**, *15*, 6612-6618). Copyright (**2009**) Wiley-VCH.

This tetraphosphonate ligand with lanthanum yielded, La[(O$_3$PCH$_2$)(HO$_3$PCH$_2$)NH(CH$_2$)$_6$NH(CH$_2$PO$_3$H)$_2$·7H$_2$O], [La(H$_5$DTMP)·7H$_2$O]. This solid is characterized by an open 3D pillared framework, composed of corrugated layers in the plane *bc* and interconnected by the organic linker. Each layer is built by chains of LaO$_6$ polyhedra, which are formed exclusively by six phosphonate oxygen atoms from six different H$_5$DTMP^{3-} anions and interconnected by bridging phosphonate tetrahedra. The resulting 8- and 16-membered rings form 1D channels filled with seven lattice water molecules. [La(H$_5$DTMP)·7H$_2$O] exhibits a proton conductivity as high as 8 x 10^{-3} S·cm^{-1} at 24ºC and 98% RH, with a low activation energy of 0.25 eV *(Colodrero et al., 2012a).* Upon dehydration below 150 ºC, an anhydrous derivative La-(H$_5$DTMP) resulted, which remained stable up to 250 ºC (see Figure 1.11). Furthermore, the anhydrous phase [La(H$_5$DTMP)] is an ultramicroporous material with a specific surface from CO$_2$ adsorption of 84 m^2·g^{-1} The dehydrated phase showed affinity for water, but no complete rehydration was observed.

(a)   (b)

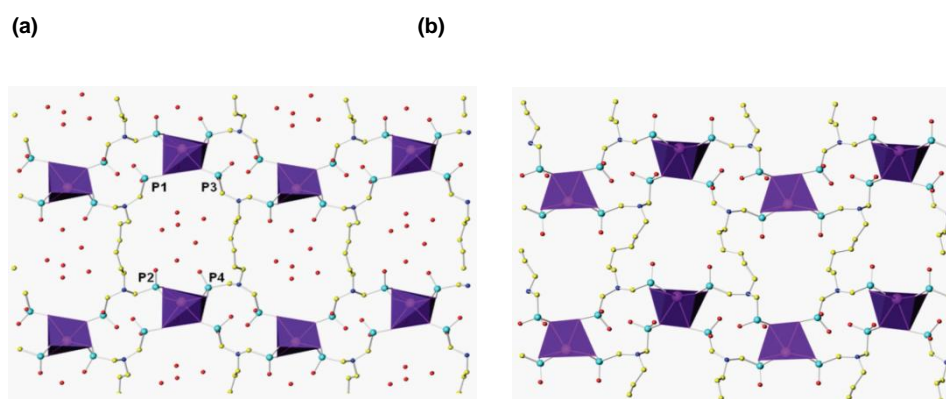**Figure 1.11.** Crystal structures of the hybrids showing the structural changes during the dehydration / rehydration processes: a) La(H$_5$DTMP)·7H$_2$O; b) La(H$_5$DTMP). Reprinted with permission from: Colodrero et al., *Dalton Trans.* **2012***, 41,*4045-4051*).* Copyright (**2012**) Royal Society of Chemistry.

Compounds with a higher number of methylene groups in the flexible organic chain have also been reported. For instance, with Mg^{2+} and octamethylenediamine-N,N,N',N'-tetrakis(methylenephosphonic acid [$(H_2O_3PCH_2)_2NH$-$(CH_2)_8NH(CH_2PO_3H_2)_2$, ($H_8ODTMP$)], a crystalline compound $Mg[(HO_3PCH_2)_2NH(CH_2)_8NH(CH_2PO_3H)_2]·2H_2O·0.5DMF$, [$Mg(H_6ODTMP)·2H_2O·0.5DMF$], was reported by Colodrero et al. (2012*b*). The magnesium compound synthesized by a high-throughput methodology is characterized by a 3D pillared open framework, containing cross-linked 1D channels filled with water and DMF molecules. Upon evacuation of H_2O and DMF molecules from the channels, thermally or under vacuum, the rehydration of the compound led to a new crystalline phase with much higher water content, $Mg(H_6ODTMP)·6H_2O$ (see Figure 1.12). This compound presented high proton conductivity of 1.6 x 10^{-3} S·cm^{-1} at 19 ºC and RH of ~100%, with an activation energy of 0.31 eV.
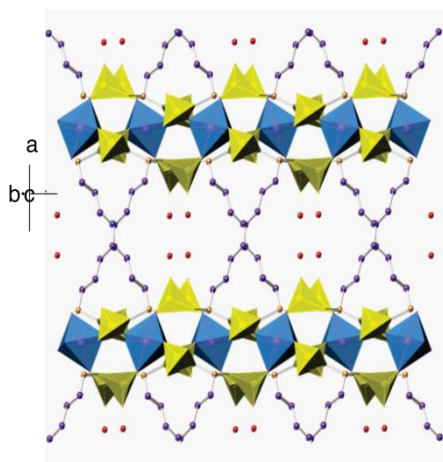
Figure 1.12. View along the *c* axis of 3D pillared-framework for $Mg(H_6ODTMP)·2H_2O·0.5DMF$, constructed by MgO_6 and CPO_3 polyhedra plus ball and stick for the organic ligand, with lattice water molecules shown as red spheres. Reprinted with

permission from (Colodrero et al., *Inorg. Chem.* **2012***, 51,* 7689-7698)*. C*opyright (**2012**) American Chemical Society.

1.1.3. APPLICATIONS OF MULTIFUNCTIONAL METAL PHOSPHONATES.

The use of functionalized phosphonic acid has notoriously boosted the metal phosphonates chemistry giving rise to novel and versatile structures for multiple purposes. A number of possible applications, such as gas adsorption, catalysis, ion-exchange, proton conductivity, magnetiism and photoluminescence properties, corrosion inhibition, etc., have recently been reported in books, such as "Metal Phosphonate Chemistry: From Synthesis to Applications" *(Clearfield and Demadis, 2012)* and "Organic-Inorganic Materials" *(Brunet et al., 2015)*, as well as, in reviews *(Ma and Yuan, 2011).* What follows is a brief summary of the some of most relevant applications of multifunctional metal phosphonates.

1.1.3.1. CATALYSIS AND PHOTOCATALYSIS.

A) CATALYSIS

For some heterogeneous catalysed reactions, metal phosphonates may represent an alternative to the frequently used zeolites. For instance, a 3-D porous rutile-type zinc(II)-phosphonocarboxylate, $[(Zn_3(C_6H_3(PO_3)(COO)_2)_2)\cdot2H_3O]_n$ showed excellent size-selective properties for Friedel–Crafts benzylation. Its catalytic activity was related to the presence of Brönsted acid centers in specific sites of the network *(Liao et al., 2010)*.

Functionalized lanthanide organophosphonates [La($C_6H_3(CH_2PO_3H_2)(CH_2PO_3H)_2$)($C_6H_3(CH_2PO_3H)(CH_2PO_3H_2)_2(H_2O)_2$]· $3H_2O$, La[(H_4BMT)(H_5BMT)($H_2O)_2$]·$3H_2O$ and [Ln_2(($C_6H_3(CH_2PO_3H)_3)_2$ ($H_2O)_2$]·$3H_2O$ [$Ln_2(H_3BMT)_2(H_2O)_2$]·H_2O (Ln= La, Ce, Pr, Nd) were also investigated as heterogeneous catalysts. As an example, [La(H_4BMT)(H_5BMT)($H_2O)_2$]·$3H_2O$ shows a high activity in the methanolysis of styrene oxide with nearly complete conversions after 30 min of reaction without the need for catalyst regeneration *(Vilela et al., 2013a and 2013b)*.

Beier et al., (2012) investigated a Co-based N,N'-piperazinebis(methylenephosphonic acid) [(H_2O_3P-CH_2-NC_4H_8N-$CH_2PO_3H_2$), STA-12] material, [[$Co_2(H_2O)_2(O_3PCH_2N(C_4H_8)$-$NCH_2PO_3$)·$xH_2O$, STA-12(Co)], to ascertain its feasibility as catalyst, in the aerobic epoxidation of olefins. It showed a high activity as compared with the Co-doped zeolite catalysts that are typically used in this reaction. The reaction was found to proceed mainly heterogeneously and the catalyst was reusable with only a small loss of activity *(Beier et al., 2012)*.

Adsorption and catalytic properties have been reported for a semicrystalline porous nickel tetraphosphonate based on ligand H_8DTMP. It exhibited catalytic activity and selectivity for the reduction of nitrobenzenes to the respective anilines, in the presence of $NaBH_4$ as the reducing agent *(Dutta, et al., 2012)*.
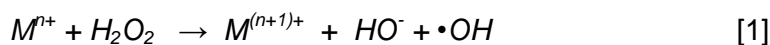
B) PHOTOCATALYSIS

Photocatalysis is a methodology, useful to solve environmental issues such as air and water pollution. Since the pioneering work of Fujishima and Honda in 1972, much research has focused on

semiconductor-based photocatalysts and photocatalytic processes using titanium dioxide TiO_2 *(Fujishima and Honda, 1972)*. This semiconductor material is non-toxic, abundant and inexpensive *(Ma et al., 2010a and 2010b)*.

Within the advanced oxidation processes (AOPs), photocatalysis relies on in-situ production of highly reactive hydroxyl radicals (•OH). These reactive species are the strongest oxidants that can be applied in water and can oxidize most compounds present in the water matrix. Hydroxyl radicals are produced with the help of one or more primary oxidants (e.g. O_3, H_2O_2, O_2) and/or energy sources (e.g. ultraviolet o visible light) or catalysts such as TiO_2.

The most important advanced oxidation treatments based on the use of H_2O_2 are Fenton and photo-Fenton processes. The Fenton reaction was discovered by Fenton in 1894 *(Fenton, 1894)*. Forty years later the mechanism was postulated and it revealed that the effective oxidative agent in the Fenton reaction is the hydroxyl radical (•OH) *(Haber and Weiss, 1934)*. The Fenton reaction and photo-Fenton process can be outlined by reactions (1-3) as follows:

$$M^{n+} + H_2O_2 \;\rightarrow\; M^{(n+1)+} \;+\; HO^- + \bullet OH \qquad\qquad [1]$$

M^{n+} is a transition metal such as Fe or Cu.

$$Fe^{3+} + H_2O + h\vartheta \;\rightarrow\; Fe^{2+} \;+\; \bullet OH + H^+ \qquad\qquad [2]$$

$$Fe^{2+} + H_2O_2 \;\rightarrow\; Fe^{3+} + OH^- + \bullet OH \qquad\qquad [3]$$
$$H_2O_2 + h\vartheta \;\rightarrow\; 2\bullet OH \;\; (\lambda < 400\ nm) \qquad\qquad [4]$$
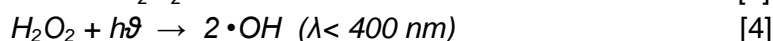
Photo-reduction of ferric ions (Fe^{3+}) is the proposed mechanism for photochemical regeneration of ferrous ions (Fe^{2+}). The newly generated ferrous ions react with H_2O_2 generating a second (•OH) radical and ferric ion, and the cycle continues (reactions 2-3).

Fenton and photo-Fenton reaction depend not only on H_2O_2 concentration and iron added, but also on the operating pH value. The oxidative decomposition and transformation of organic substrates by Fenton's reagent, H_2O_2/Fe^{2+} has economic advantages as compared to other pollutant degradation processes by the low cost of H_2O_2 and iron sources.

Basic chemistry, as well as applications of Fe^{2+}/H_2O_2 and Fe^{3+}/H_2O_2 system for hazardous waste treatment is used. Ferrous ion combined with hydrogen peroxide reacts stoichiometrically to give ($\cdot$OH) according to reaction (3).

In the dark, the reaction is retarded after complete conversion of Fe^{2+} to Fe^{3+}. Further enhancement of oxidizing power of the Fenton system is achieved by irradiation with UV or UV-visible light. This effectiveness has been proven with the total mineralization of many organic compounds in aqueous solution. The reason for the positive 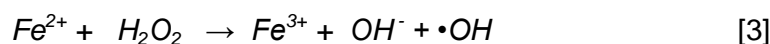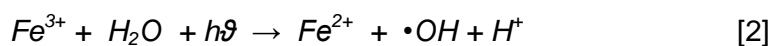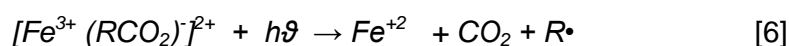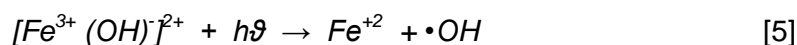effect of irradiation on the degradation rate include the photo-reduction of Fe^{3+} to Fe^{2+} ions, which produce new ($\cdot$OH) radicals with H_2O_2 according to reactions 2 and 4.

The main species absorbing light in the Fenton system are ferric ion complexes, e.g. $[Fe^{3+}(OH)^-]^{2+}$ and $[Fe^{3+}(RCO_2)^-]^{2+}$, which produce additional Fe^{+2} by following photo-induced, ligand-to-metal charge-transfer reactions, according to reactions 5 and 6 *(Sagawe et al., 2001)*.

$$[Fe^{3+}(OH)^-]^{2+} + h\vartheta \rightarrow Fe^{+2} + \cdot OH \qquad\qquad [5]$$
$$[Fe^{3+}(RCO_2)^-]^{2+} + h\vartheta \rightarrow Fe^{+2} + CO_2 + R\cdot \qquad\qquad [6]$$

Additionally, the first equation yields ($\cdot$OH) radicals, while the second equation results in a reduction of the total organic carbon

(TOC) content of the system due to the decarboxylation of organic acid intermediates. Both reactions, in turn, form the ferrous ions required for the Fenton reaction. The overall degradation rate of organic compounds is considerably increased in the photo-Fenton process, even at lower concentration of iron salts present in the system.

Photo-Fenton was found more efficient in decreasing pollution load of waste water as compared to others because of fast generation of hydroxyl in the presence of light and involvement of Fe^{3+} in visible light-absorbing complexes that increase the production rate of hydroxyl radicals *(Muneer et al., 2012 and Bilal et al., 2014).*

Recent research has showed that metal-organic frameworks (MOFs) are quite effective in the photocatalytic degradation of organic pollutants under UV/visible. *(Horiuchi et al., 2013, Zhang and Lin, 2014; Li and Xu, 2013; Laurier et al., 2013; Nasalevich et al., 2014; Wang, et al., 2014a; Ai et al., 2014).*

There are few works reporting the use of functionalized metal phosphonates in photocatalysis processes. Crystalline lanthanide-containing organodiphosphonate-functionalized polyoxomolybdate cages have been found as effective catalysts in decolouration of rhodamine B and other dyes under UV irradiation, although mineralization data were not given *(Niu, et al., 2012)*. Titanium phosphonates, obtained by surfactant-assisted synthesis were shown to be useful catalysts for the photodegradation of rhodamine B under solar light-analogous radiation *(Ma et al., 2009, 2010a and 2010b).*

1.1.3.2. PROTON CONDUCTIVITY.

Proton exchange membrane fuel cells (PEMFCs) are believed to be the most promising devices for transportation applications. Its operating temperature is near 100ºC with ultra-low or zero emissions of environmental pollutants. The high proton conductivity is one of the important factors for evaluating the PEMFCs *(Li and Xu, 2013),* but proton conductor performances remains a critical issue. Apart from perfluorinated polymers, such as Nafion[®], which work efficiently in the presence of water at temperatures lower than 80 ºC, development of new proton conductors having high proton conductivity (over 0.1 S·cm^{-1}) and operating in a wider temperature range (25–300 ºC) is required to increase the efficiency of fuel cells. Coordination polymers are possible candidates with the necessary requirements as electrolites and, furthermore, their crystallinity provide insights into molecular-level transport mechanisms *(Jiménez-García et al., 2011; Clearfield and Demadis, 2012; Li and Xu, 2013; Yoon et al., 2013 and Horike et al., 2013).*

Proton conducting MOFs can be classified in two categories: water-mediated and anhydrous or non-water mediated proton-conductors. In the case of anhydrous or non-water mediated proton conductors, H$^+$ conductivity can be achieved by accumulating protonic organic molecules in the pores *(Yoon et al., 2013 and Horike et al., 2013).* For water-mediated proton conductors, the *vehicle* and *Grotthuss-type mechanisms* have been described. The first type of mechanism implies diffusion of a proton on a carrier species or proton-containing groups (e.g., H$_3$O$^+$, NH$_4^+$), where, these groups act as a vehicle for the proton. The occupied vehicle travels through the solvent filled channel in a framework, while the unoccupied vehicles diffuse

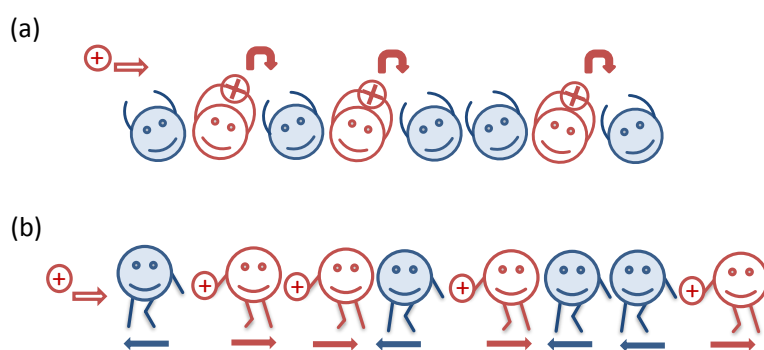back in the opposite direction, resulting in proton conduction via diffusion (Figure 1.13), *(Kreuer et al., 1982).*

(a)

(b)

Figure 1.13. Scheme of proton conduction models: (a) Grotthuss mechanism and (b) vehicle mechanism. Adapted from reference *(Ren, et al., 2013).*

The Grotthuss-type mechanism involves a proton being transported by hopping through an infinite hydrogen-bonding network *(Agmon, 1995)*. There a series of oxygen atoms (proton acceptor sites) line a pore surface, allowing a proton that is bound to one oxygen atom to hydrogen bond to the neighboring atom. The proton can then hop to the next available site, but then a structural reorientation needs to occur to allow the proton to continue hopping. Proton acceptor sites are not restricted solely to dangling functional groups on a surface, but can also involve solvent or guest molecules within the pore. Proton conduction in MOFs is not limited to either the Grotthuss or the vehicle mechanism, but can be a combination of the two. Determining which mechanism is present in a material is normally done by analyzing the activation energies (Ea) process. Low Ea (e.g., 0.1-0.4 eV) is characteristic of Grotthuss mechanism, and the vehicular mechanism is more dominant when the E_a is larger (e.g., 0.5-0.9 eV) *(Agmon,*

1995; Kreuer et al., 1982; Colomban and Novak, 1988). Recently, hydroxide ion conduction has also been reported in MOFs *(Sadakiyo et al., 2014).* Considering OH^- ions are opposite in change to proton, there are two approaches to introducing OH^- ions into MOFs: OH^- ions are inserted as counteranions into the pores, or hydroxide salts are incorporated into the voids *(Sadaliyo et al., 2009).* Nevertheless, it is important to consider the stability of the frameworks for a strong base, such as the OH^- ions.

Metal phosphonates may offer acidic sites for proton exchange, some degree of structural adaptability, high crystallinity and pores filled with guest molecules (e.g. H_2O, heterocycles, etc.) that act as proton carriers. In addition, some robust metal phosphonates are susceptible of post-synthesis modifications, by processes such as sulfonation, to increase the proton conductivity *(Clearfield and Demadis, 2012; and Cabeza et al., 2015).*

Table 1.1 displays the conductivity properties of selected crystalline functionalized metal phosphonates. Here, conductivity values for metal phosphonates/polymer composites or pure phosphonic acids have been omitted. Table 1.1 shows that a large number of metal phosphonates presenting significant proton conductivity are multifunctionalized structures.

Table 1.1. Proton conductivities for functionalized metal phosphonates.

Proton Conducting Phosphonates Systems	Highest H$^+$ σ (S/cm)	Ea (eV)	T (°C)	Relative Humidity (%)	Reference
[C$_6$(OH)$_3$(SO$_3$Na)$_3$]$_{0.66}$[C$_6$H$_3$(PO$_3$HNa)$_3$]$_{0.34}$·0.75H$_2$O *PCMOF-2.5*	2.1 x 10^{-2}	0.21	85	90	Kim et al., 2013
La[(O$_3$PCH$_2$)(HO$_3$PCH$_2$)-NH(CH$_2$)$_6$NH(CH$_2$PO$_3$H)$_2$·7H$_2$O *LaH$_5$DTMP·7H$_2$O*	8 x 10^{-3}	0.25	24	98	Colodrero et al., 2012a
La(HO$_3$PCH$_2$)$_4$(O$_3$PCH$_2$)C$_6$H$_2$(H$_2$O)$_4$ *PCMOF-5*	4.0x 10^{-3}	0.16	60	98	Taylor et al., 2013
[UO$_2$(HO$_3$PC$_6$H$_5$)$_2$(H$_2$O)]$_2$·8H$_2$O	3.0 x 10^{-3}	0.36	RT	80	Grohol et al., 1996
Mg[(HO$_3$PCH$_2$)$_2$NH(CH$_2$)$_8$NH(CH$_2$PO$_3$H)$_2$]·6H$_2$O *MgH$_6$ODTMP·6H$_2$O*	1.6 x 10^{-3}	0.31	19	98	Colodrero et al., 2012b
Mn-(m-C$_{12}$H$_{18}$O$_{12}$N$_2$P$_4$)·2H$_2$O	1.5 x 10^{-3}	-	140	100	Feyand et al., 2013
Zr$_2$ (PO$_4$)H$_5$(L)$_2$·H$_2$O [L=(O$_3$PCH$_2$)$_2$NCH$_2$COO]	1.0 x 10^{-3}	0.15	140	95	Donnadio et al., 2014
Gd$_3$(H$_{0.75}$O$_3$PCHOHCOO)$_4$·16H$_2$O *GdHPA-II*	3.2 x 10^{-4}	0.23	25	98	Colodrero et al., 2012c
ZrH$_4$(O$_3$PCH$_2$)$_2$N-C$_6$H$_{10}$-N(O$_3$CH$_2$P)$_2$·5.5 H$_2$O *ZrChDTMP_lp@H*	1 x 10^{-4}	0.09	80	95	Costantino et al., 2012
Zn$_3$[C$_6$H$_3$(PO$_3$)$_3$](H$_2$O)$_2$·2H$_2$O, *PCMOF-3*	5.0 x 10^{-5}	0.17	25	98	Taylor et al., 2010
Zn-(p-C$_{12}$H$_{18}$O$_{12}$N$_2$P$_4$)·2H$_2$O	4.3 x 10^{-5}	-	140	100	Feyand et al., 2013

Materials exhibiting the highest proton conductivity are those containing sulfonic groups, incorporated by post-synthesis sulfonation or forming part of the phosphonate moiety *(Taylor et al., 2013 and Kim et al., 2013)*. However, the absence of crystallinity in many compounds, make difficult to establish a clear relationship between

their crystal structures and conductivity mechanisms *(Adani et al., 1998; Zima et al., 2010; Jang et al., 2003).*

The 3D lanthanum derivate of 1,2,4,5-tetrakisphosphonomethylbenzene $[(H_2O_3PCH_2)_4C_6H_2]$ ligand, $[La(HO_3PCH_2)_4(O_3PCH_2)C_6H_2(H_2O)_4]$ $[La(H_5L)(H_2O)_4$, PCMOF-5] constitutes an example of the importance of having phosphonic groups for the proton conduction. This compound contains uncoordinated diprotic phosphonic acid groups that points toward the hydrated channels. The presence of these acidic groups and the hydrated nature of the channel provide a chance of generating well defined hydrogen bond pathways. This compound exhibited good humidity stability and proton conductivity of 4×10^{-3} S·cm^{-1} at 60 ºC and 98% RH with low activation energy (0.16 eV) *(Taylor et al., 2013).*

Values of proton conductivity similar to those of PCMOF-5 were reported for a gadolinium multifunctional phosphonates, $Gd_3(H_{0.75}O_3PCHOHCOO)_4 \cdot 16H_2O$, which exhibited a proton conductivity value of 3.2×10^{-4} S·cm^{-1} at 25 ºC and 98% RH and Ea of 0.23 eV *(Colodrero et al., 2012c)*. However, a polymorphic phase of $La_3(H_{0.75}O_3PCHOHCOO)_4 \cdot 15H_2O$, shows conductivity values ~2 orders of magnitude lower than that of the Gd^{3+} derivative. Although both compounds display microporous frameworks, with 1D channels decorated with P-OH groups and filled with water molecules; the different arrangements of the water molecules inside the channels, both metal-bonding and non-coordinated water, likely leads to markedly different proton pathways *(Colodrero et al., 2012c).*

Functionalized metal phosphonates of low dimensionality, such as Mn-(m-$C_{12}H_{18}O_{12}N_2P_4$)·2H$_2$O and Zn-(p-$C_{12}H_{18}O_{12}N_2P_4$)·2H$_2$O, also

exhibit significant proton conductivities. Their crystal structures contain H-bounded water molecules that are filling the space between the hydrophilic portions of the layers. The layered Mn-(m-$C_{12}H_{18}O_{12}N_2P_4$)·2H$_2$O shows a high proton conductivity at 140 ºC and maximum value of RH (proton conductivity value of 1.5 x 10^{-3} S·cm^{-1}), but it decays abruptly by decreasing 10% the RH *(Feyand et al., 2013).*

Various compounds of di-, tri- and tetravalent phosphonates contain the N,N,N',N'-diaminotetramethylene-phosphonate moiety, have been reported as good proton conductors *(Colodrero et al., 2012a, b; Costantino et al., 2012*). These metal phosphonates exhibit quite frequently a pillared layered or a 3D open framework with 1D channel decorated with free P-OH groups. These cavities are regularly occupied with lattice water molecules that establish H-bonds interactions with each other and with the non-coordinated phosphonate groups, creating an extended H-bond network through the channels. For instance, proton conductivity studies on [Mg[(HO$_3$PCH$_2$)$_2$NH(CH$_2$)$_8$NH(CH$_2$PO$_3$H)$_2$]·6H$_2$O, Mg(H$_6$ODTMP)· 6H$_2$O] showed a large humidity dependence, but gave a high conductivity value of 1.6 x 10^{-3} S·cm^{-1} at 19 °C and ~100% RH due to the large number of free acidic protons *(Colodrero et al., 2012b).*

[La[(O$_3$PCH$_2$)(HO$_3$PCH$_2$)NH(CH$_2$)$_6$NH(CH$_2$PO$_3$H)$_2$·7H$_2$O, La(H$_5$DTMP)·7H$_2$O] exhibited higher proton conductivity, 8 x 10^{-3} S·cm^{-1} at 24 ºC and 98% of relative humidity and a low activation energy of 0.25 eV *(Colodrero et al., 2012a)*. This network favors the exchange of the protons, which explains the relative low activation energies measured, typical of a Grotthuss mechanism. LaH$_5$DTMP·7H$_2$O and MgH$_6$ODTMP·6H$_2$O experience a diminution in their proton

conductivities upon dehydration. This behavior may be explained in terms of framework flexibility. A high flexibility, as that in La^{3+} and Mg^{2+} derivatives, implies that water removal is accompanied by structural changes. Alternatively, water removal decreases the number of available sites for proton conductor the Grotthuss mechanism.

$[C_6(OH)_3(SO_3Na)_3]_{0.66}[C_6H_3(PO_3HNa)_3]_{0.34} \cdot 0.75H_2O$, $[Na_3L_1]_{0.66}$ $[Na_3H_3L_2]_{0.34} \cdot 0.75H_2O$ (PCMOF-2.5) was obtained by isomorph replacement of deprotonated organosulfonate (2,4,6-trihydroxy-1,3,5-benzenetrisulfonate, $[C_6(OH)_3(SO_3Na)_3]$) with the organohydrogenphophonate (1,3,5-benzenetriphosphonate $[C_6H_3(PO_3H_2)_3$, $H_6BTP]$) ligand. PCMOF-2.5 presents a structure with 1D channels with hydrogen phosphonate and sulfonate groups. This compound is the highest proton conductor with a conductivity value of 2.1×10^{-2} S·cm^{-1}, at 85 ºC and 90% RH *(Kim et al., 2013)*.

CHAPTER 2
OBJECTIVES

OBJECTIVES

In this work, proton conduction, photocatalytic and photoluminescence properties are investigated for a series of multifunctional metal phosphonates. These materials have been prepared by incorporation of active metal ions and/or specific organic functions in different structural systems. In order to establish the correlations between crystal structures and properties, synthetic methods have been optimized for obtaining materials with a high degree of crystallinity.

The following tasks have been addressed to achieve this main objective:

■ Synthesis of crystalline metal phosphonates by suitable combination of one of the three phosphonic acids employed: $HO_2CCH(OH)PO_3H_2$ (HPAA), $C_6H_3(H_2PO_3)(CO_2H)_2$ (PiPhtA) or $N(CH_2PO_3H_2)_3$ (H_6AMP) and a salt of a metal, selected according to the properties to be investigated in each case (alkaline: Li^+, Na^+, K^+ and Cs^+; alkaline earth: Ca^{2+} or transition metal ion: Fe^{2+} or lanthanides). A preliminary study using organic functional groups (sulfonic) other than those above specified is also included in order to evaluate their possible effects.

■ Structural resolution and chemical characterization of the obtained solids by using single crystal diffraction, when possible, and laboratory or synchrotron radiation powder X-ray diffraction. For basic chemical characterization, a wide variety of instrumental techniques, such as DTA-TG, IR spectroscopy, UV-

Vis, XPS, SEM and elemental analysis, among others, are employed.

■ Photodegradation study of standard water pollutants (phenol and chlorophenol) by using Fe(II) phosphonate as a heterogeneous photocatalyst in advanced oxidation processes. Evaluation of the main parameters influencing pollutant photo-oxidation reactions, as well as the optimum conditions of pollutant mineralization.

■ Study of the proton conduction properties for those materials with structures exhibiting potential proton transfer pathways through hydrogen bonding networks. Measurements of proton conductivity and activation energy within a temperature (<100 °C) and relative humidity range. Data are analyzed by establishing correlations with the corresponding crystal structures. Finally, reactions of the as-synthesized solids with ammonia vapors are conducted in order to check the possible structural modifications and their effects on proton conductivity.

CAPÍTULO 2
OBJETIVOS

OBJETIVOS

En la presente memoria se investigan las propiedades de conducción protónica, fotocatalíticas y fotoluminiscentes de fosfonatos metálicos multifuncionales, preparados por incorporación de iones metálicos activos y/o funciones orgánicas específicas en diferentes sistemas estructurales. Para estudiar las correlaciones existentes entre estructura y propiedades, los métodos de síntesis se han optimizado, con el propósito de obtener materiales que posean un elevado grado de cristalinidad.

La consecución de este objetivo principal se ha abordado mediante las siguientes etapas de trabajo:

■ Síntesis de fosfonatos metálicos cristalinos mediante la combinación adecuada de uno de los tres ácidos fosfónicos empleados: $HO_2CCH(OH)PO_3H_2$ (HPAA), $C_6H_3(H_2PO_3)(CO_2H)_2$ (PiPhtA) o $N(CH_2PO_3H_2)_3$ (H_6AMP) y una sal de un metal, seleccionado según las propiedades que se desean investigar en cada caso (alcalinos: Li^+, Na^+, K^+ y Cs^+, alcalinotérreos: Ca^{2+} ; de transición: Fe^{2+}; o lantánidos). También, se incluye un estudio preliminar usando otras funcionalidades orgánicas (grupos sulfónicos) con el objeto de evaluar sus posibles efectos.

■ Resolución estructural y caracterización química de los sólidos obtenidos. Para elucidar las estructuras cristalinas se emplea difracción de monocristal, cuando esto sea posible, y difracción de rayos X de polvo, tanto de

laboratorio como radiación sincrotrón. La caracterización química se realiza empleando un amplio abanico de técnicas instrumentales: ATD-TG, espectroscopía IR, UV-Vis, XPS, análisis elemental y microscopía SEM, entre otras.

■ Estudio de la fotodegradación de contaminantes ambientales presentes frecuentemente en las aguas naturales, tales como fenol, clorofenol y/o colorantes de diversas naturalezas mediante el uso de un fosfonato de Fe(II) como fotocatalizador heterogéneo para procesos avanzados de oxidación. Se pretende determinar los parámetros que influyen en la fotooxidación y las condiciones óptimas de mineralización del contaminante orgánico seleccionado.

■ Estudio de las propiedades de conducción protónica en aquellos materiales cuya estructura presenta potenciales trayectorias de transferencia protónica, a través de redes de enlace de hidrógeno. Se determina la conductividad protónica y la energía de activación del proceso en un intervalo de temperaturas no superior a 100 ºC y diversas condiciones de humedad relativa. Estos datos se analizan estableciendo correlaciones con la estructura cristalina correspondiente. Finalmente, se investiga la reacción de los sólidos sintetizados con amoniaco en fase vapor, con el objeto de comprobar las modificaciones estructurales introducidas y su efecto sobre la conductividad protónica.

CHAPTER 3
ARTICLE SECTION

Montse Bazaga-Garcia, Aurelio Cabeza, Pascual Olivera-Pastor, Isabel Santacruz, Rosario M. P. Colodrero, y Miguel A. G. Aranda

"*Photodegradation of Phenol over a hybrid organo-inorganic metal: Iron(II) hydroxyphosphonoacetate*"

Abstract:

Water treatment is a hot topic, and it will become much more important in the decades ahead. Advanced oxidation processes are being increasingly used for organic contaminant removal, for example using photo-Fenton reactions. Here we report the use of an organo-inorganic hybrid, $Fe[HO_3PCH(OH)COO]\cdot 2H_2O$, as Fenton photocatalyst for phenol oxidation with H_2O_2 under UVA radiation. Preactivation, catalyst content, and particle size parameters have been studied/optimized for increasing phenol mineralization. Upon reaction, iron species are leached from the catalyst making a homogeneous catalysis contribution to the overall phenol photo-oxidation. Under optimized conditions, the mineralization degree was slightly larger than 90% after 80 min of irradiation. Analysis by X-ray photoelectron spectroscopy revealed important chemical modifications occurring on the surface of the catalyst after activation and phenol photodegradation. The sustained slow delivery of iron species upon phenol photoreaction is advantageous as the mixed heterogeneous−homogeneous catalytic processes result in very high phenol mineralization.

Montse Bazaga-García, Rosario M. P. Colodrero, Maria Papadaki, Piotr Garczarek, Jerzy Zoń, Pascual Olivera-Pastor, Enrique R. Losilla, Laura León-Reina, Miguel A. G. Aranda, Duane Choquesillo-Lazarte, Konstantinos D. Demadis, y Aurelio Cabeza.

"Guest Molecule-Responsive Functional Calcium Phosphonate Frameworks for Tuned Proton Conductivity"

Abstract:

We report the synthesis, structural characterization, and functionality (framework interconversions together with proton conductivity) of an open-framework hybrid that combines Ca^{2+} ions and the rigid polyfunctional ligand 5-(dihydroxyphosphoryl)isophthalic acid (PiPhtA). $Ca_2[(HO_3PC_6H_3COOH)_2]_2[(HO_3PC_6H_3(COO)_2H)(H_2O)_2]\cdot 5H_2O$ (Ca-PiPhtA-I) is obtained by slow crystallization at ambient conditions from acidic (pH ≈ 3) aqueous solutions. It possesses a high water content (both Ca coordinated and in the lattice), and importantly, it exhibits water-filled 1D channels. At 75 °C, Ca-PiPhtA-I is partially dehydrated and exhibits a crystalline diffraction pattern that can be indexed in a monoclinic cell with parameters close to the pristine phase. Rietveld refinement was carried out for the sample heated at 75 °C, Ca-PiPhtA-II, using synchrotron powder X-ray diffraction data, which revealed the molecular formula $Ca_2[(HO_3PC_6H_3COOH)_2]_2[(HO_3PC_6H_3(COO)_2H)(H_2O)_2]$. All connectivity modes of the "parent" Ca-PiPhtA-I framework are retained in Ca-PiPhtA-II. Upon Ca-PiPhtA-I exposure to ammonia vapors (28% aqueous NH_3) a new derivative is obtained (Ca-PiPhtA-NH_3) containing 7 NH_3 and 16 H_2O molecules according to elemental and thermal analyses. Ca-PiPhtA-NH_3 exhibits a complex X-ray diffraction pattern with peaks at 15.3 and 13.0 Å that suggest partial breaking and transformation of the parent pillared structure. Although detailed structural identification of Ca-PiPhtA-NH_3 was not possible, due in part to nonequilibrium adsorption conditions and the lack of crystallinity, FT-IR spectra and DTA-TG analysis indicate profound structural changes compared to the pristine Ca-PiPhtA-I. At 98% RH and T = 24 °C, proton conductivity, σ, for Ca-PiPhtA-I is 5.7×10^{-4} S·cm^{-1}. It increases to 1.3×10^{-3} S·cm^{-1} upon activation by preheating the sample at 40 °C for 2 h followed by water equilibration at room temperature under controlled conditions. Ca-PiPhtA-NH_3 exhibits the highest proton conductivity, 6.6×10^{-3} S·cm^{-1}, measured at 98% RH and T = 24 °C. Activation energies (Ea) for proton transfer in the above-mentioned frameworks range between

0.23 and 0.4 eV, typical of a Grothuss mechanism of proton conduction. These results underline the importance of internal H-bonding networks that, in turn, determine conductivity properties of hybrid materials. It is highlighted that new proton transfer pathways may be created by means of cavity "derivatization" with selected guest molecules resulting in improved proton conductivity.

Montse Bazaga-García, Maria Papadaki, Rosario M. P. Colodrero, Pascual Olivera-Pastor, Enrique R. Losilla, Belén Nieto-Ortega, Miguel Ángel G. Aranda, Duane Choquesillo-Lazarte, Aurelio Cabeza, y Konstantinos D. Demadis.

"Tuning proton conductivity in alkali metal phosphonocarboxylates by cation size-induced and water-facilitated proton transfer pathways"

Abstract:

The structural and functional chemistry of a family of alkali-metal ions with racemic R,S-hydroxyphosphonoacetate (M-HPAA; M = Li, Na, K, Cs) are reported. Crystal structures were determined by X-ray data (Li$^+$, powder diffraction following an ab initio methodology; Na$^+$, K$^+$, Cs$^+$, single crystal). A gradual increase in dimensionality directly proportional to the alkali ionic radius was observed. [Li$_3$(OOCCH(OH)PO$_3$)-(H$_2$O)$_4$]·H$_2$O (Li-HPAA) shows a 1D framework built up by Li-ligand "slabs" with Li$^+$ in three different coordination environments (4-, 5-, and 6-coordinated). Na-HPAA, Na$_2$(OOCCH(OH)PO$_3$H)(H$_2$O)$_4$, exhibits a pillared layered "house of cards" structure, while K-HPAA, K$_2$(OOCCH(OH)PO$_3$H)(H$_2$O)$_2$, and Cs-HPAA, Cs(HOOCCH(OH)-PO$_3$H), typically present intricate 3D frameworks. Strong hydrogen-bonded networks are created even if no water is present, as is the case in Cs-HPAA. As a result, all compounds show proton conductivity in the range 3.5×10^{-5} S · cm^{-1} (Cs-HPAA) to 5.6×10^{-3} S · cm^{-1} (Na-HPAA) at 98% RH and T = 24 °C. Differences in proton conduction mechanisms, Grothuss (Na$^+$ and Cs$^+$) or vehicular (Li$^+$ and K$^+$), are attributed to the different roles played by water molecules and/or proton transfer pathways between phosphonate and carboxylate groups of the ligand HPAA. Upon slow crystallization, partial enrichment in the S enantiomer of the ligand is observed for Na-HPAA, while the Cs-HPAA is a chiral compound containing only the S enantiomer.

CHAPTER 4
RESULTS & DISCUSSION

4. RESULTS AND DISCUSSION

This chapter examines the relationships between crystal structure and various properties resulting from the combination of rigid or flexible multifunctional phosphonate ligands with mono, di- or trivalent metal ions.

The chapter has been divided in three different families of multifunctional phosphonic acids: (1) mono- and divalent derivatives of *R,S*-2-hydroxyphosphonoacetic acid [$HOOCCH(OH)PO_3H_2$], HPAA; (2) Calcium derivatives of 5-(dihydroxyphosphoryl)isophthalic acid [$C_6H_3(H_2PO_3)(COOH)_2$], PiPhtA; (3) Trivalent derivatives of amino-*tris*-(methylenephosphonic) acid [$N(CH_2PO_3H_2)_3$], (see Figure 4.1). Finally, some preliminaries results will be shown for the polyfunctonalized acid $(H_2O_3PCH_2)_2$-N-$(CH_2)_2SO_3H$

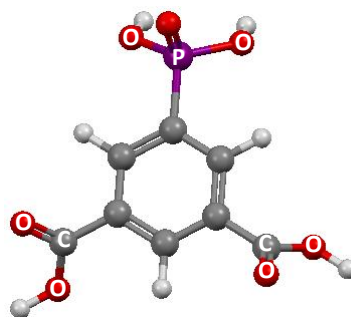*R,S* 2-hydroxyphosphonoacetic acid [$HOOCCH(OH)PO_3H_2$], HPAA is a commercially available simple ligand, chemically stable, cost-effective and environmentally safe product. Moreover, the presence of a chiral carbon in its backbone opens the possibility to synthesize non-centrosymmetric metal-organic coordination polymers.

5-(dihydroxyphosphoryl)isophthalic acid, PiPhtA is a highly functionalized rigid ligand with one phosphonic and two carboxylic acidic groups susceptible to create H-bonding networks in metal phosphonates with potential applications as proton conductors.

The tripodal ligand amino-*tris*-(methylenephosphonic) acid H_6AMP, characterized by the presence of three phosphonic groups in the same organic linker, has been used in this work as a representative example of tri-phosphonate ligands.
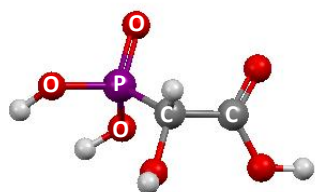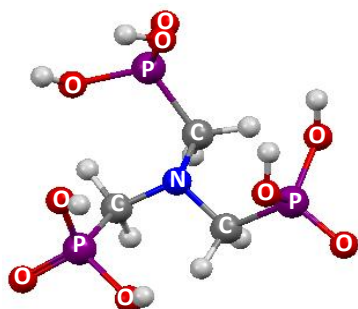
(a) **HPAA**

(b) **PiPhtA**

(c) **H₆AMP**

Figure 4.1. Molecular structures of functional phosphonic acids used as building blocks of metal phosphonates. (a) *R,S* 2-hydroxyphosphonoacetic acid (HPAA), (b) 5-(dihydroxyphosphoryl)isophthalic acid (PiPhtA), (c) amino-*tris*-(methylenephosphonic) acid (H₆AMP).

An ample selection of mono-, di- and trivalent metal ions has been chosen to study the structural and properties variability of the resulting metal phosphonate solids. The selected metal ions were: Li^+, Na^+, K^+, Cs^+, Ca^{2+}, Mg^{2+}, Co^{2+}, Zn^{2+}, Fe^{2+}, and rare earth ions as representative trivalent metal ions. The latter were preferentially chosen by their rich coordination chemistry and ability to confer multifunctionality in organo-inorganic frameworks, such as photoluminescence, proton conductivity and catalysis.

The main techniques employed for the chemical and structural characterization of these solids have been: X-ray diffraction, thermogravimetric-thermodifferential analysis (TGA-DTA), spectroscopy techniques (IR, NMR, UV-VIS, Mössbauer) and X-ray photoelectron spectroscopy (XPS). The photocatalytic activity and proton conductivity were monitored by Total Organic Carbon (TOC) analysis and impedance spectroscopy, respectively.

4.1. METAL *R,S* 2-HYDROXYPHOSPHONOACETATES.

Alkali (Li$^+$, Na$^+$, K$^+$, and Cs$^+$) and iron (II) derivatives of HPAA have been prepared and studied in this work. Alkaline metal compounds present a rich variety of structural architectures and topologies, from one-dimensional (1D) to three-dimensional (3D). A peculiar behaviour observed for these alkali metal hydroxyphosphonoacetates is the gradual variation in the dimensionality of the framework according to the size of the alkali metal ion. The structure−proton conductivity relationships will be discussed on the basis of the possible pathways involved in proton conduction processes.

On the other hand, Fe[HO$_3$PCH(OH)COO]·2H$_2$O, *FeHPAA*, is a layered material already reported in literature *(Fu et al., 2005a)*. Here, this compound has been studied as an example of a multifunctional material exhibiting both photocatalytic and proton conduction capabilities *per se* and upon derivatization by soft treatments.

In the next sections, the crystal structures as well as targeted properties for all these compounds are highlighted.

4.1.1. ALKALI-METAL HYDROXYPHOSPHONOACETATES.

4.1.1.1 SYNTHESIS AND STRUCTURAL CHARACTERIZATION.

A family of alkali-metal ions (Li, Na, K and Cs) was isolated by combination of the racemic *R,S* 2-hydroxyphosphonoacetic acid [$HOOCCH(OH)PO_3H_2$, HPAA] with the corresponding alkaline hydroxides (LiOH and KOH) or metal salt (NaCl and CsCl). All of them were isolated by slow crystallization at room temperature in water or water/DFM mixtures and pH ∼ 2 and using an excess of the alkaline metal [**a#3**, Bazaga-García et al., *Chem. Mater.* **2015**, *27*, 424-435]. The stoichiometries obtained for the different solids are given in Table 4.1 together with the dimensionality of the resulting frameworks.

Table 4.1. Stoichiometry and structural architecture of alkali metal-HPAA derivatives as reported in this work.

Stoichiometry	Acronym	Structure
$Li_3(OOCCH(OH)PO_3)(H_2O)_4 \cdot H_2O$	Li-HPAA	1D
$Na_2(OOCCH(OH)PO_3H)(H_2O)_4$	Na-HPAA	2D
$K_2(OOCCH(OH)PO_3H)(H_2O)_2$	K-HPAA	3D
$Cs(HOOCCH(OH)PO_3H)$	Cs-HPAA	3D

The crystal structure of alkali-metal derivatives was obtained from single crystals data, except for **Li-HPAA**, constituted by small thin needles. Its structure was solved following an *ab initio* methodology from laboratory X-ray powder diffraction.

From a structural point of view, alkali metal carboxyphosphonates show wide coordination chemistry, with 4- and 5- coordinated environments for Li$^+$ derivative up to 9-coordinated environment for Cs$^+$ (see Figure 4.2).
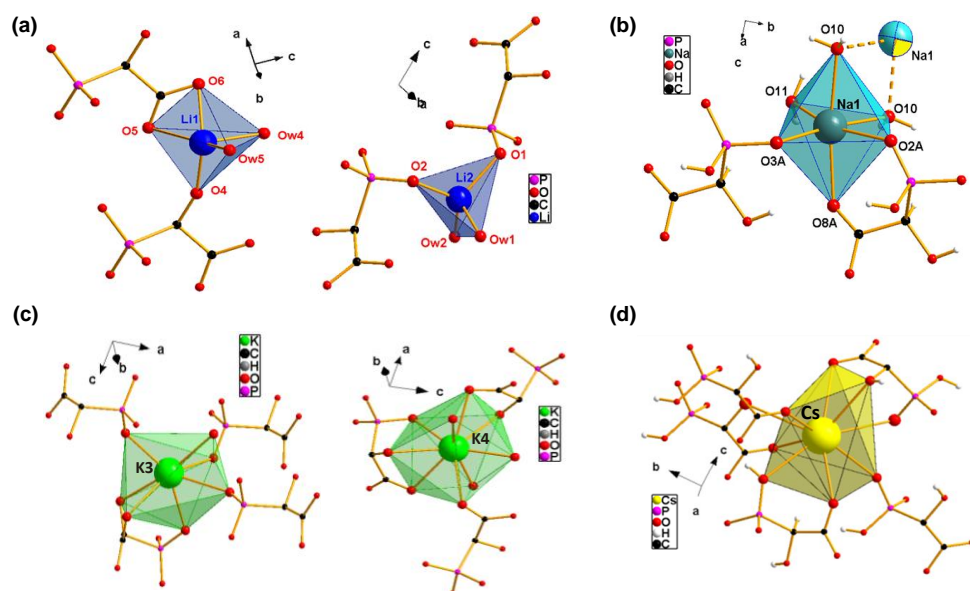

Figure 4.2. Selected coordination environments for **M-HPAA** compounds: Li (a), Na (b), K (c) and Cs (d). Reprinted with permission from (**a#3**, Bazaga-García et al., *Chem. Mater.* **2015**, *27*, 424-435). Copyright (**2015**) American Chemical Society.

The different protonation degree of the ligand together with the presence of water molecules for the lighter ions make possible this variability of coordination modes what leads to solids with different crystal structures, from 1D (**Li-HPAA**) through pillared-layered (**Na-HPAA**) to 3D (**K-HPAA** and **Cs-HPAA**). So, **Li-HPAA** shows a 1D framework consisting in linear ribbon or "slabs" built up from Li$^+$ ions in three different coordination environments (4-, 5-, and 6-coordinated) and deprotonated HPAA^{3-} ligand (see Figures 4.3a and 4.3b-d).

In its structure there are five water molecules, four of which are coordinated to Li$^+$ ions and one is situated in the lattice and positioned between the 1D slabs, apparently stabilizing the supramolecular structure through four hydrogen bonds.
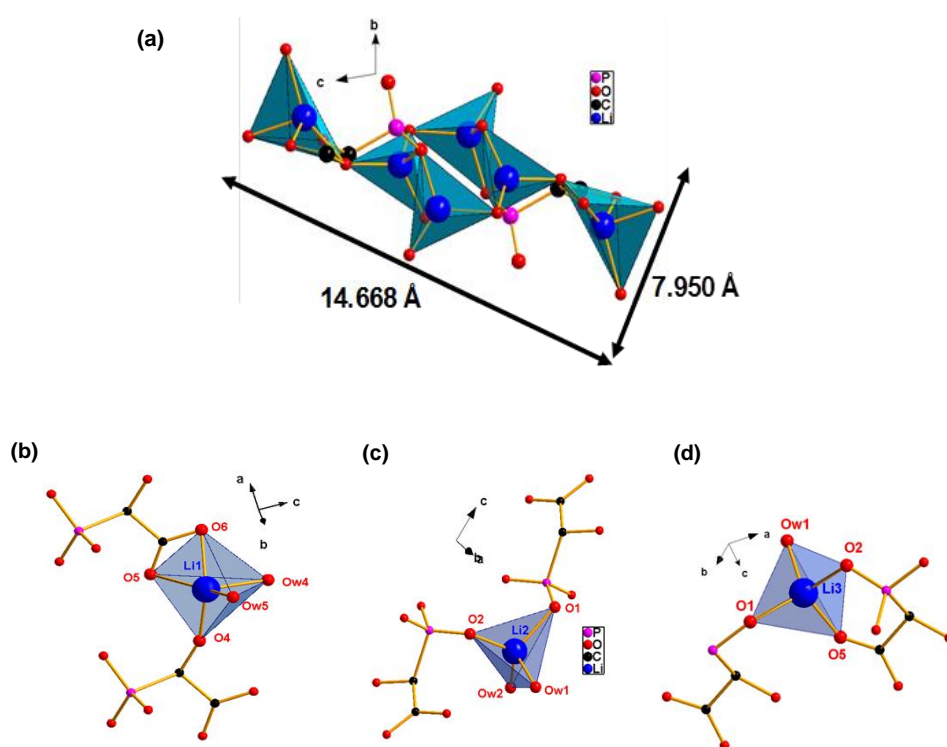

Figure 4.3. (a) View of a portion of the "slab" in the structure of [Li$_3$(OOCCH(OH)PO$_3$)(H$_2$O)$_4$]·H$_2$O, **Li-HPAA**. (b), (c) and (d) different views of the coordination environment of the three Li$^+$. Reprinted with permission from (**a#3**, Bazaga-García et al., *Chem. Mater*. **2015**, *27*, 424-435). Copyright (**2015**) American Chemical Society.

Na-HPAA exhibits a pillared layered structure (Figure 4.4c) formed by the intersection (at an angle of 71.3°) of two layers built up from NaO$_6$ octahedra and HPAA^{2-} ligands which in turn are linked together via water molecules (see Figure 4.4b).
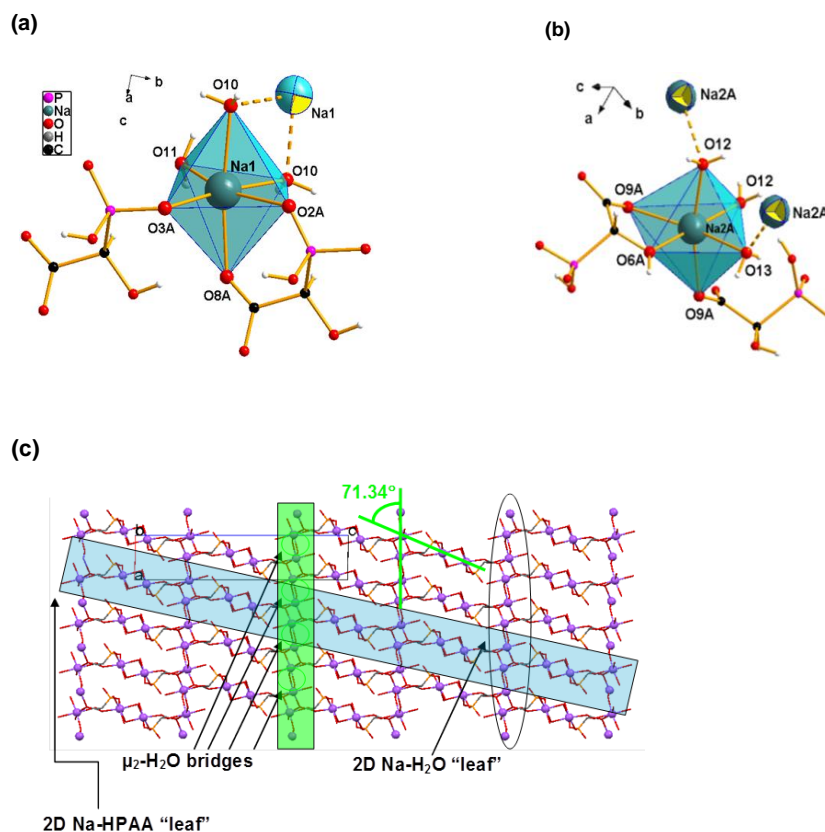
Figure 4.4. (a) And (b) coordination environments of the two Na$^+$ cations in the structure of [Na$_2$(OOCCH(OH)PO$_3$H)(H$_2$O)$_4$] (***Na-HPAA***). Bonds that bridge neighboring Na$^+$ cations are drawn with dotted lines. (c) 3D structure view of ***Na-HPAA*** viewed down the *a*-axis. Reprinted with permission from (**a#3**, Bazaga-García et al., *Chem. Mater.* **2015**, *27*, 424-435). Copyright (**2015**) American Chemical Society.

There are two Na$^+$ ions (Na1 and Na2) and one HPAA^{2-} ligand in the asymmetric unit of this structure. It is noticed that both HPAA ligand and Na2 atom are disordered over two alternatives metal atom positions, Na2a and Na2b, with different occupancy factors. This disorder can be considered as the result of an enantiomeric excess of the ligand ($\sim$ 20%) in the structure. Furthermore, the coordination mode of the bis-deprotonated HPAA^{2-} to Na$^+$ ions resembles that found in other Ca^{2+} derivatives *(Demadis et al., 2010b and Colodrero et al.,*

2011). So, HPAA^{2-} ligand is coordinated through its phosphonate moiety with two distorted Na2O$_6$ octahedra, while the P−OH group remains uncoordinated. Its carboxylate and hydroxyl groups are also used to bridge two other Na1O$_6$ distorted octahedral.

K-HPAA and *Cs-HPAA* present intricate 3D frameworks and both of them crystallize without lattice water (Figure 4.5). The crystal structure of *K-HPAA* contains four K$^+$ ions, (K$^+$ are 7- and 9-coordinated), and two doubly deprotonated HPAA^{2-} ligands (Figure 4.2c). This contrasts with *Cs-HPAA* in which there is only an independent Cs$^+$ cation (9-coordinated) and HPAA$^-$ ligand with a phosphonate group monodeprotonated (-PO$_3$H$^-$), and a carboxy group protonated (-COOH) (Figure 4.2d). The coordination of Cs centers creates a 3D structure when strong H-bonding networks even in absence of water.

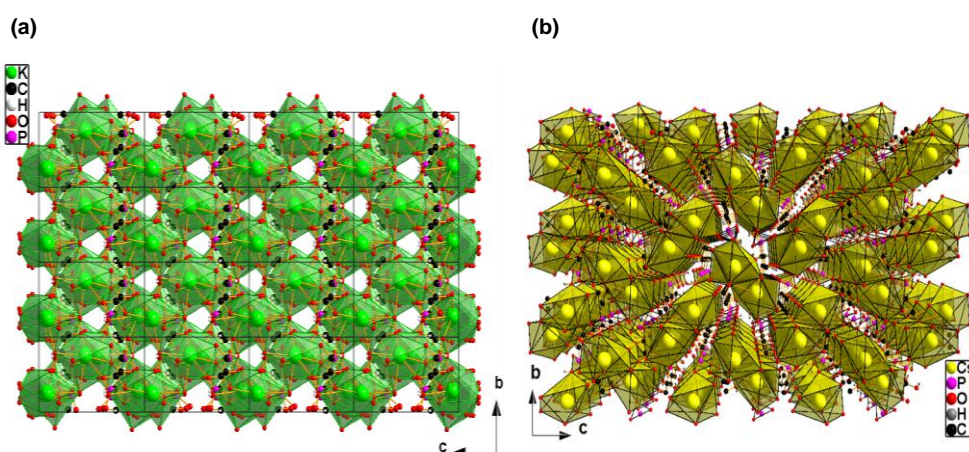(a)   (b)

Figure 4.5. 3D structures for (a) K$_2$(OOCCH(OH)PO$_3$H)(H$_2$O)$_2$ (*K-HPAA*), and (b) [Cs(HOOCCH(OH)PO$_3$H)] (*Cs-HPAA*), viewed along the *a*-axis. Reprinted with permission from (**a#3**, Bazaga-García et al., *Chem. Mater.* **2015**, *27*, 424-435). Copyright (**2015**) American Chemical Society.

The gradual increase in dimensionality observed for **M-HPAA** compounds is correlated with the alkali metal ion radius and, hence, the average M-O bond distance. This behavior has also been reported for alkaline-earth metal ions with HPAA or *(Clearfield and Demadis, 2012)* AMP linkers *(Demadis et al., 2004, 2005 and 2006a-b).*

Although there are many metal derivatives of *R,S*-HPAA reported, all of them contain both *S* and *R* isomers in their crystal structure. **M-HPAA** family constitutes a rare example of spontaneous enantiomeric enrichment from a racemic mixture. Thus, both enantiomers of the ligand are incorporated to the crystal structures of **Li-HPAA***,* **Na-HPAA** and **K-HPAA**. However, **Cs-HPAA** crystallizes in a chiral space group and only contains the *S*-HPAA ligand. In order to corroborate the chirality proposed, this compound was investigated in solution by Electronic Circular Dichroism (ECD) and computational methods. As shown in Figure 4.6 the ECD spectrum of the solution of **Cs-HPAA** exhibits a negative dichroic signal at 210 nm, that is absent in the reference samples (*R,S*-HPAA solution and *R,S*-CsHPAA obtained by fast precipitation). In addition, the spectrum of **Cs-HPAA** calculated by using crystallographic data without further optimization agrees well with that obtained experimentally, leading a negative signal between 200-300 nm and confirming an enantiomeric excess in the sample obtained by slow crystallization.
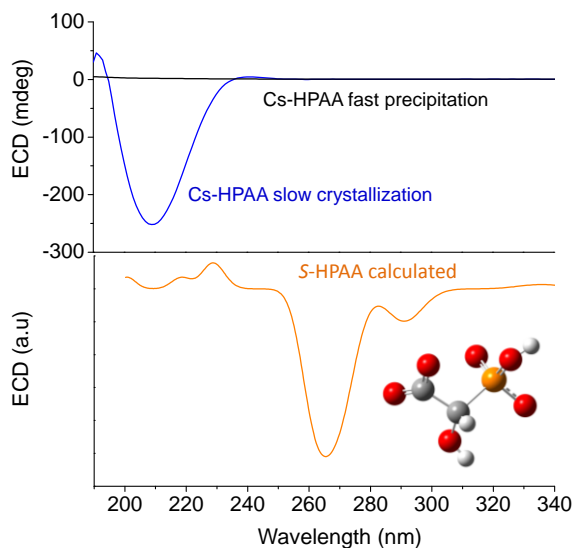
Figure 4.6. Electronic Circular Dichroism (ECD) spectra for ***Cs-HPAA*** prepared by slow (blue line) and fast crystallization (black line), and the calculated dichroic spectrum for the *S*-HPAA enantiomer. Reprinted with permission from (**a#3**, Bazaga-García et al., *Chem. Mater.* **2015**, *27*, 424-435). Copyright (**2015**) American Chemical Society.

4.1.1.2. PROTON CONDUCTIVITY.

The formation of strong hydrogen-bonded networks in all these structures, even if water is absent, prompted us to evaluate the proton conductivity of these materials. Measurements were carried out at different temperatures (from 10 ºC to 24 ºC) and 98% relative humidity (RH) using porous C electrodes. Figure 4.7 depicts the complex impedance spectra at different temperatures and 98% of RH. As can be seen in Figure 4.7, the inclination of the spike and the associated capacitance ($\sim$1 μF) suggest a partial-blocking electrode response what it is characteristic of ionic species.

All compounds show proton conductivity at 24 ºC and 98% of RH, in the range of 3.5×10^{-5} S·cm^{-1} (***Cs-HPAA***) to 5.6×10^{-3} S·cm^{-1} (***Na-HPAA***). The proton conductivity for ***Na-HPAA*** is larger than those

reported for other M^{3+}-HPAA·nH_2O (M^{3+} = La, Gd and n=15-16) recently reported and highly hydrated, for instance GdHPAA (3.2×10^{-4} S·cm^{-1} at 21 ºC and 98% of RH) *(Colodrero et al., 2012c)*, but similar to those of some tetraphosphonates of Mg *(Colodrero et al., 2012b)*, and Ln derivatives *(Colodrero et al., 2012a).*
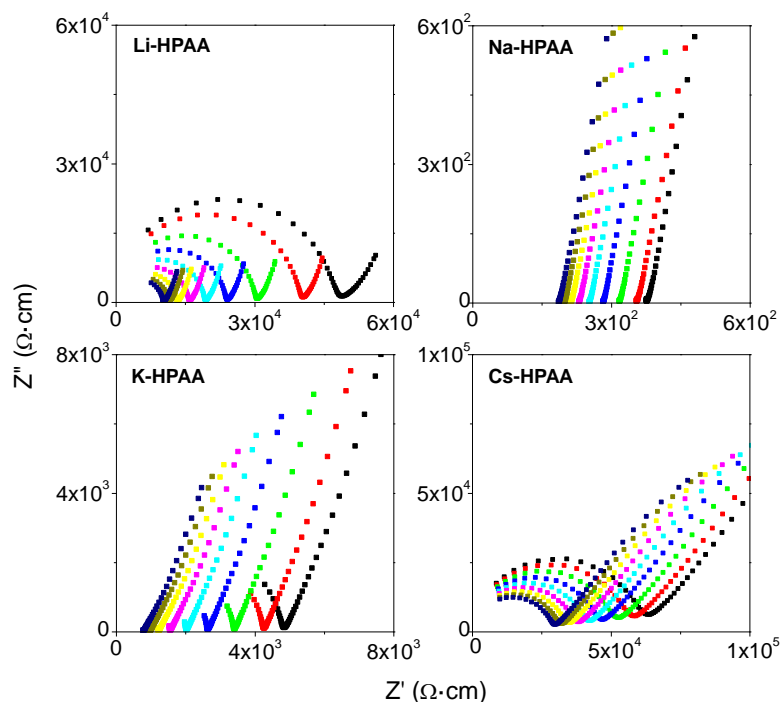

Figure 4.7. Plot of complex impedance plane for the as-synthesized (***M-HPAA*** ; M=Li, Na, K and Cs) compounds at 98% relative humidity: 10 ºC (black), 11 ºC (red), 12 ºC (green), 14ºC (blue), 16 ºC (cyan), 18 ºC(magenta), 20 ºC (yellow), 22 ºC (dark yellow) and 24 ºC (navy). Reprinted with permission from (**a#3**, Bazaga-García et al., *Chem. Mater.* **2015**, *27*, 424-435). Copyright (**2015**) American Chemical Society.

The possibility of alkali ion conduction was ruled out by using, for the highest conductive material, ***Na-HPAA***, nonblocking electrodes to protons, under 5% H_2-Ar and 100% H_2 gas flows. Figure 4.8 shows only one semicircle values due to electrode polarization between 3 and

0.1 mF·cm^{-1}, for 5% H$_2$-Ar and 100% H$_2$ gas flow, respectively. The absence of the spike indicates that the material shows a purely resistive behaviour, and, therefore, it is exclusively a proton conductor.
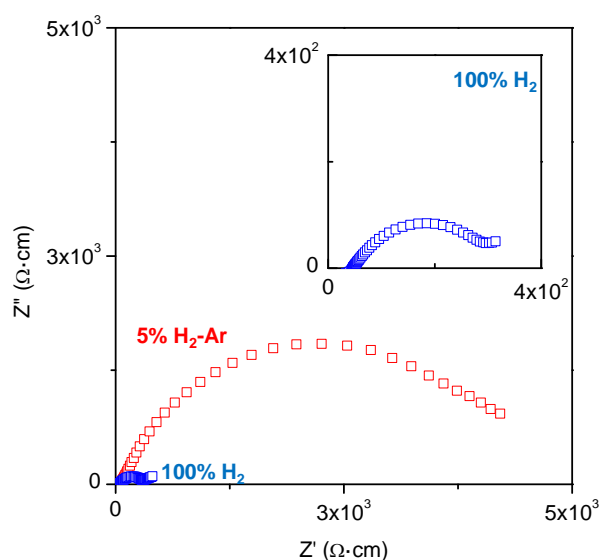

Figure 4.8. Plots of complex impedance plane for the as-synthesized *Na-HPAA* equilibrated at 24 °C and 98% RH, in flowing 5% H$_2$−Ar and 100% H$_2$. Measurements were performed using Pt−C gas diffusion electrodes, Reprinted with permission from (**a#3**, Bazaga-García et al., *Chem. Mater.* **2015**, *27*, 424-435). Copyright (**2015**) American Chemical Society.

From the Arrhenius plots, activation energy (Ea) values were calculated for the proton conduction process in the M-HPAA series (Figure 4.9a). Ea values for *Na-HPAA* (0.39 eV) and *Cs-HPAA* (0.40 eV) are within the characteristic range of a Grothuss transfer mechanism via water molecules (0.1 - 0.4 eV) *(Colomban, et al., 1992)*. On the contrary, *Li-HPAA* and *K-HPAA* present Ea values (0.84 eV and 0.98 eV, respectively) typical of a vehicular mechanism. These differences in proton conduction mechanisms are attributed to the different roles played by water molecules and/or proton transfer

pathways (see Figure 4.9b). So, Na-derivative containing both lattice and bound water and having a certain structural disorder has been demonstrated to exhibit a high proton conductivity of 5.6 × 10^{-3} S·cm^{-1}. **Cs-HPAA** exhibits a certain conductivity (3.5 × 10^{-5} S·cm^{-1}) due to strong H-bond interactions between neighbouring -P-OH and -COOH groups, as well as the presence of equidistant shared protons between phosphonate and carboxylate groups, which create short proton transport pathways. **K-HPAA** has intermediate conductivity value (1.3 × 10^{-3} S·cm^{-1}) as well as structural characteristics and water content between Na- and Cs-derivatives. **Li-HPAA** shows lower conductivity (1.1 × 10^{-4} S·cm^{-1}) than Na- and K-derivatives, what can mainly be due to the absence of acidic groups and the low mobility of strongly coordinated water in the former.
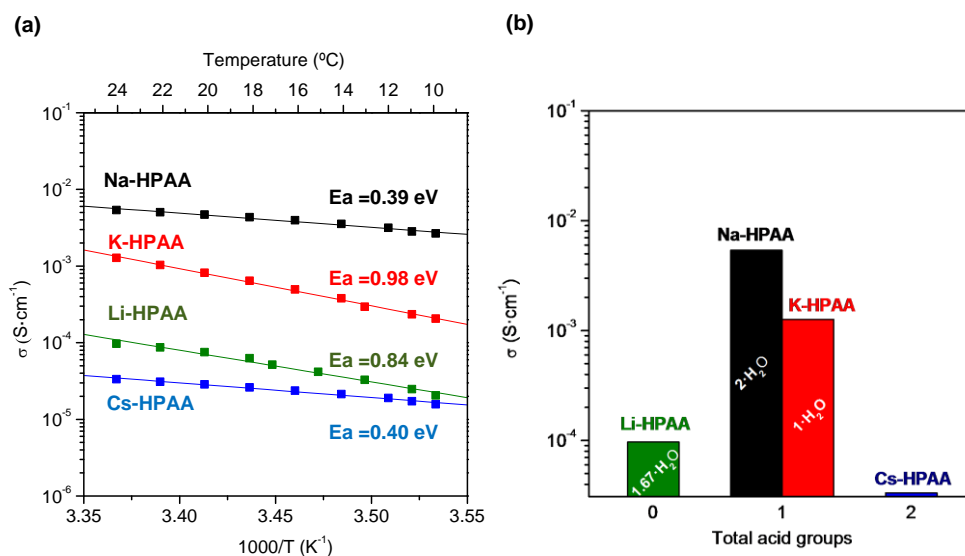

Figure 4.9. (a) Plot of log σ versus 1000/T for **M-HPAA** (M= Li, Na, K and Cs) series as synthesized at differences temperatures and 98% of RH. (b) Plot of log σ versus number of total acid groups for **M-HPAA** (M= Li, Na, K and Cs) series as synthesized at 24 ºC and 98% of RH. Reprinted with permission from (**a#3**, Bazaga-García et al., *Chem. Mater.* **2015**, *27*, 424-435). Copyright (**2015**) American Chemical Society.

However, the conductivity value determined for it is very close to those reported for other 1D divalent tetraphosphonates, in which a vehicular mechanism is also implied *(c#1, Colodrero et al., 2013; Feyand et al., 2013)*. Significantly, the protonation degree of the ligand, which increases from Li, through Na and K, to Cs is not directly correlated to the conductivity value.

It must be underlined that Li-, K- and **Cs-HPAA** materials do no experiment neither structural nor water content changes after measuring proton conductivities, according to the X-ray diffraction and TG analyses. However, **Na-HPAA** displays a significant water gain without important changes in its powder pattern. This fact suggests that its pillared structure can still host more water molecules keeping the basic pillared framework, behaviour that was also corroborated by water adsorption-desorption isotherms (Figure 4.10). Moreover, the lack of reversibility in the sorption/desorption profile indicates that the moisture (up to 1 H_2O molecule) is absorbed inside the structure rather than being adsorbed on the surface of the material.
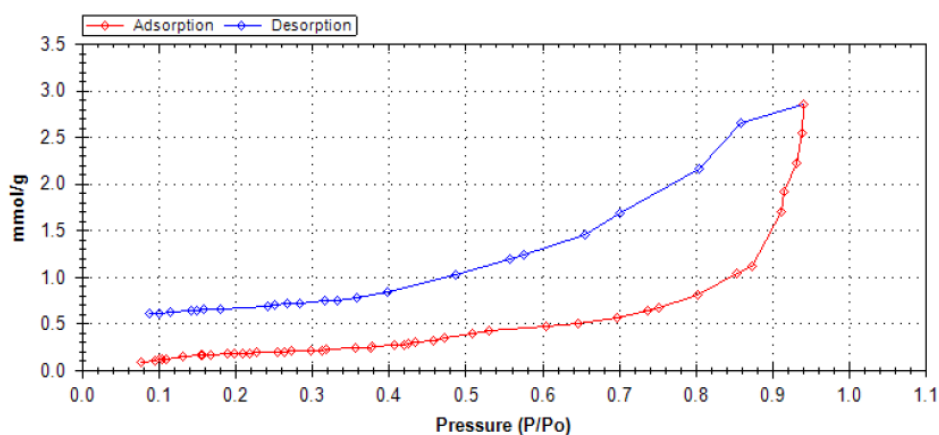

Figure 4.10. Water vapour adsorption-desorption isotherm for **Na-HPAA** at 24 °C. Reprinted with permission from (**a#3**, Bazaga-García et al., *Chem. Mater.* **2015**, *27*, 424-435). Copyright (**2015**) American Chemical Society.

4.1.2. IRON(II) *R,S* 2-HYDROXYPHOSPHONOACETATES.

As indicated in section 1.1.4.1, iron(II) salts have been successfully used in Fenton and photo-Fenton reactions to generate hydroxyl radicals, which are highly oxidant species capable to mineralize numerous organic compounds. These reactions have been proven more efficient than other photocatalytic processes, but require low pHs and removing iron from water.

In this section we propose a double use of Fe(II) *R,S* 2-hydroxyphosphonoacetates, $Fe[HO_3PCH(OH)CO_2]\cdot 2H_2O$ (***FeHPAA***): (1) as heterogeneous photocatalyst in photo-Fenton reactions; and (2) as proton conductors with tuneable conductivity upon exposure to ammonia vapours. So, it will be shown that FeHPAA can be considered as an example of a multifunctional compound displaying both, photocatalytic and proton conductivity properties, and the latter increased by soft structural modifications. Some of these results have already been published [**a#1**, Bazaga-García et al., *J. Phys. Chem. C* **2012**, 116, 14526-14533].

4.1.2.1. SYNTHESIS OF Fe(HO₃PCH(OH)COO)·2H₂O, (*FeHPAA*).

$Fe[HO_3PCH(OH)CO_2]\cdot 2H_2O$, ***FeHPAA***, was firstly reported by Fu et. al (2005a). It is isostructural with other layered M(II)-HPAA·2H₂O, (M= Mg, Mn, Fe, Co and Zn) compounds, *(Colodrero et al., 2010; Fu et al., 2005a)* which structures were described in section 1.1.2.2. Iron(II) compound was chosen due to its potential photo-Fenton properties as well as other characteristic of this phosphonic acid such as its wide availability, its chemical stability, low carbon content, non-toxic intermediates, and low cost.

FeHPAA was synthesized by hydrothermal method according to literature procedure. *(Fu et al., 2005a)*. This method uses a mixture of $FeSO_4 \cdot 7H_2O$, NaF, HPAA solution and acetic acid as reagents. The final solution is transferred to a Teflon-lined autoclave and heated to 140 ºC for four days (pH ~ 3).

The synthetic procedure was simplified in order to remove unnecessary additives, such as NaF and acetic acid, and to decrease time and temperature of reaction. The established synthesis conditions were:

(a) Mixture of $FeSO_4 \cdot 7H_2O$, NaF, HPAA solution and acetic acid (*FeHPAA-2*).

(b) Mixture of $FeSO_4 \cdot 7H_2O$ and HPAA solution (*FeHPAA-3*).

(c) Mixture of $FeSO_4 \cdot 7H_2O$, HPAA solution and acetic acid (*FeHPAA-4*).

Figure 4.11 shows the XRPD patterns of the samples prepared at the different synthesis conditions previously indicated and compared to the pattern simulated from single crystal data (CCDC nº 285712). As can be seen, all powder patterns agree well with the reference material. Therefore, hereafter, the synthetic route was modified conveniently by refluxing the reagents for 48 h without adding NaF or acetic acid. Nevertheless, the highest crystallinity was obtained for the solid prepared under hydrothermal conditions.
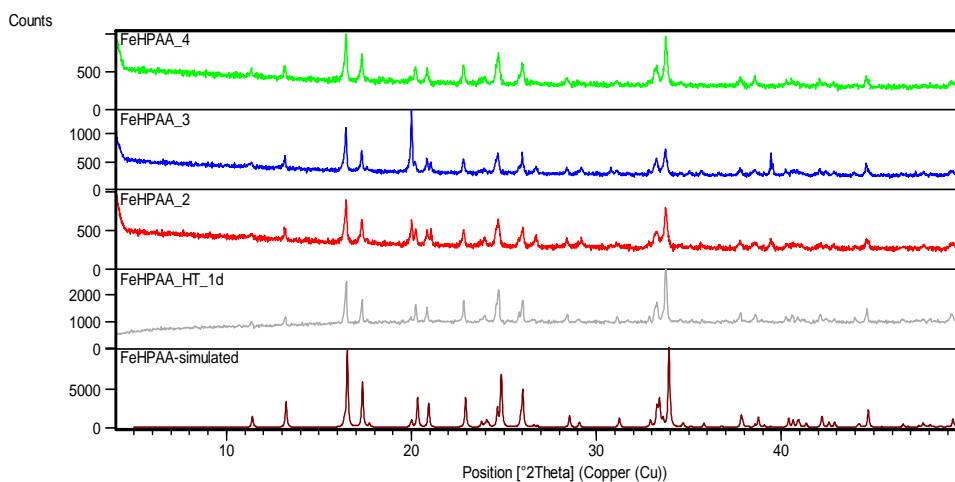
Figure 4.11. Comparison of the powder X-ray diffraction patterns (XRPD) of samples obtained under reflux (*FeHPAA-2*, *FeHPAA-3* and *FeHPAA-4*) or hydrothermally (140 ºC, 1 day) (*FeHPAA_HT-1d)* with that simulated for a single crystal of the same material (*FeHPAA*, CCDC nº 285712).

On the other hand, the Mössbauer effect study (Figure 4.12) reveals that the iron local environments correspond to Fe^{2+} in all bulk samples, including a sample recovered after running the phenol photocatalytic test. This indicates that the oxidation state of iron is preserved as Fe(II), even though highly oxidant species, as OH radicals were formed in solution upon phenol photodegradation, as it will be discussed later. Hence, FeHPAA behaves as a true photocatalyst in photo-Fenton reactions.
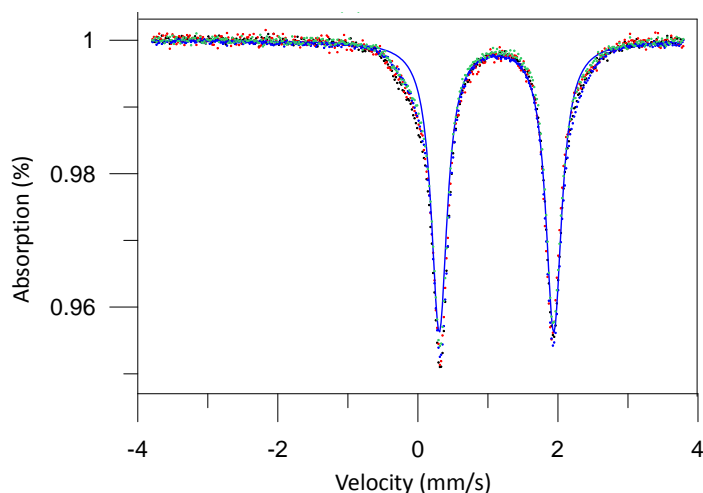
Figure 4.12. Mössbauer absorption spectra for *FeHPAA* at room temperature: (black) *FeHPAA_HT-1d* as-synthesized; (red) *FeHPAA_HT-1d* as-synthesized after a photocatalytic test; (green) *FeHPAA-3* as-synthesized and (blue) *FeHPAA-4* as-synthesized.

Additionally, for *FeHPAA* obtained hydrothermally, the effect of milling (vibratory) on the photocatalytic properties was also studied. Figure 4.13 shows the SEM images corresponding to different milling times (0, 4 and 6 h). As it is observed, the use of 4 h of vibratory milling significantly reduced the initial average size of the particles (30 μm) to ∼10 μm, after 4 h, and lower than 2 μm after 6 h. The milling does not affect to the crystal structure as shown in Figure 4.14 (intermediate), but increases considerably the surface area, from 0.8 to 16.9 m^2/g after 4 hours milling. For sample synthesized under refluxing, SEM images show an initial average size of lower than 6 μm, closed to those sizes corresponding to the sample prepared hydrothermally and milled for 4 h.
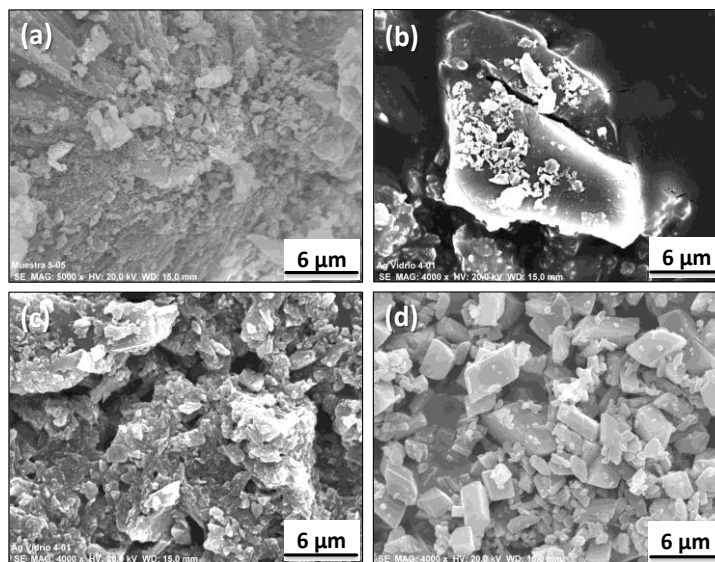
Figure 4.13. Selected SEM images for *FeHPAA* (a) as-synthesized, (b) after 4 h and (c) after 6 h of milling; and (d) obtained by refluxing.
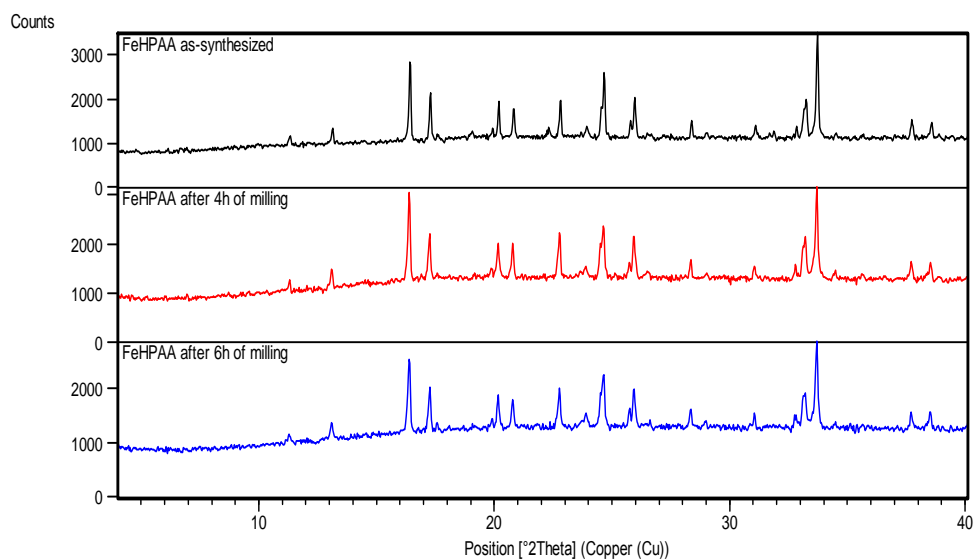

Figure 4.14. XRPD patterns for the *FeHPAA* at different milling times.

On the other hand, the UV-vis spectra (Figure 4.15) for the sample milled exhibits a substantial widening of the absorbance at the used UVA wavelength region, as compared with the TiO_2 and ***FeHPAA*** as-synthesized spectra what may increase the photocatalytic activity of the compound.
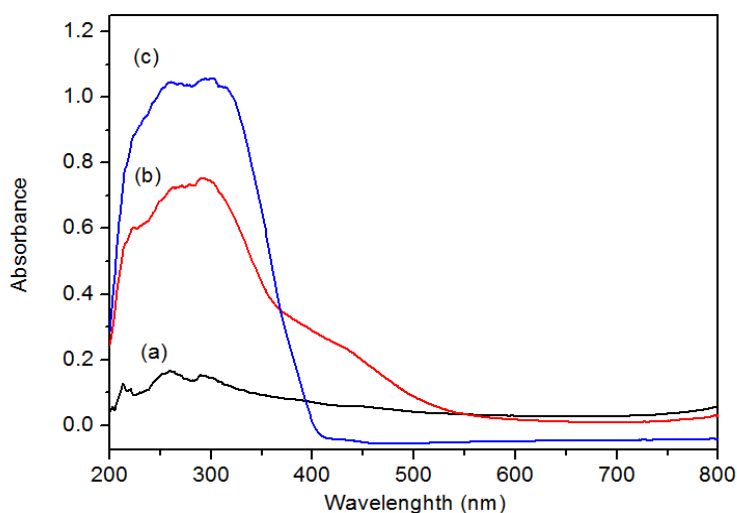

Figure 4.15. UV-vis spectra for 150 mg of the catalysts, mixed with 350 mg of BaSO4: (a) as-synthesized ***FeHPAA***, (b) catalyst after 4 h of vibratory milling of as-synthesized FeHPAA and (c) TiO_2 (Degussa-P25). Reprinted with permission from (**a#1**, Bazaga-García et al., *J. Phys. Chem. C* **2012**, *116*, 14526-14533). Copyright (**2012**), American Chemical Society.

4.1.2.2. PHOTOCATALYTIC MINERALIZATION OF PHENOL

We have undertaken the study of the photocatalytic behaviour of ***FeHPAA*** using the degradation of phenol as a standard probe of monitoring pollutant removal *(Wang, et al., 2014a; Hasan and Jhung, 2015).*

In the preliminary photocatalytic study, the stability of the ligand HPAA in solution was analysed under UVA light and in the presence of H_2O_2. As it is shown in Figure 4.16, the ligand HPAA is stable during

the first 30 min, but at 80 min of irradiation, about 50% of the initial amount is mineralized. However, when forming part of *FeHPAA*, no mineralization was detected during the whole exposure time to UVA irradiation.
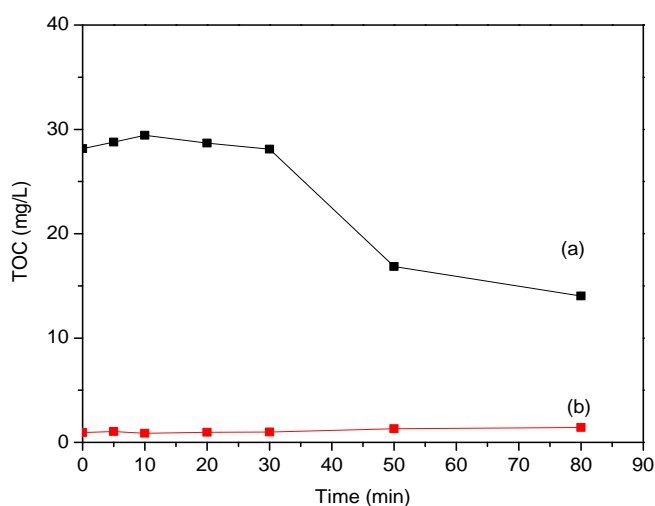
The photoactivity of *FeHPAA* was initially studied using the following conditions: [Phenol] = 50 mg/L; [H_2O_2] = 250 mg/L (stoichiometry amount for the full mineralization of phenol, lower values diminished the efficiency of mineralization); pH_0=4.0 (no adjusted); and [FeHPAA] = 220 mg/L. The same conditions were established without catalyst and using a well-known TiO_2 catalyst (P25 from Degussa) for the sake of comparison (see Figure 4.17). It can be seen that phenol undergo only a small mineralization in absence of the catalyst; however, when the as-prepared catalyst was present, phenol has fully

reacted in 50 min and TOC removal was increased with about 30% of TOC being removed after 80 min, see Figure 4.17 (top).
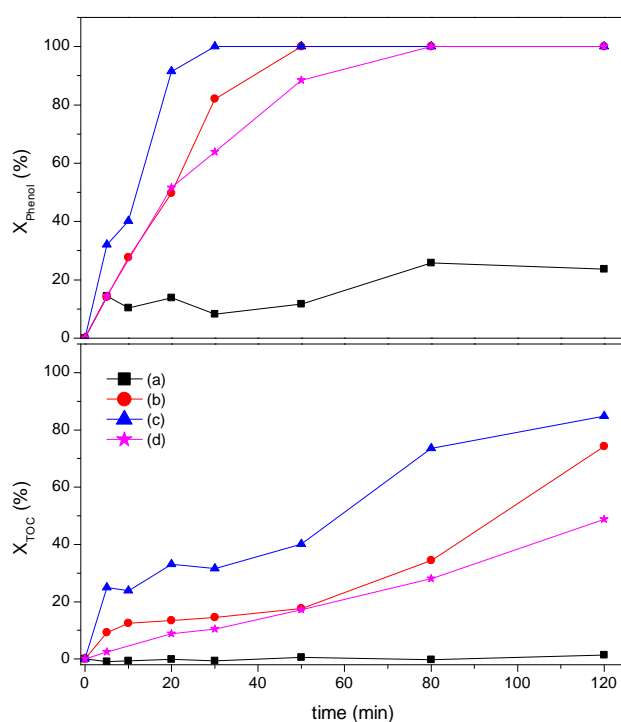

Figure 4.17. Time evolution plot of phenol (top) and TOC (bottom) conversions under UVA irradiation: (a) without catalyst, (b) with as-prepared *FeHPAA* catalyst, (c) with as-prepared FeHPAA catalyst previously activated by UVA irradiation for 30 min, and (d) with standard TiO$_2$ catalyst (Degussa-P25) under exactly the same conditions. Reprinted with permission from (**a#1**, Bazaga-García et al., *J. Phys. Chem. C* **2012**, *116*, 14526-14533). Copyright (**2012**), American Chemical Society.

Furthermore, the efficiency was improved when the catalyst was subjected to a pretreatment with UVA radiation and 50 mg/L of H$_2$O$_2$ for 30 min, in the absence of phenol. After pretreatment, the photocatalytic test indicated that the TOC removal reached to 75% at 80 min of irradiation, see Figure 4.17 (bottom). This activity was much higher than that displayed by the standard photocatalyst TiO$_2$.

In order to establish the optimum catalyst concentration, the phenol photodegradation and mineralization were studied with different loads of the catalyst (220, 500 and 700 mg/L) and at different values of initial pH (3.5, 4, 5 and 6) using the pre-activated catalyst under UVA radiation. The evolutions of the TOC removal with these two variables are given in Figure 4.18 and 4.19, respectively. Figure 4.18 shows larger conversions for higher loadings of the catalyst in both the phenol degradation and TOC removal suggesting that the reaction rate is related to the amount of sites of iron exposed to light radiation. About 90% of phenol mineralization was achieved at 80 minutes for catalyst loading of 700 mg/L at initial pH~4 under UVA radiation. On the other hand, Figure 4.19, indicates that independently of the initial pH similar TOC conversions were reached.
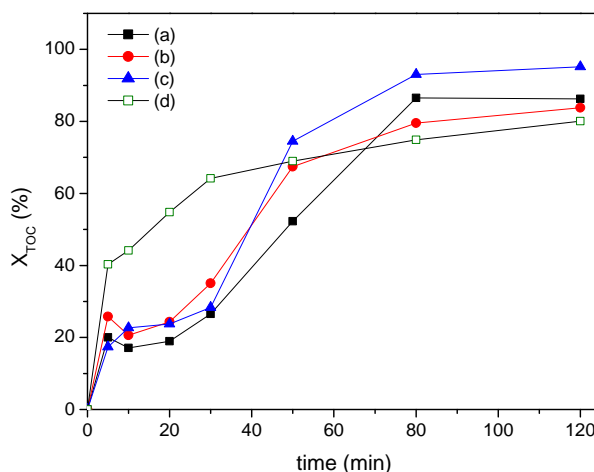

Figure 4.18. Time evolution of TOC conversions under contents of as-synthesized FeHPAA catalyst: (a) 220, (b) 500, and (c) 700 mg/L, and (d) a test in homogeneous conditions, 3 ppm of Fe. Reprinted with permission from (**a#1**, Bazaga-García et al., *J. Phys. Chem. C* **2012**, *116*, 14526-14533). Copyright (**2012**), American Chemical Society.
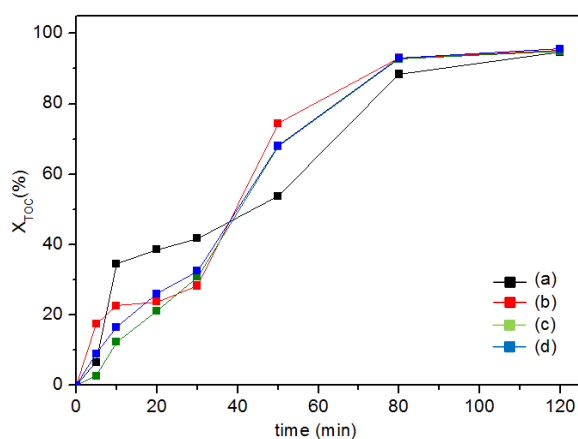
Figure 4.19. Time evolution of the TOC conversion at different initial pH values: (a) pH=3.5, (b) pH=4.0; (c) pH=5.0; and (d) pH=6.0. Reprinted with permission from (**a#1**, Bazaga-García et al., *J. Phys. Chem. C* **2012**, *116*, 14526-14533). Copyright (**2012**), American Chemical Society.

The time-dependence pH values and the concentration of iron leached for the catalytic reaction were also stablished for different loads of catalyst (Figure 4.20a-b). As it is shown in Figure 4.20a, the tendency observed in the pH values is independent of the amount of catalyst. The initial pH ranges between 3.9 and 4.3 and drop to 3.3 during the first 30 min.

Figure 4.20. Time evolution of (a) pH and (b) total iron leached, for the photocatalytic reactions with different contents of as-synthesized FeHPAA catalyst; (a) 220 mg/L; (b) 500 mg/L; and (c) 700 mg/L and (d) without phenol. Reprinted with permission from (**a#1**, Bazaga-García et al., *J. Phys. Chem. C* **2012**, *116*, 14526-14533). Copyright (**2012**), American Chemical Society.
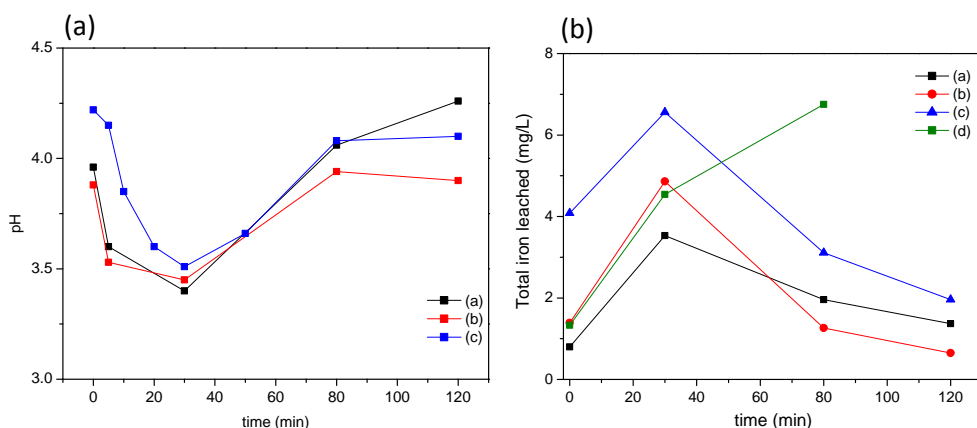
Afterward, it starts to increase up to values closed to 4.0. The drop to pH 3.3 has also been reported before *(Priya and Madras, 2006; Sivalingam et al., 2004)* and it is very likely joined to the production of acidic intermediate species for phenol degradation. The following scheme shows a general pattern of phenol degradation *(Liu, et al., 2013)* in which the main reactions are aromatic ring oxidation (hydroquinone, catechol), as it was observed by HPLC-MS (Figure 4.21), and ring cleavage compounds (f.i. oxalic acid or formic acid). Finally, low carbon content carboxylic acids are formed at the end of the photocatalytic reaction, although in our study also phosphonic $(HPO(OH)_2)$ and orthophosphoric acids were obtained in solution as byproducts of partial photodegradation of the ligand HPAA.
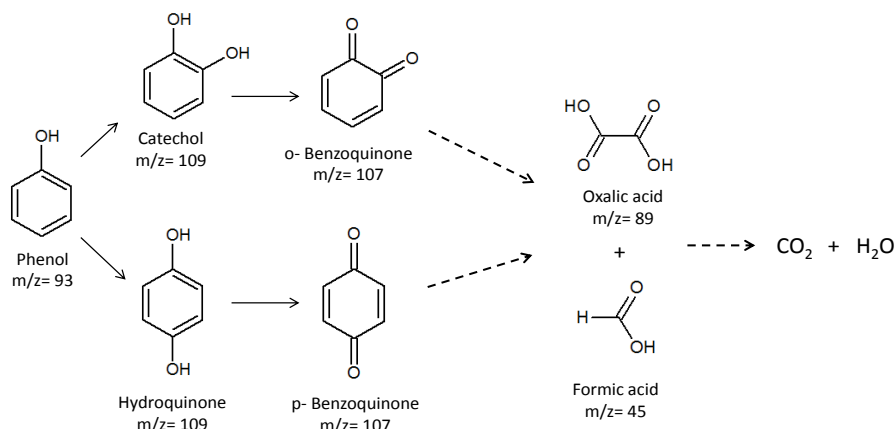
Figure 4.21. Probable mechanism for the photocatalytic degradation of phenol.

On the other hand, the evolution of lixiviated iron shows a volcano shape, as reported previously *(Adán et al., 2011; Bozzi, et al., 2004)*, that is attributed to an initial leaching, likely due to the low pH, with a subsequent re-adsorption process favours by the increment of the pH. This behaviour is quite different from that observed in the absence of phenol where a continue increment of lixiviated iron is observed (higher than 7 ppm, after 80 min). However, the amount of dissolved iron is very important. So, the photocatalytic test carried out under homogeneous conditions (3 ppm of Fe^{2+} and pH = 3.8 and other equivalent conditions) shows an important contribution to the overall phenol photo-oxidation (see Figure 4.18d). Therefore, **FeHPAA** photocatalyst can be considered as a complex liquid-solid mixed phase photocatalyst where the sustained slow delivery of iron upon reaction could be considered as an advantage in advanced photocatalytic processes.

The effect of particle size upon the photocatalytic reaction has also been analysed. The samples milled for 4h and 6h showed similar

behaviors giving the best results for phenol photodegradation in the first 50 min with a TOC conversion above 85% (Figure 4.22). However, a quick consumption of H_2O_2 take place as consequence of the small particle size of the milled *FeHPAA* samples, with no measurable content for reaction times of 50 minutes or longer. It is also important to note that total leached iron for the milled catalyst is much larger than that for *FeHPPA* as synthesized.
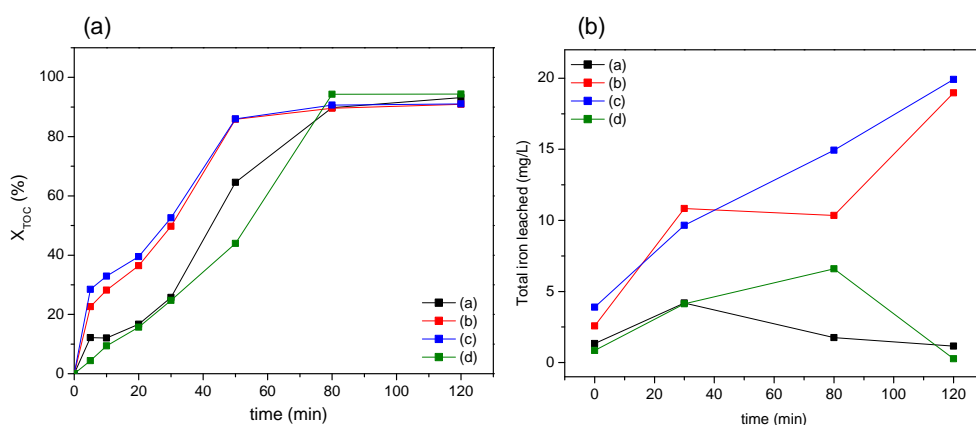
Figure 4.22. Time evolution of (a) TOC conversions and (b) total iron leached, for the photocatalytic reactions under contents of *FeHPAA* catalyst (a) as-synthesized, (b) after 4 h and (c) after 6 h of milling; and (d) as-synthesized obtained by refluxing. Reprinted with permission from (**a#1**, Bazaga-García et al., *J. Phys. Chem. C* **2012**, *116*, 14526-14533). Copyright (**2012**), American Chemical Society.

Finally, the recyclability of the *FeHPAA* catalyst was studied by running a second test cycle (see Figure 4.23). An increasing in TOC removal was found for the latter test, this effect pointing to favourable surface modifications after a first reaction cycle that improve performances in further cycles.

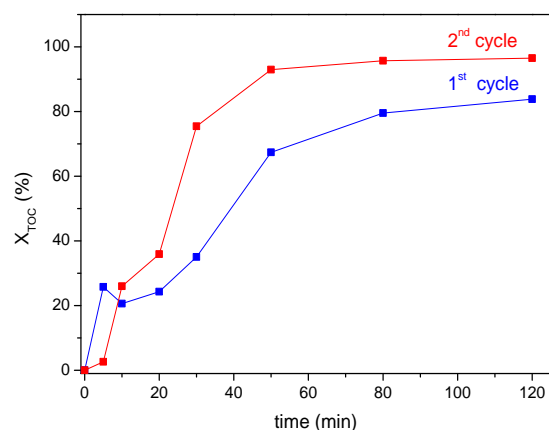**Figure 4.23.** Changes in TOC conversions for two repeated processes with *FeHPAA*. Reprinted with permission from (**a#1**, Bazaga-García et al., *J. Phys. Chem. C* **2012**, *116*, 14526-14533). Copyright (**2012**), American Chemical Society.

It must be noticed, that although the bulk structure of *FeHPAA* remains unchanged after phenol mineralization according to its powder diffraction pattern, important chemical modifications occur on the surface of the catalyst upon pre-activation under UVA and after phenol photodegradation, as revealed by X-ray photoelectron spectroscopy. So, pretreatment increased almost twofold the iron concentration on the catalyst surface, although the ratio Fe(II)/Fe(III) was roughly maintained, i.e. 60/40 (see Figure 4.24b). Furthermore, photolytic process would eventually lead to the formation of charged iron species, probably Fe(III) carboxylates, acting as initiators of the photocatalytic reaction and a main source of iron in solution, through a photo-Fenton process *(Adán et al., 2011).* Therefore, the role of UVA pre-activation is double: i) increases the surface iron concentration; and ii) generates photoactive iron species by leaching at the start of the photocatalytic reaction. Both modifications help to increase the photodegradation of phenol at early reaction times. Moreover, the reduction of particle sizes to 10 - 5 μm by milling of the sample (4 h) or by preparing the sample

by refluxing allow to increase the surface Fe(II)/Fe(III) to values closed to 2, what leads to the highest TOC conversions (Figure 4.22a).
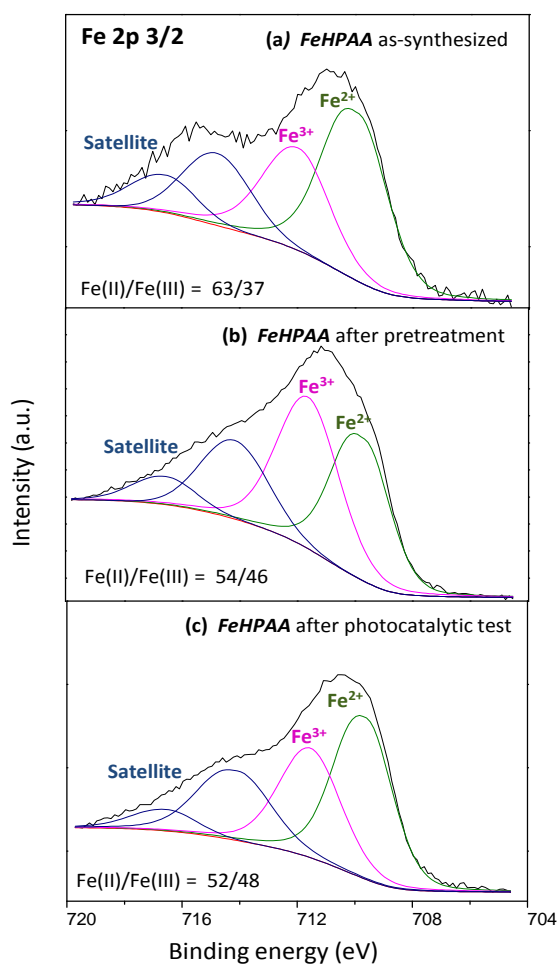
Figure 4.24. XPS Fe2p$^{3/2}$ raw data for *FeHPAA*: (a) as-synthesized; (b) as-synthesized after pre-treatment and (c) as-synthesized after a photocatalytic test. Reprinted with permission from (**a#1**, Bazaga-García et al., *J. Phys. Chem. C* **2012**, *116*, 14526-14533). Copyright (**2012**), American Chemical Society.

The O1s and Fe 2p$^{3/2}$ regions have been studied by XPS for *FeHPAA* as-synthesized after a photocatalytic test. Figure 4.25 shows

the O1s XPS spectrum that displays a main peak located at 531.3-531.4 eV that is mostly attributed to Fe–O–P and Fe–O–H type-oxygen, and possibly strongly adsorbed water. The shoulder at 532.8-533.1 eV may be assigned to oxygens belonging to both phosphonic, POH, and carboxylic, CO_2H groups. After photoreaction, (Figure 4.25, top) the area of this second component markedly decreases at the expense of the main peak, probably due to an increased presence of Fe-OH bonds on the catalyst surface. It is also remarkable the absence of segregated iron oxide in the studied catalysts (peak centrered at 530 eV).
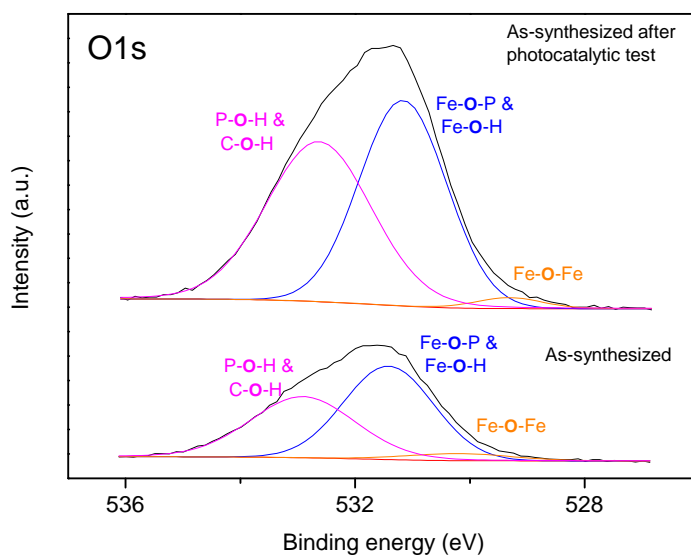
Figure 4.25. XPS O1s raw data for *FeHPAA*: (bottom) as-synthesized; (top) as-synthesized after a photocatalytic test. Reprinted by permission from American Chemical Society: **a#1**, Bazaga-García et al., *J. Phys. Chem. C* **2012**, 116, 14526-14533, copyright **2012**.

Finally, Figure 4.24 shows the XPS spectra for the Fe 2p$^{3/2}$ region corresponding to two representative samples: *FeHPAA* as synthesized (Figure 4.24a) and after photocatalytic test (Figure 4.24c).

The key finding is the higher Fe(II)/Fe(III) ratio found in the used catalyst after photoreaction. This measurement supports the idea that iron is re-adsorbed on the catalyst surface as Fe(II) species. This assumption is further confirmed by the fact that this process just starts at low H_2O_2 concentrations, i.e. at times latter than approximately 50 minutes *(Paszternak et al., 2010).*

**4.1.2.3. PROTON CONDUCTIVITY FOR *FeHPAA* AND ITS DERIVATIVES.**

The layered structure of ***FeHPAA*** is amenable for post-synthesis modifications through the adsorption of guest molecules which may impart/enhance properties for potentials applications. Based on the derivatization procedure followed with ***Ca-PiPhtA*** (see next section), a new family of ammonia-intercalated iron(II) metal phosphonates as potential candidates as proton conductors have been prepared from ***FeHPAA*** by exposing to ammonia vapours (28% aqueous NH_3) at different times (1, 5, 24 and 48 h). All samples, called ***(NH_3/H_2O)-FeHPAA***, were characterized by elemental analysis, XRPD, and impedance spectroscopy.

Table 4.2 gives the elemental analysis and the total weight losses determined by thermal analysis. Crystalline compound incorporate ammonia up to 1 mol per formula after 24 h. Longer times of ammonia exposure slightly increase the ammonia content but the solid become amorphous (Figure 4.26).

Table 4.2. Elemental analysis for selected samples *(NH₃/H₂O)-FeHPAA_xh.*

t(h)	Formula	%C Exp. Calc.	%N Exp. Calc.	%H Exp. Calc.	%Weight loss (700ºC) Exp. Calc.
0	$Fe(HO_3PCHOHCO_2)(H_2O)_{2.5}$	9.57 9.41	- -	3.13 3.16	39.75 40.81
5	$Fe(HO_3PCHOHCO_2)(H_2O)_{2.5}(NH_3)_{0.2}$	9.09 9.29	0.99 1.08	3.16 3.35	41.06 41.59
5*	$Fe(HO_3PCHOHCO_2)(H_2O)_{2.6}(NH_3)_{0.18}$	8.90 9.24	0.99 0.97	3.01 3.39	40.70 41.91
24	$Fe(HO_3PCHOHCO_2)(H_2O)_3(NH_3)$	8.24 8.54	5.05 4.98	3.92 4.30	46.50 46.29
24*	$Fe(HO_3PCHOHCO_2)(H_2O)_{3.2}(NH_3)$	8.09 8.43	4.92 4.92	3.70 4.39	48.01 46.98

* After impedance measurements.
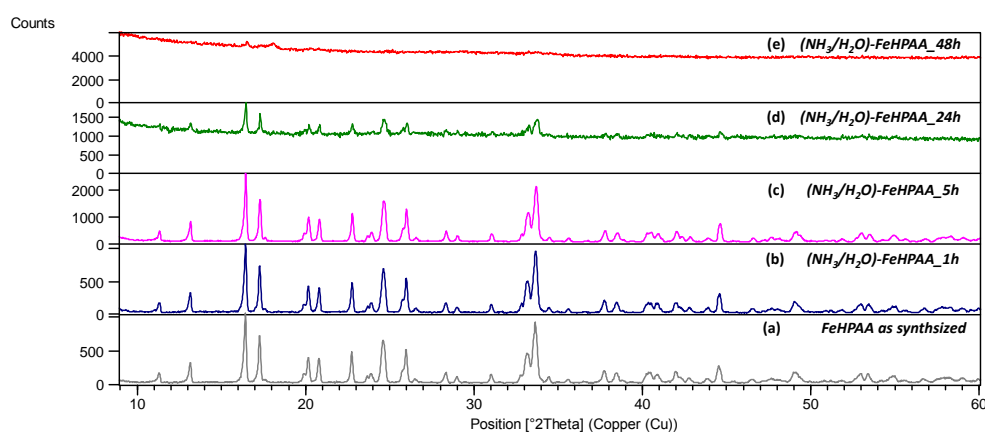
Figure 4.26. XRPD patterns for the [(*NH₃/H₂O)-FeHPAA*] at different times ((a) 0, (b) 1, (c) 5, (d) 24 and (e) 48 hours respectively) of exposure to ammonia vapours.

In order to check possible chemical changes on the surface of samples *(NH₃/H₂O)-FeHPAA_xh*, the Fe $2p^{3/2}$ region has been studied

by XPS. The ratio Fe(II)/Fe(III) was roughly maintained, i.e. 70/30 (see Figure 4.27), after ammonia exposure, indicating that no oxidation of Fe(II) has taken place.
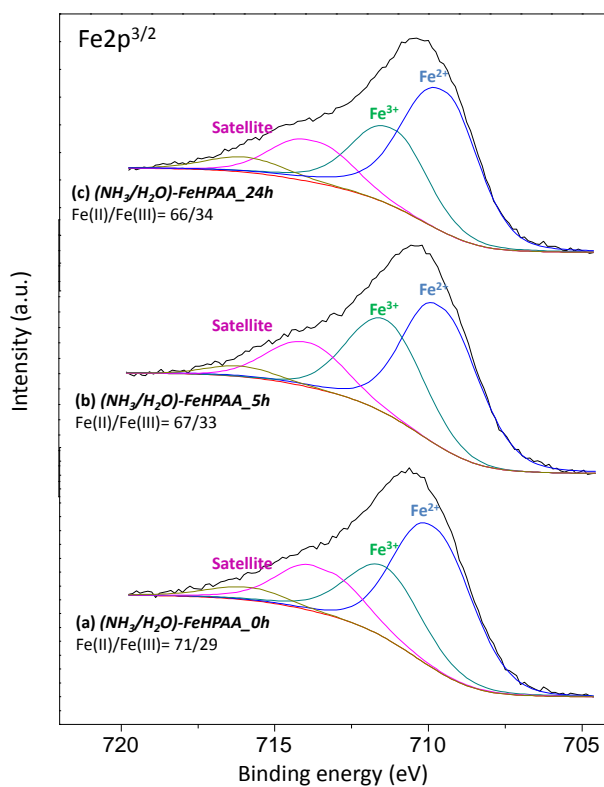
Figure 4.27. XPS Fe2p$^{3/2}$ raw data for the [*(NH$_3$/H$_2$O)-FeHPAA*] at different times ((a) 0, (b) 5 and (c) 24 hours respectively) of exposure to ammonia vapours.

Proton conductivity measurements were carried out for *FeHPAA* and its intercalated derivatives using cylindrical pellets (diameter ~5 mm and thickness ~1 mm). The pellets were equilibrated by successive heating/cooling cycles from 21 to 80 °C at 0.2 °C/min and 95% relative humidity (% RH) up to no deviation of the conductivity (see Figure 4.28). Sample cell was placed inside a temperature and humidity

controlled chamber (Espec SH-222). AC impedance data were collected over the frequency range from 20 Hz to 1 MHz with an applied voltage of 1 V. Figure 4.28 gives the plots of complex impedance plane, measured at 25 ºC and 95% RH, for all analysed samples except for *(NH₃/H₂O)-FeHPAA_48h* as the values overlap with those of *(NH₃/H₂O)-FeHPAA_24h*.

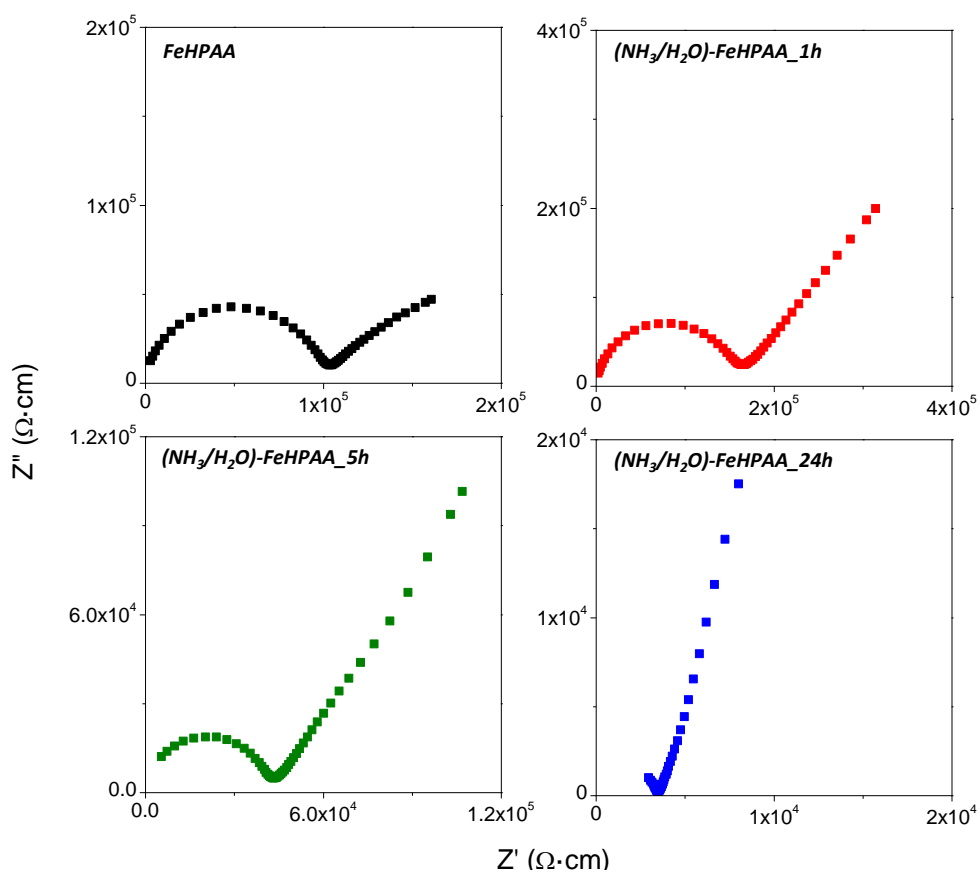**Figure 4.28.** Plots of complex impedance plane for the [*(NH₃/H₂O)-FeHPAA*] at different times (0, 1, 5 and 24 hours) of exposure to ammonia vapours, the measurements were realized at 25 ºC and 95% of RH.

On ammonia exposure, a substantial and gradual increase in proton conductivity, measured at 95% RH and 80 °C, from 1.1×10^{-5} S·cm^{-1} (**FeHPAA**) up to 2.5×10^{-3} S·cm^{-1} [**(NH₃/H₂O)-FeHPAA_24h**] was observed. This increment is attributed to a higher amount of adsorbed guest (NH$_3$/H$_2$O) species. According to the TG analysis, samples **FeHPAA_0h**, **(NH₃/H₂O)-FeHPAA_5h** and **(NH₃/H₂O)-FeHPAA_24h** display weight losses at 100 ºC of 0.25, 2.71 and 11.6 %, respectively. The nitrogen content is kept almost invariable after impedance measurements (Table 4.2).

Figure 4.29 shows the proton conductivity values at different times of exposure and the corresponding calculated activation energies. The latter values were between 0.32 and 0.36 eV, all of them within the range typically attributed to a Grotthuss transfer mechanism.
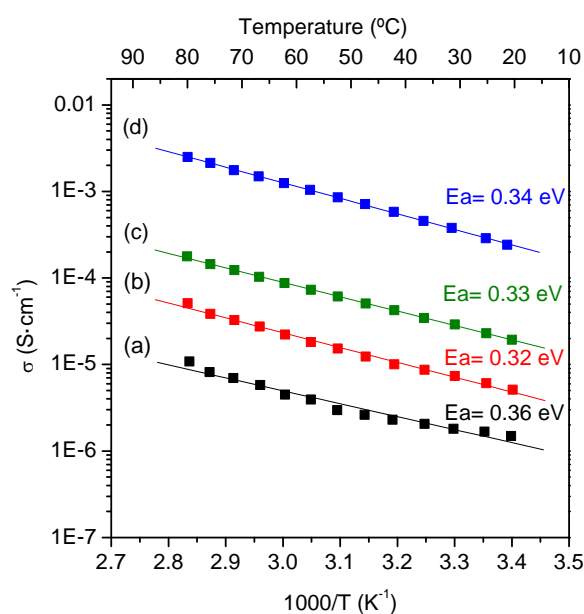
Figure 4.29. Plot of Log σ versus 1000/T for [**(NH₃/H₂O)-FeHPAA**] at times (a) 0, (b) 1, (c) 5 and (d) 24 hours of exposure to ammonia vapours and measured at 95% of RH.

The quantification of amorphous content was determined by Rietveld method *(Rietveld, 1969)* and the internal standard method. The refinement were carried out employing the GSAS package *(Toby, 2001; Larson and von Dreele, 2004)* and as starting models was used the crystal structure of **FeHPAA** previously reported from single crystal data (*Fu et al., 2005a*). ZnO (20% w/w) was used as internal standard and all refinements were realized using soft constraints to maintain chemically reasonable geometries for the phosphonate, chain and carboxylic groups. As example, Figure 4.30 depicts the final Rietveld plot for [*(NH₃/H₂O)-FeHPAA_24h*].

Figure 4.30. Rietveld plot for [*(NH₃/H₂O)-FeHPAA_24h*].

Table 4.3 shows representative crystallographic parameters for the crystalline **FeHPAA** fraction contained for samples **(NH_3/H_2O)-FeHPAA_xh** as well as the amorphous content, A, that was determined from the following equation:
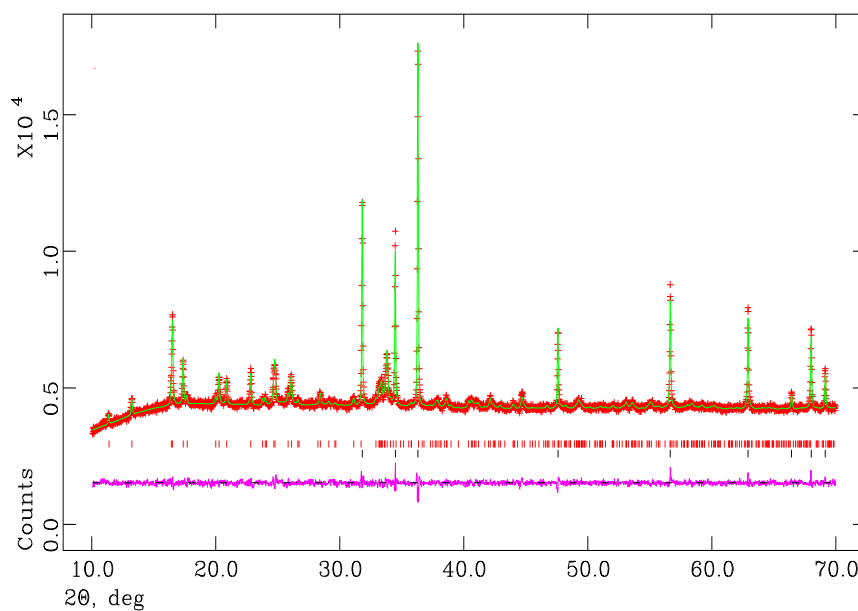
$$\% \ A = (1 - W_S/R_S)(100 - W_S)^{-1} \ 10^4$$

where W_S stands for the weighted concentration of the internal standard and R_S stands for the Rietveld analysed concentration of the internal standard *(De La Torre et al., 2001).*

According to Rietveld refinement (Table 4.3), exposure of layered **FeHPAA** to ammonia vapours the fraction of amorphous phase is kept constant despite an aparent progressive amorphization was observed in the XRD pattern of the as-prepared samples. The elemental analysis of samples mixed with ZnO shows similar nitrogen contents (~ 1.40 %) and quite closed to the original sample [**(NH_3/H_2O)-FeHPAA_5h**]. This suggests that sample preparation conditions (milling effects) for determination of amorphous content decreases the adsorbed ammonia in the solid. Due to the similar ammonia content in these samples, no significant variations in amorphous content as well as in the unit cell parameters should be expected, as experimentally determined.

Table 4.3. Selected crystallographic parameters and amorphous content.

| t(h) exposure $NH_{3(g)}$	(NH_3/H_2O)-FeHPAA_xh		
	0	5	24
Space group	P 1 21/c 1	P 1 21/c 1	P 1 21/c 1
λ (Å)	1.5406	1.5406	1.5406
a (Å)	5.7453(4)	5.7444(3)	5.7447(5)
b (Å)	15.599(1)	15.599(1)	15.596(1)
c (Å)	7.8837(7)	7.8847(6)	7.8853(7)
β (º)	109.699(5)	109.697(5)	109.70485)
V (Å^3)	665.21(7)	665.22(7)	665.09(7)
A (%)	28.2	25.1	27.6
R_{wp}	0.0171	0.0159	0.0154
R_p	0.0130	0.0120	0.0118

4.1.3. CALCIUM 5-(DIHYDROXYPHOSPHORYL) ISOPHTHALIC MATERIALS.

Crystalline calcium derivative of 5-(dihydroxyphosphoryl)isophthalic acid, (hereinafter referred to as ***Ca-PiPhtA***) have been prepared and characterized. In the next section, the crystal structure and the functionality (framework interconversions together with proton conductivity) of this open-framework material that combines Ca^{2+} ions and the rigid polyfunctional ligand 5-(dihydroxyphosphoryl)isophthalic acid $((C_6H_3(H_2PO_3)(COOH)_2,$ PiPhtA) are discussed [**a#2**, Bazaga-García et al., *J. Am. Chem. Soc.* **2014**, *136,* 5731-5739].

4.1.3.1 SYNTHESIS OF 5-(DIHYDROXYPHOSPHORYL) ISOPHTHALIC ACID (*Ca-PiPhtA*).

The polyfunctional ligand (PiPhtA) is not a commercial ligand and its synthesis was carried out by Garczarek, P. and Zón J. of University of Technology of Wroclaw (Poland), the ligand was synthesized through a number of intermediates, shown in Schema 4.1, as follows.

The product ***Ca-PiPhtA-I,*** $Ca_2[(HO_3PC_6H_3COOH)_2]_2$ $[(HO_3PC_6H_3(COO)_2H)(H_2O)_2]\cdot 5H_2O$, was obtained from a solution of the ligand (PiPhtA) and Ca^{2+} ions (molar ratio ligand:Ca=1) by slow crystallization at room temperature and at a relatively low reaction pH~3.0.
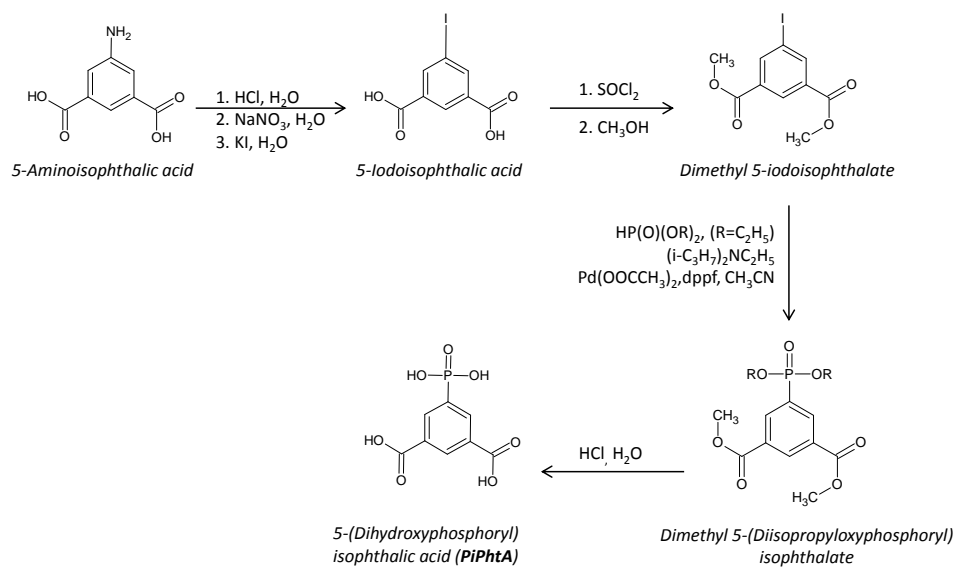
Scheme 4.1. Synthetic route for the preparation of 5-(dihydroxyphosphoryl)-isophthalic acid (PiPhtA).

4.1.3.2. SYTHESIS AND STRUCTURAL CHARACTERIZATION OF *Ca-PiPhtA.*

At pH~3.0 the carboxylic acid groups are expected to be deprotonated, whereas the phosphonic acid group is monodeprotonated. This would render the ligand tri-anionic, and a possible 1:1 adduct with Ca^{2+} would be anionic. Compound (*Ca-PiPhtA-I)* crystallizes in the orthorhombic system, space group *Pca2$_1$* and unit cell a=23.112(4) Å, b=6.9534(13) Å, c=22.638(4) Å and V=3638.1(12) Å^3.

Ca-PiPhtA-I, which crystal structure was solved from single crystal data, shows a complex pillared layered structure with a unit cell containing two calcium atoms, three PiPhtA ligands, and seven water

molecules, two are Ca coordinated and the remaining five are situated within the lattice.

The coordination geometry of both calcium centers is pentagonal bipyramidal (see Figure 4.31a). In this geometry, four of the equatorial positions are occupied by oxygen atoms of three different phosphonate groups and a fifth equatorial coordination position is occupied by an oxygen atom of a carboxylate group. Equatorial oxygen atoms belong to two ligands, P2 and P3, which configure edge-sharing calcium polyhedral chains and connect them into the layers, while leaving alternately arranged free carboxylic groups inside the interlayer space. While the axial positions of the calcium polyhedron are occupied by one water molecule and phosphonate or carboxylate oxygen of the third organic ligand, P1, which is pillaring adjacent layers (Figure 4.31b).

The arrangement of phosphonate and carboxylate moieties within the layers creates H-bond rings contributing to the stabilization of the pillared layered structure. The third dicarboxyphosphonate ligand, P1, is linking adjacent layers only by one phosphonate oxygen, by one side, and one carboxylate oxygen atom, from the other side. This connectivity mode leaves a POH and a free carboxylic group inside the interlayer space (Figure 4.31b).

Ca-PiPhtA-I presents a general structure with interlayer hydrophilic 1-D channels running parallel to the *b* axis. These channels are filled with 5 H_2O lattice water per unit cell forming zigzag chains inside the cavities (Figure 4.31b). The parallel zigzag chains display a left-handed helix and a right-handed helix along the *c* axis. The water-to-water interactions between these lattice waters create an extended network of H bonds along the 1-D channels and therefore a potential

proton transfer pathway, which may play an important role in the proton conductivity.

In contrast with **Ca-PiPhtA-I**, $Ca_2(H_2O)[H(OOC)_2C_6H_3PO_3H]_2$ *(Bauer and Stock, 2007b),* only contains discrete Ca_2O_{12} dimers in its structure instead of lineal chains. In addition, the connectivity of the carboxylic and phosphonic groups is also modified, and show higher connectivity of the hydrogen phosphonate groups relative to the carboxylate/ carboxylic groups.
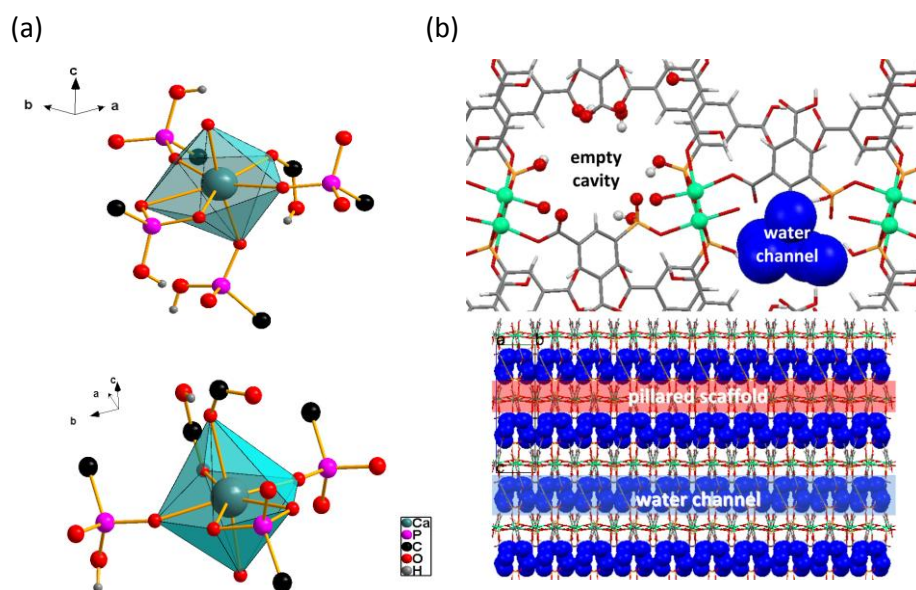
(a) (b)

Figure 4.31. (a) The coordination environment of the two Ca centers in the structure of **Ca-PiPhtA-I**. (b) *(Top)* 3D structure of **Ca-PiPhtA-I** along the *b* axis, showing the relative arrangement of the water-filled 1D channels and the moieties protruding from the channel wall to the interior. *(Bottom)* longitudinal view (*b*-axis horizontal) of the 1D water columns within the pillared scaffold. Reprinted with permission from (**a#2**, Bazaga-García et al., *J. Am. Chem. Soc.,* **2014***,136,* 5731-5739). Copyright (**2014**) American Chemical Society.

The TG-DTA analysis and the thermodiffractometric study of **Ca-PiPhtA-I** display some slight structural changes between room

temperature and 75 °C, temperature at which a partial dehydration takes place to give $Ca_2[(HO_3PC_6H_3COOH)_2]_2[(HO_3PC_6H_3(COO)_2H)(H_2O)_2]$ *(Ca-PiPhtA-II)*. This framework remains stable upon heating up to 135 °C. Between this temperature and 220 °C, others structural changes (Figure 4.32) associated to the removal of the coordinated water, are observed together with a progressive loss of crystallinity. However, the crystallinity is restored when the sample preheated at 220 °C is exposed to air for a long time or placed in contact with a controlled humidity atmosphere.
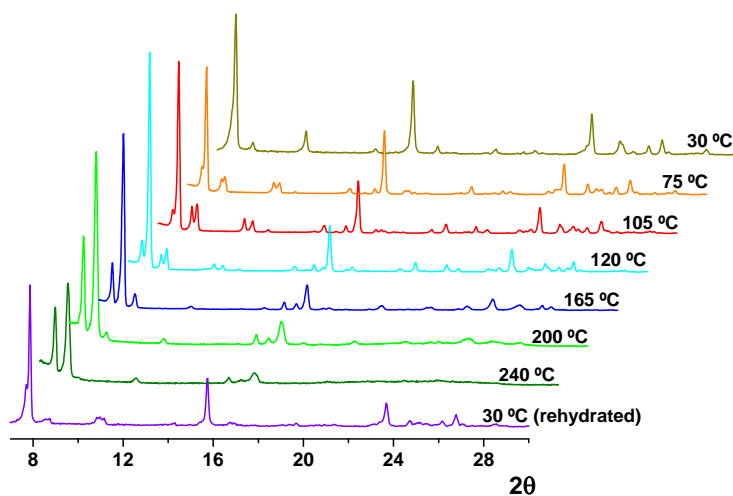
Figure 4.32. Thermodiffractometric study for *Ca-PiPhtA-I* at selected temperatures. Reprinted with permission from (**a#2**, Bazaga-García et al., *J. Am. Chem. Soc.,* **2014***,136,* 5731-5739). Copyright (**2014**) American Chemical Society.

The crystal structure of *(Ca-PiPhtA-II)* was determined by Rietveld refinement (Figure 4.33) using synchrotron powder X-ray diffraction data. The crystal structure of **Ca-PiPhtA-I** was used as starting model lowering the symmetry from the initial space group *P ca2₁* to P *a*]. Although all connectivity modes of **Ca-PiPhtA-I** framework are retained in **Ca-PiPhtA-II**, a higher distortion of the calcium

polyhedra takes place what leads to the formation of an alternate interlayer region with slightly different cavity dimensions (Figure 4.34) and, hence, slightly different 1-D channels.
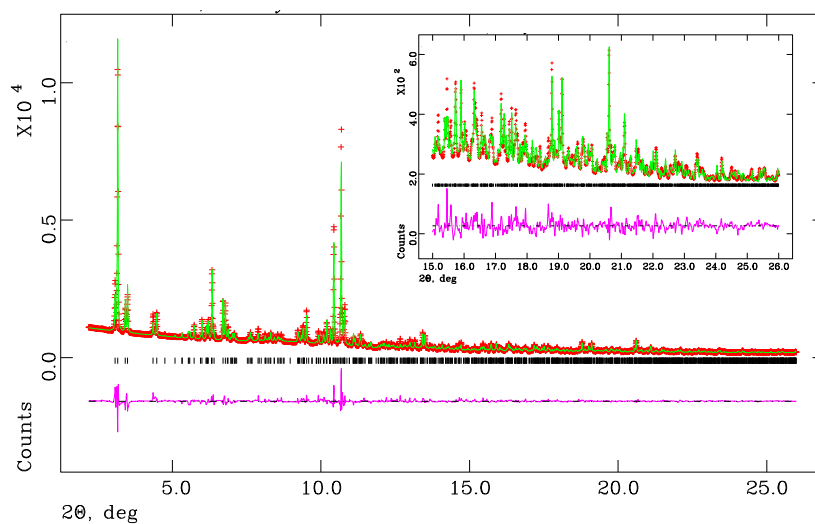
Figure 4.33. Rietveld refinement powder for *Ca-PiPhtA-II*. The inset shows the fit for the angular region range between 15 and 26° (2θ). Reprinted with permission from (**a#2**, Bazaga-García et al., *J. Am. Chem. Soc.,* **2014***,136,* 5731-5739). Copyright (**2014**), American Chemical Society.

Figure 4.34. *b*-axis view (*a*-axis horizontal) of the crystal structures for *Ca- PiPhtA-I* (left) and *Ca-PiPhtA-II* (right) showing the slightly different conformation of the 1D

channels along the *c* axis. Reprinted with permission from (**a#2**, Bazaga-García et al., *J. Am. Chem. Soc.,* **2014***,136,* 5731-5739). Copyright (**2014**), American Chemical Society.

4.1.3.3. THERMAL EVOLUTION AND REACTIVITY OF *Ca-PiPhtA-I* WITH AMMONIA VAPORS.
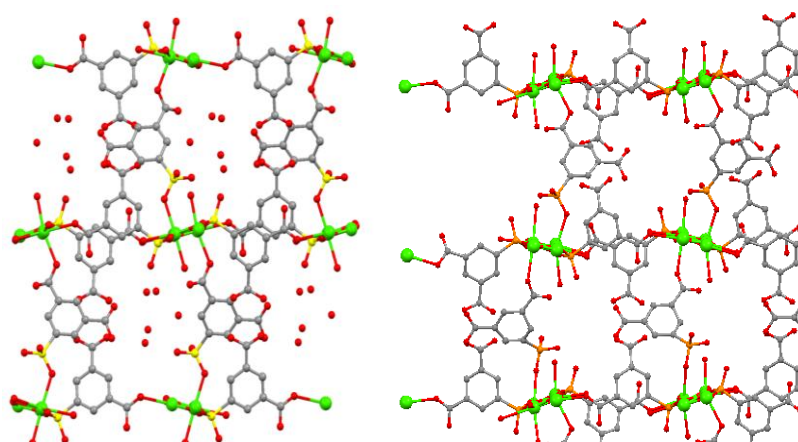
Upon exposure of ***Ca-PiPhtA-I*** to ammonia vapors (from 28% NH_3 aqueous solution for 2 hours) a new derivative is obtained (***Ca-PiPhtA-NH₃***) which contains 7 NH_3 and 16 H_2O molecules. ***Ca-PiPhtA-NH₃*** exhibits a complex X-ray diffraction pattern that suggests partial breaking and transformation of the parent pillared structure (Figure 4.35). A detailed structural analysis of ***Ca-PiPhtA-NH₃*** was not possible, due, in part, to the lack of crystallinity. ***Ca-PiPhtA-NH₃*** is likely a multiphase compound with peaks at 15.3 and 13 Å corresponding to $d_{(001)}$ basal spacing of two new layered phases originated by rupture of the interlayer phosphonate/Ca^{2+} or carboxylate/Ca^{2+} bonds (see figure 4.36).
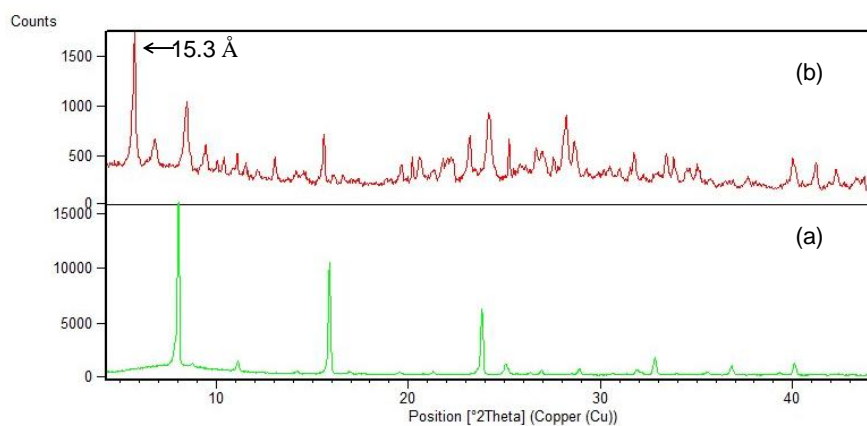

Figure 4.35. X-ray diffraction patterns (XRPD) for (a) ***Ca-PiPhtA-I*** and (b) ***Ca-PiPhtA-NH₃***. Reprinted with permission from (**a#2**, Bazaga-García et al., *J. Am. Chem. Soc.,* **2014***,136,* 5731-5739). Copyright (**2014**), American Chemical Society.
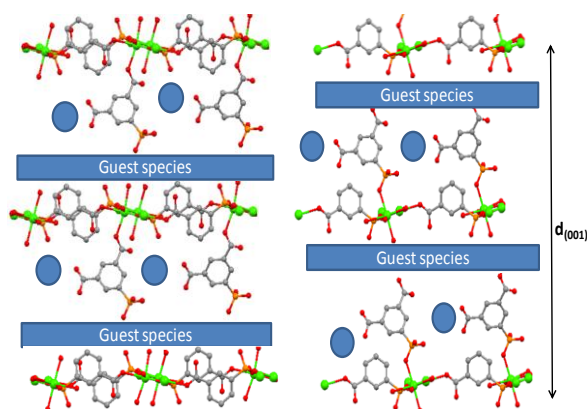
Figure 4.36. Schematic representation for the rupture of the 3D-framework to give new 2D intercalated derivatives. Reprinted with permission from (**a#2**, Bazaga-García et al., *J. Am. Chem. Soc.,* **2014***,136,* 5731-5739). Copyright (**2014**), American Chemical Society.

This hypothesis is supported by the inability of the original narrow 1-D channels to accommodate the high number (23) of intercalated guest species (weight loss observed 38.66%); and, especially by its IR spectra what suggests profound structural changes compared to the pristine *Ca-PiPhtA-I*. So, the IR spectrum of *Ca-PiPhtA-NH₃* shows a shift to lower wave numbers in the water stretching vibrations region, which is indicative of the existence of strong hydrogen bonds between intercalated water and ammonia guest molecules (Figure 4.37). In addition, the characteristic bands corresponding to the carboxylic *(Danilich, et al., 1995; Chaplais et al., 2003; Demadis and Katarachia, 2004*; *Kim et al., 2001)* ($\sim$1700 cm^{-1}) and hydrogen phosphonate *(Zenobi et al., 2008)* (915−930 cm^{-1}) groups are almost absent in the vibrational spectrum of *Ca-PiPhtA-NH₃* as a consequence of the reaction of these acidic groups with NH$_3$. On the other hand, the thermodiffraction of *Ca-PiPhtA-NH₃* shows a progressive amorphization of the sample with the loss of the guest species although the peak at 15.3 Å

(corresponding to the new intercalated phase) persists up to 125 °C, what suggests a high stability for this phase (see Figure 4.35).
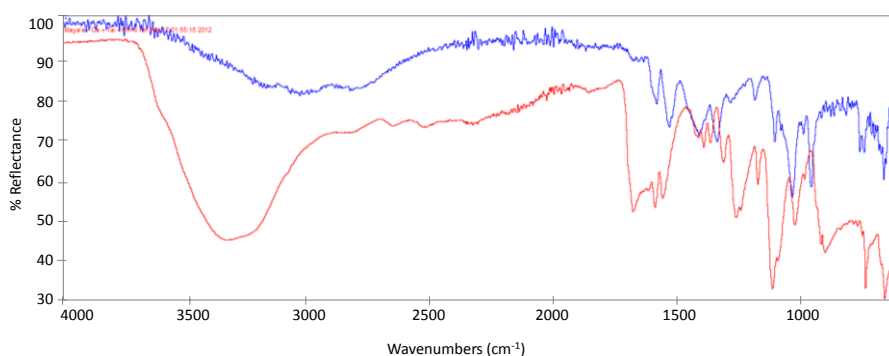

Figure 4.37. ATR-IR spectra for ***Ca-PiPhtA-I*** (red) and ***Ca-PiPhtA-NH₃*** (blue). Reprinted with permission from (**a#2**, Bazaga-García et al., *J. Am. Chem. Soc.,* **2014***,136,* 5731-5739). Copyright (**2014**), American Chemical Society.

Measurements of the proton conductivity for ***Ca-PiPhtA-I*** and ***Ca-PiPhtA-NH₃*** were carried out at 98% of relative humidity (RH) and different temperatures. The impedance plots are depicted in Figure 4.38 at 98% RH and T=24 °C, proton conductivity for ***Ca-PiPhtA-I*** is $\sigma=5.7 \times 10^{-4}$ S·cm^{-1}. It increases up to 1.3×10^{-3} S·cm^{-1} upon activation by preheating the sample at 40 °C for 2 h followed by water equilibration at room temperature under controlled conditions *(**Ca-PiPhtA-III**)*. This preactivation (Figure 4.39) would imply small, but effective, structural and/or textural changes (surface effect) as neither its X-ray powder diffraction and its thermal analysis show important changes when compared to the related traces of the pristine solid.

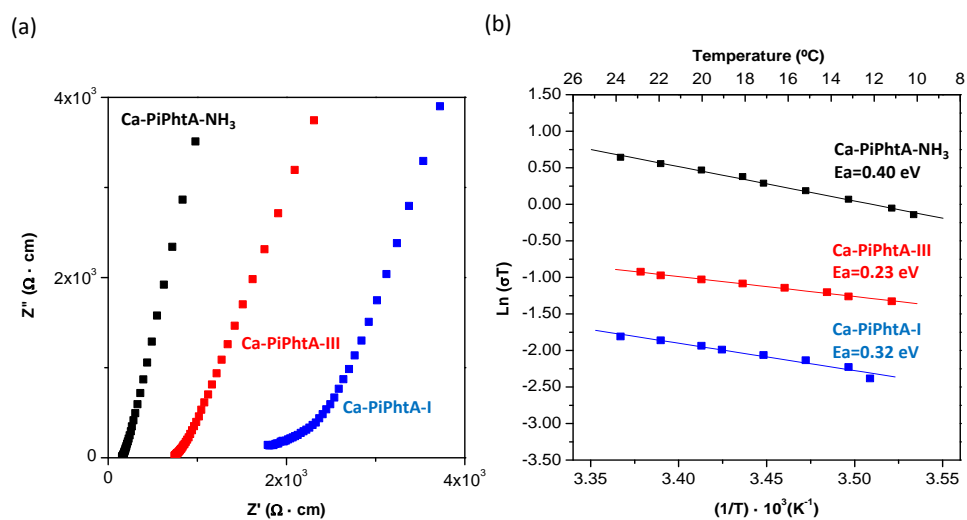**Figure 4.38.** (a) Plot of the complex impedance plane for *Ca-PiPhtA* compounds at 24 °C and 98% RH. (b) Arrhenius plots vs T^{-1} from 10 to 24 °C. Reprinted with permission from (**a#2**, Bazaga-García et al., *J. Am. Chem. Soc.,* **2014***,136,* 5731-5739). Copyright (**2014**), American Chemical Society.
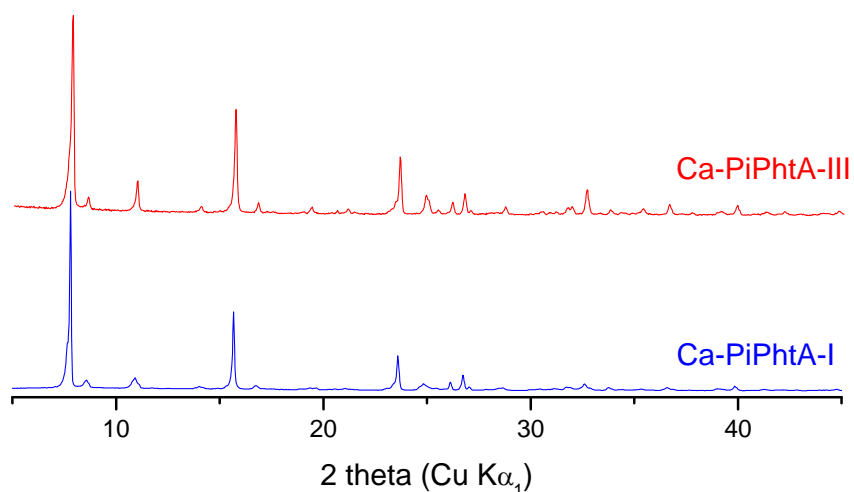

Figure 4.39. Powder X-ray diffraction pattern (XRPD) for *Ca-PiPhtA-I* and *Ca-PiPhtA-III*.

The conductivity value obtained for **Ca-PiPhtA-III** (after thermal activation) is of the same magnitude as for other functionalized metal phosphonates, from 1.6×10^{-3} S·cm^{-1} for Mg[(HO$_3$PCH$_2$)NH(CH$_2$)$_8$NH(CH$_2$PO$_3$H)$_2$]·6H$_2$O, Mg(H$_6$ODTMP)·6H$_2$O *(Colodrero et al., 2012b)*, to 8×10^{-3} S·cm^{-1} for La[(O$_3$PCH$_2$)(HO$_3$PCH$_2$)NH(CH$_2$)$_6$NH(CH$_2$PO$_3$H)$_2$]·7H$_2$O, La-(H$_5$HDTMP)·7H$_2$O *(Colodrero et al., 2012a)*, and other MOF materials, some of them reaching 10^{-2} S·cm^{-1} *(Kim et al., 2013; Ponomareva et al., 2012)*. However, the proton conductivity of **Ca-PiPhtA** materials is higher than those reported for other Ca-based MOFs, the latter exhibiting values in the range from 10^{-5} to 4×10^{-4} S·cm^{-1} under similar experimental conditions *(Liang et al., 2013; Kundu et al., 2012)*.

Ca-PiPhtA-NH$_3$ exhibits the highest proton conductivity, 6.6×10^{-3} S·cm^{-1}, measured at 98% RH and T=24 °C (Figure 4.38). These results underline the importance of internal H-bonding networks that, in turn, determine the proton conductivity properties of organo-inorganic materials. It is highlighted that new proton transfer pathways may be developed by means of cavity "derivatization" with selected guest molecules resulting in improved proton conductivity.

Activation energies (Ea) for proton transfer in the above-mentioned frameworks range between 0.23 and 0.40 eV (see Figure 4.38b). These values are typical for a Grothuss mechanism of proton conduction *(Colomban, et al., 1992)*. The lower Ea value is obtained for the sample pre-heating at 40 °C. This indicates that the preactivation could induce small structural and/or textural changes which enhance proton transfer through a pathway of sites separated by a smaller energy barrier.

4.2. LANTHANIDE AMINO-*TRIS*-(METHYLENE PHOSPHONATES).

Amino-*tris*-(methylenephosphonic) acid (N(CH$_2$PO$_3$H$_2$)$_3$, H$_6$AMP), with three phosphonic groups in tripodal arrangement has been selected for preparing a new family of lanthanide phosphonate derivatives with multifunctional properties.

4.2.1. STRUCTURAL CHARACTERIZATION AND PROPERTIES.

Lanthanide amino-tris-methylenephosphonate compounds (***Ln-AMP***), with Ln = La^{3+}, Pr^{3+}, Sm^{3+}, Gd^{3+}, Tb^{3+}, Dy^{3+} and Ho^{3+}, have been synthesized at room temperature from the reaction of the phosphonic acid, H$_6$AMP, with lanthanide nitrate salts, using a ligand to metal molar ratio of 5:1 and pH < 1. *(Bazaga-García et al., 2015, unpublished results).* This series of materials is represented by the general formula {Ln[(HN(CH$_2$PO$_3$H)$_3$(H$_2$O)$_4$]Cl}.

The TGA-DTA curves, illustrated in Figure 4.40 for ***Gd-AMP***, showed a weight loss in three steps. First stage, up to ~ 120-150 ºC, corresponds to the loss of three water molecules, two lattice ones and one coordinated to the Ln^{3+} ion (calc. 9.6%, obs. 9.5%). Second stage, up to 200-220 ºC, is characterized by a weight loss of about 3,3% that corresponds to removal of the remaining bound water. Third weight loss stage (~5.4%), up to 350-400 ºC is accompanied of a small endothermic effect and matches with removal of HCl (calc. 6.6%) but slightly overlapped with initial thermal decomposition of the ligand, which is completed at about 650 ºC, with an associated total weight loss about 27% (calc. 30.6%).
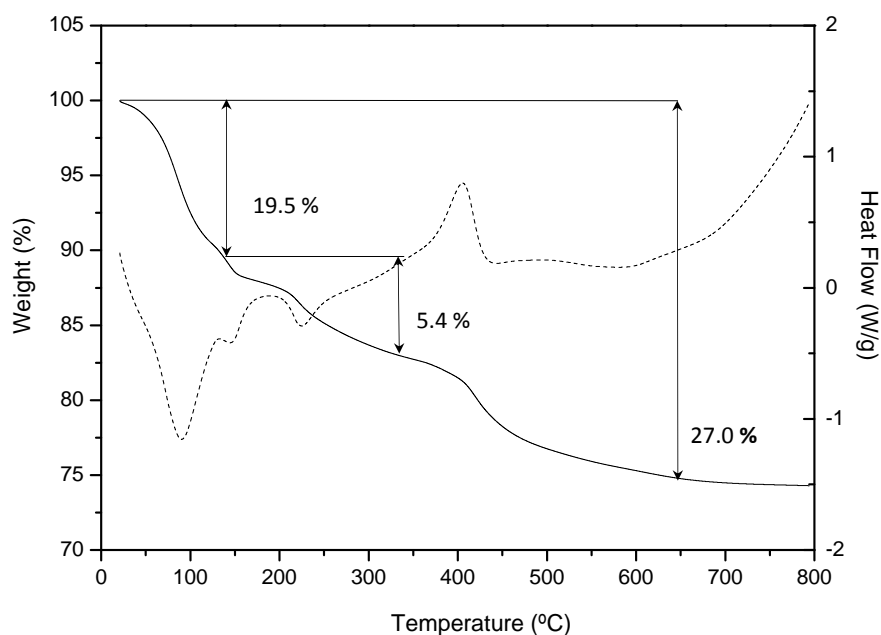
Figure 4.40. TGA curve (solid line) and DTA curve (dashed line) for *Gd-AMP*.

The isostructural *Ln-AMP* compounds crystallize in the space group *Cc*. Only La-, Pr- and Ho-derivatives were obtained as single crystals, while the remaining compounds of the series were obtained as polycrystalline samples. The crystal structures of the latter compounds were determined by Rietveld refinement using that of *La-AMP* as the starting structural model. Tables 4.4 and 4.5, report crystallographic data for these solids and Figure 4.41 shows the Rietveld plot for *Gd-AMP* as an example.
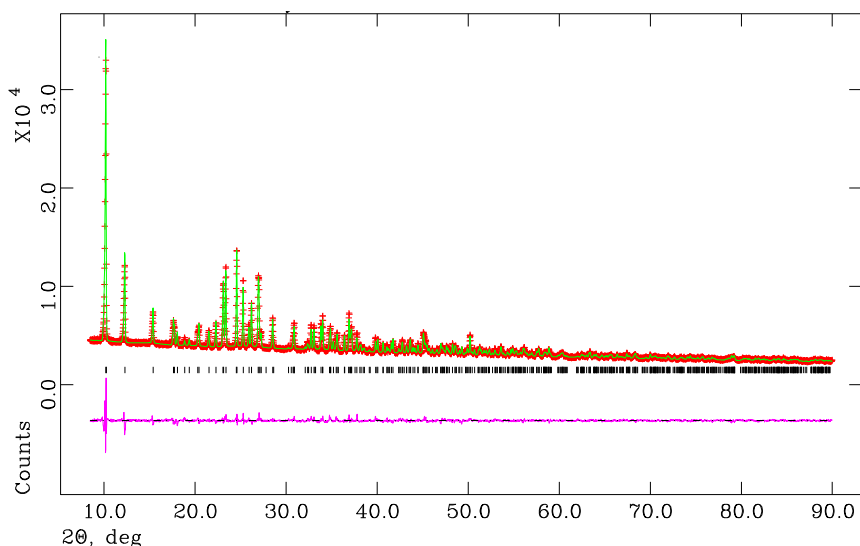
Figure 4.41. Rietveld plot for *Gd-AMP*.

The crystal structures of these compounds can be described as built up from 2D positively charged layers with chloride ions and water molecules in the interlayer region (see Figure 4.42a). The asymmetric part of the unit cell consist of one seven-coordinated Ln^{3+} metal center, two oxygen atoms from two bonded water molecules, one AMP^{2-} anionic ligand, two uncoordinated water molecules and one uncoordinated chloride ion (Figure 4.42b). It must be noticed that the three crystalllographically independent phosphonate groups are monoprotonated as well as the nitrogen atoms of the amine group having a zwitterionic behavior, very common in other aminophosphonate-type compounds *(Cabeza et al., 2015).* Two of the three phosphonate groups (P2 and P4) act as both, a chelating and a bridging linker, while the third group, P3, acts solely as a bridging moiety. Free P-OH groups point towards the interlayer region and weakly interact with chloride ions (Figure 4.43).

Table. 4.4. Selected crystallographic data for {***Ln[(HN(CH₂PO₃H)₃(H₂O)₄]Cl***}, (Ln= La, Pr, Sm and Gd) compounds.

$^{a}R1(F) = \Sigma||Fo| - |Fc||/\Sigma|Fo|; wR2(F^2) = [\Sigma w(Fo^2 - Fc^2)^2/\Sigma F^4]^{1/2}$

	La-AMP	*Pr-AMP*	*Sm-AMP*	*Gd-AMP*
Empirical formula	$C_3H_{18}ClNO_{13}$ P_3La	$C_3H_{18}ClNO_{13}$ P_3Pr	$C_3H_{18}ClNO_{13}$ P_3Sm	$C_3H_{18}ClNO_{13}$ P_3Gd
F.W. (g mol^{-1})	543.45	544.88	555.89	561.89
λ (Å)	0.71073	1.54178	1.5406	1.5406
a (Å)	11.3510(2)	11.2998(8)	11.2137(3)	11.1734(2)
b (Å)	17.5960(4)	17.7086(12)	17.6416(3)	17.6294(4)
c (Å)	8.7010(2)	8.6894(6)	8.6012(3)	8.5670(2)
α (°)	90.0	90.0	90.0	90.0
β (°)	115.4310(13)	115.830(2)	115.410(2)	115.416(2)
γ (°)	90.0	90.0	90.0	90.0
V (Å^3)	1569.48(6)	1565.06(19)	1536.96(9)	1524.73(6)
Z	4	4	4	4
$V_{non\,H\,atom}$ (Å^3·atom^{-1})	17.84	17.78	17.46	17.33
Data/Restrains/Parameters	3532/2/199	2390/2/199	4645/41/115	4864/44/116
Nº reflections	3532	2390	623	619
R_{wp}			0.0336	0.0289
R_p			0.0234	0.0201
R_F			0.0572	0.0539
GOF, F^2	1.086	1.098		
R factor [I>2σ(I)]	^{a}R1=0.02019 ^{a}wR2=0.0453	^{a}R1=0.0594 ^{a}wR2=0.1593		
R factor (all data)	^{a}R1=0.0219 ^{a}wR2=0.0458	^{a}R1=0.0596 ^{a}wR2=0.1596		

Table. 4.5. Selected crystallographic data for {**Ln[(HN(CH$_2$PO$_3$H)$_3$(H$_2$O)$_4$]Cl**}, (Ln= Tb, Dy and Ho) compounds.

[a]R1(F) = Σ||Fo| − |Fc||/Σ|Fo|; wR2(F^2) = [Σw(Fo^2 − Fc^2)^2/ΣF^4]$^{1/2}$

	Tb-AMP	Dy-AMP	Ho-AMP
Empirical formula	C$_3$H$_{18}$ClNO$_{13}$P$_3$Tb	C$_3$H$_{18}$ClNO$_{13}$P$_3$Dy	C$_3$H$_{18}$ClNO$_{13}$P$_3$Ho
F.W. (g mol^{-1})	562.89	567.90	569.47
λ (Å)	1.5406	1.5406	0.71073
a (Å)	11.1464(2)	11.1205(3)	11.0600(6)
b (Å)	17.6301(2)	17.6102(4)	17.4160(8)
c (Å)	8.5503(2)	8.5324(1)	8.4728(4)
α (º)	90.0	90.0	90.0
β (º)	115.440(1)	115.400(1)	115.1570(10)
γ (º)	90.0	90.0	90.0
V (Å^3)	1517.31(6)	1509.42(6)	1477.23(13)
Z	4	4	4
V$_{non\ H\ atom}$ (Å^3·atom^{-1})	17.23	17.15	16.78
Data/Restrains/ Parameters	4689/43/116	4645/41/115	4391/2/ 210
Nº reflections	618	614	4391
R$_{wp}$	0.0310	0.0447	
R$_p$	0.0231	0.0320	
R$_F$	0.049	0.0758	
GOF, F^2			1.159
R factor [I>2σ(I)]			[a]R1=0.0140 [a]wR2=0.0397
R factor (all data)			[a]R1=0.0140 [a]wR2=0.0397
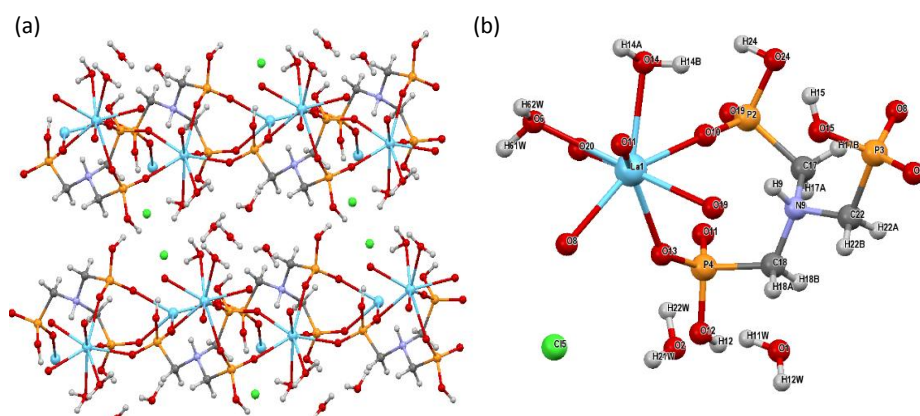
Figure 4.42. (a) 2D-arrangement for *Ln-AMP* viewed along the *c*-axis. (b) Expanded asymmetric part showing the coordination environment of Ln^{3+} ions and the coordination mode of the ligand.

The layers are built up from isolated LnO_8 polyhedra and bridge chelating AMP^{2-} ligands. This connectivity creates infinite chains of interconnected LnO_8 polyhedra (see Figure 4.43).

Figure 4.43. View of a single layer of *La-AMP* with details of the interaction of chloride ion with the P-OH groups and lattice water.

A single lanthanide center in a two-dimensional network is also observed in **Pr-(AMP)·1.5H₂O** *(Cunha-Silva et al., 2007),* where the ligand exhibits single unidentate, chelate bidentate and chelate tridentate interactions with the metal cen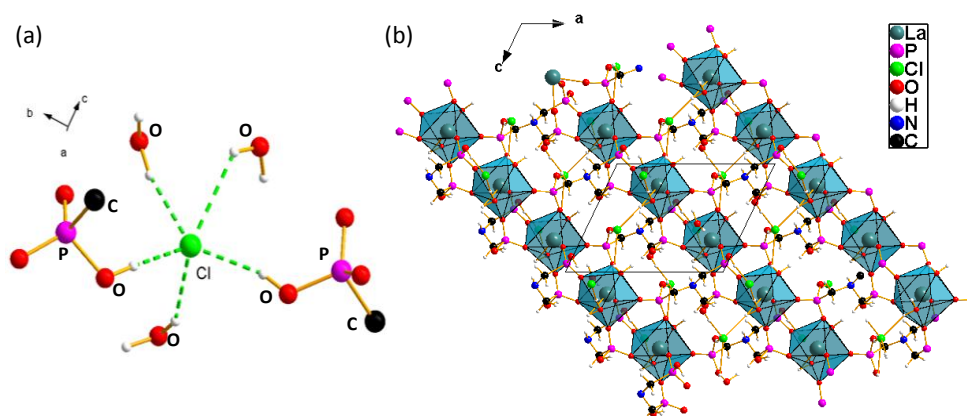ter, such high connectivity leading to a sterically hindered environment, which prevent inclusion of water molecules in the first coordination sphere. Because molecules other than water may perhaps be introduced (and removed) in between this network, tuning the photoluminescence properties has been anticipated for compounds **Ln-(AMP)·1.5H₂O.** Conversely to **La-(AMP)·1.5H₂O**, anhydrous **La-AMP** *(Silva et al., 2011)* does not have any solvent molecules incorporated into the network, and upon heating, the structure is transformed into a dense 3D or a layered 2D material.

Differently, a 1D coordination polymer, $[La_2(AMP)_2(H_2O)_4]\cdot 4.5H_2O$, is formed when Ln^{3+} metal centers are coordinated to two water molecules and seven oxygen atoms originating from neighbouring phosphonate groups. In this case, a distorted tricapped trigonal LaO_9 coordination environment results, with uncoordinated water molecules occupying the interstitial spaces between adjacent polymers *(Mendes et al., 2015).*

Overall, the structural variations observed in lanthanide amino-*tris*-methylenephosphonate compounds show that small changes in metal-ligand connectivity can promote important changes in properties and, hence, it could be possible to exploit them for specific purposes.

Because an extended H-bonded network is formed in the interlayer space of **Ln-AMP,** due to the presence of coordinated and unbounded water molecules, together with P-OH groups, proton conductivity could be anticipated for this kind of materials. Preliminary measurements were performed for **Gd-AMP** as a representative compound of this series. The procedure of data acquisition has been previously described for **Fe-HPAA** (section 4.1.2.3). Under this conditions, **Gd-AMP** exhibits a

proton conductivity of 3.96×10^{-4} S·cm^{-1}, at 80 ºC and 95% RH, with a remarkably low activation energy (Ea) of 0.2 eV typical of a Grothuss mechanism of proton conduction *(Colomban, et al., 1992).*

The photoluminescence study for the complete ***Ln-AMP*** series is underway. Meanwhile, absorbance and luminescence spectra recorded for selected examples are here reported. The observed transitions are attributed solely to *f-f* transitions of the lanthanide ions present, as the tri-phosphonate organic groups had no measurable absorption or luminescent properties.

The electronic spectra for studied samples show strong absorption bands below ~250 nm assumed to arise from charge transfer transitions, i.e. *$4f^n \rightarrow 4f^{n-1}5d^1$*, which are 'allowed' under all the selection rules and, therefore, they have been excluded from tables of band assignments.

Absorption and emission bands are specified in Table 4.6 for ***Pr-AMP*** as well as the corresponding band assignments. Its UV-vis absorption and photoluminescence spectra (under excitation at 355 nm) are shown in Figure 4.44.

Table 4.6. Absorption and emission bands observed for ***Pr[HN(CH₂PO₃H)₃(H₂O)₄]Cl,*** (***Pr-AMP***).

Absorption		Luminescence (λ_{exc}= 355nm)	
Transition $\leftarrow {}^3H_4$	**Wavelength (nm)**	**Transition** ${}^3P_0 \rightarrow$	**Wavelength (nm)**
${}^3F_2$	1945		
${}^3F_3, {}^3F_4$	1559		
${}^1G_4$	1026		
${}^1D_2$	592	${}^3H_6$	621
${}^3P_0$	481	${}^3H_5$	535
${}^3P_1, {}^1I_6$	469	${}^3H_4$	481
${}^3P_2$	444		

The absorption spectrum of **Pr-AMP** shows several intense peaks in the visible and NIR regions with the spin allowed, $\Delta S=0$, transitions being much more intense than those which are spin forbidden. Excitation of the sample with light of wavelength 355 nm gives rise to three peaks in the visible region corresponding to the $^3P_0 \rightarrow {}^3H_J$ (J=4-6), the most intense of which is the middle one of the three $^3P_0 \rightarrow {}^3H_5$.
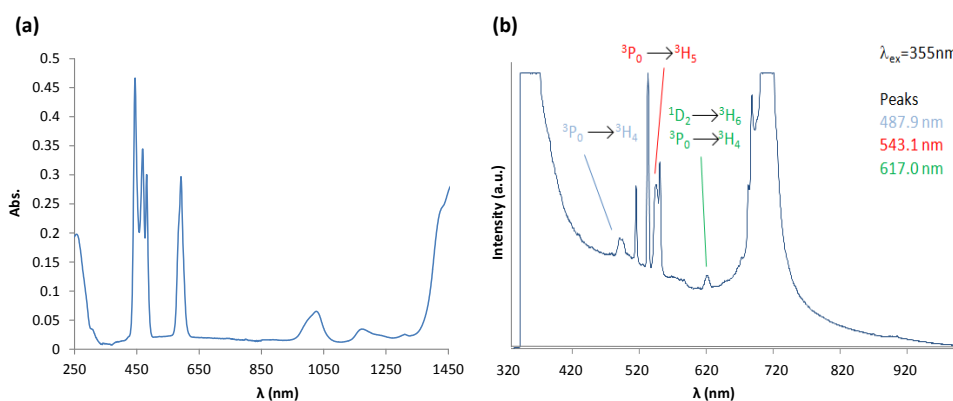
Figure 4.44. (a) UV-visible absorption and (b) photoluminescence spectra (under excitation al 355 nm) of **Pr[HN(CH$_2$PO$_3$H)$_3$(H$_2$O)$_4$]Cl, (Pr-AMP).**

For **Tb-AMP** the absorption and emission data are compiled in Table 4.7 and its UV-vis absorption and photoluminescence spectra (under excitation at 355 nm) are shown in Figure 4.45.

Table 4.7. Absorption and emission bands observed for *Tb[HN(CH₂PO₃H)₃* *(H₂O)₄]Cl*, *(Tb-AMP).*

Absorption		Luminescence (λ_{exc}= 355nm)	
Transition $\leftarrow {}^7F_6$	**Wavelength (nm)**	**Transition** ${}^5D_4 \rightarrow$	**Wavelength (nm)**
${}^7F_3$			
${}^7F_0, {}^7F_1, {}^7F_2$	1941	${}^7F_3$	620
	1446	${}^7F_4$	583
${}^5D_4$	487	${}^7F_5$	546
	379	${}^7F_6$	489
${}^5G_6, {}^5D_3, {}^5L_{10}$	371		
${}^5G_5, {}^5G_2, {}^5G_4, {}^5L_9$	352		
${}^5D_2, {}^5L_8, {}^5L_7, {}^5G_3$	342		
${}^5H_7, {}^5D_0, {}^5D_1$	318		

The *f-f* transitions in the UV-visible part of the spectrum of this compound are fairly weak. Interest lies in the breadth of the absorption envelope for this material, broadly covering all wavelengths measured below 400 nm, which means that it can be readily excited by a wide range of energies. Its photoluminescence spectrum, illuminated with light of wavelength 355 nm, displays the strong ${}^5D_4 \rightarrow {}^7F_J$ (J=3-6) peaks commonly associated with the visible green response. The most intense of these is the ${}^5D_4 \rightarrow {}^7F_5$ transition at 546 nm. Interestingly, the only 'resonance' wavelength (where absorption and emission have the same wavelength) observable is at 489 nm. This implies that excitation to higher energy excited state is followed by a non-radiative relaxation to the ${}^5D_4$ state prior to radiative relaxation to the ground states. It is

notable that a strong green emission is observed for this material despite the fact that the lanthanide content is wholly Tb. Excitation of an ion can migrate to a nearby neighbour if they are separated by only a few angstroms. The optical excitation is thus trapped at impurity or defect sites giving rise to concentration quenching via the enhancement of non-radiative relaxation, or by $^5D_3 + {}^7F_6 \rightarrow {}^5D_4 + {}^7F_0$ cross-relaxation *(Kano, 2006)*. As such it is usual to dope host materials with only 1-5 mol % of the trivalent ion. In ***Tb-AMP***, the Tb^{3+} ions are separated by distances of 5.588, 8.495, and 8.550 Å, which means that a high luminescent efficiency can be achieved even when all cation sites are occupied by Tb *(Bazaga-García et al., 2015, unpublished results)*.
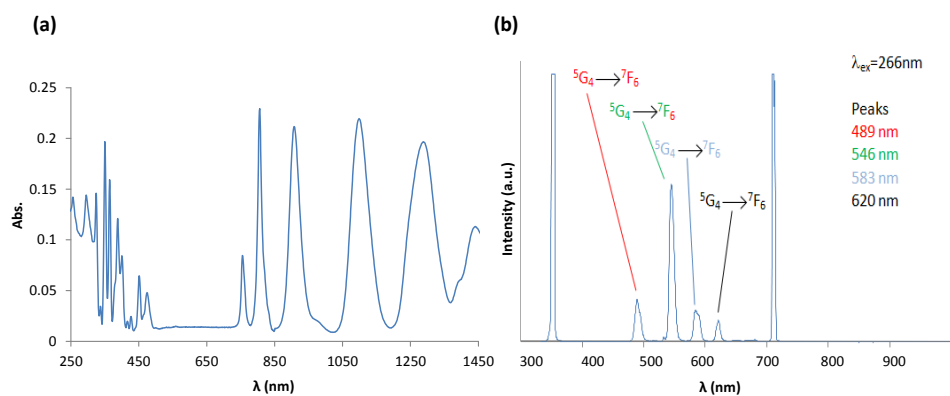
(a)

(b)

Figure 4.45. (a) UV-visible absorption and (b) photoluminescence spectra (under excitation al 266 nm) of ***Tb[HN(CH₂PO₃H)₃(H₂O)₄]Cl***, ***(Tb-AMP)***.

4.3. OTHER FUNCTIONALIZED METAL PHOSPHONATES.

In this section the polyfunctionalized phosphonic acid $(H_2O_3PCH_2)_2$-N-$(CH_2)_2SO_3H$, DVb382, has been used in order to get new materials. This ligand has been prepared in collaboration with Prof. Didier Villemin from the University of Caen (France) and it is characterized by the presence of two phosphonic groups and one sulfonic group; what makes it good candidate to attain a rich structural variability for new potential applications.

A systematic study to optimize the synthesis conditions has been carried out using a High-Throughput (HT) methodology. This one allows optimizing the experimental conditions (microscale synthesis) prior to conducting preparations at higher scale. HT methods imply four major steps: design of experiment, synthesis, characterization, and data evaluation. In this way, reaching to the pre-established goals is much shorter whereas minimum amounts of residues are generated. The HT methodologies *(Stock, 2010; Bauer and Stock, 2007a)* are acknowledged as quite helpful tools to discover new crystal structures.

By meaning of HT methodology, the reactivity of DVb382 with alkaline-earth metals (Ca, Mg), transition metals (Co, Zn) and lanthanide ions (La, Sm, Gd, Eu) under different synthesis conditions (temperature, pH, reagent molar ratio and solvents) has been tested. The experimental system consists in an autoclave block made of aluminium, which contains either 48 reaction chambers in a 6x8 array, or 24 reaction chambers in a 6x4 array (Figure 4.46).
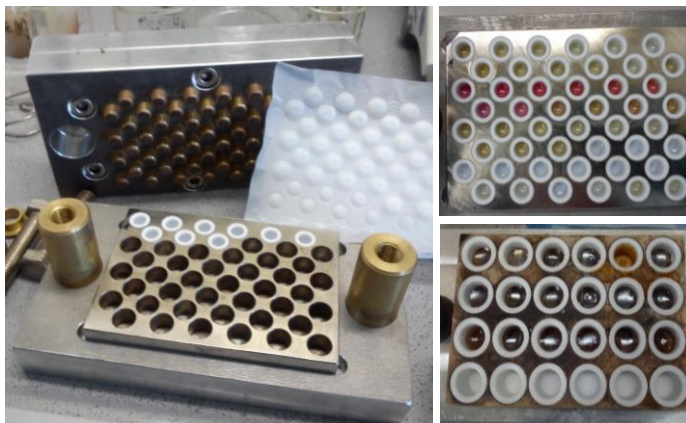
Figure 4.46. Photograph of the home-designed parallel-synthesis system.

The following parameters were analysed: metal:DVb382 molar ratios (1:1, 1:2, 2:1, 1.5:1), initial pH values (0.5-4.0), solvents (H_2O or DMF/H_2O mixtures, DMF=dimethylformamide), temperature (140 and 160 ºC). Similar parameters were also studied by microwave-assisted synthesis. Scheme 2 summarizes the established synthesis conditions and results for some experiments. Figure 4.47 shows the powder X-ray diffraction patterns for some lanthanides derivatives obtained upon different conditions and in comparison with the powder pattern for the pure phosphonic acid used as precursor.

Only some lanthanide derivatives were isolated as semicrystalline solids under hydrothermal conditions at 140 ºC, molar ratio M^{3+}:DVb382 = 2:1 and pH <2, see Figure 4.46. The work in this set of compounds is still in progress.
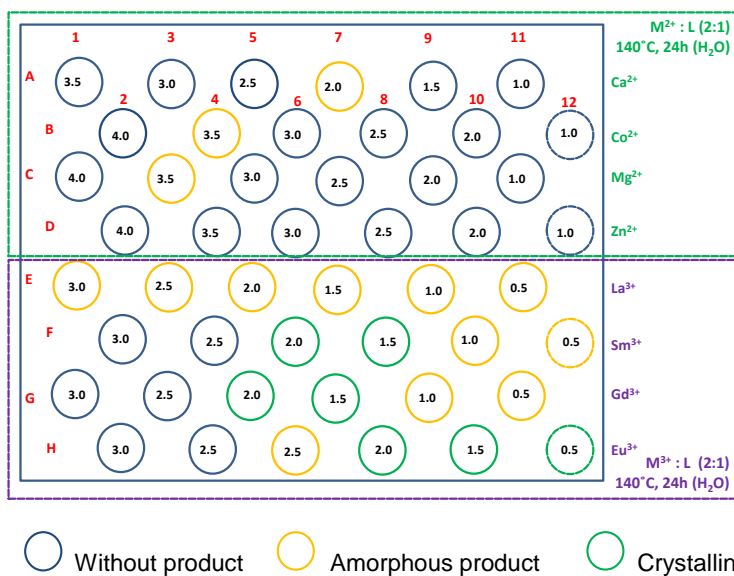
Scheme 2. Representation with synthesis conditions and results for metal derivatives of $(H_2O_3PCH_2)_2$-N-$(CH_2)_2SO_3H$ (DVb382). The number within the circle indicates the initial pH value.
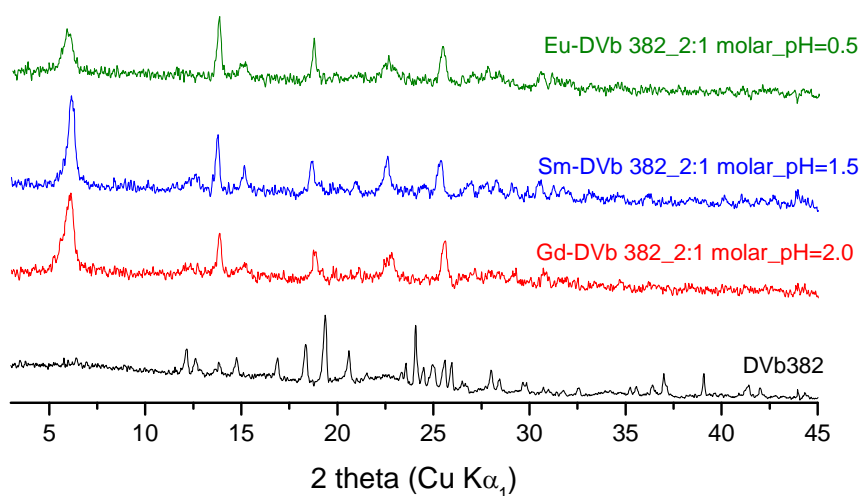

Figure 4.47. XRPD patterns for the obtained solids upon different conditions.

DISCLAIMER

I would like say that I am a member of a working group which has a vast experience in synthesis of metal phosphonates and characterization by diverse solid state techniques, particularly X-ray powder diffraction combined with Rietveld methodology. So, I would like to highlight my contribution to the synthesis of the reported compounds, except for those prepared from non-commercial organic ligands, as well as the complete characterization of all studied materials. Finally, I have also accomplished all photocatalytic and proton conductivity experiments reported in this work.

CHAPTER 5
CONCLUSIONS

CONCLUSIONS

1. Alkali-metal phosphonate compounds with the ligand *R,S* 2-hydroxyphosphonoacetic acid (HPAA) have been isolated by slow crystallization at room temperature. In ***M-HPAA*** series (M = Li$^+$, Na$^+$, K$^+$ and Cs$^+$), a gradual structural complexity is observed with increasing the size of the alkali metal ion, from one-dimensional (1D) to three-dimensional (3D). Thus, Li$^+$ derivative (Li$_3$(OOCCH(OH)PO$_3$)(H$_2$O)·H$_2$O, ***Li-HPAA***) is 1D, Na$^+$ compound (Na$_2$(OOCCH(OH)PO$_3$H)(H$_2$O)$_4$, ***Na-HPAA***) is pillared layered and those of K$^+$ (K$_2$(OOCCH-(OH)PO$_3$H)(H$_2$O)$_2$, ***K-HPAA***) and Cs$^+$ Cs(HOOCCH(OH)PO$_3$H, ***Cs-HPAA***) display 3D frameworks. These compounds exhibit different proton conductivities depending on the structural function of water and the internal hydrogen bond networks generated. ***Na-HPAA***, which shows structural disorder and contains both coordinated and uncoordinated water, exhibited the highest proton conductivity: 5.6×10^{-3} S·cm^{-1} at 24 °C and 98% relative humidity (RH). In addition, ***Cs-HPAA*** showed unusual ligand S-enantiomer enrichment.

2. Fe^{II}[HO$_3$PCH(OH)COO]·2H$_2$O, ***FeHPAA***, has been prepared from a hydrothermal reaction, slightly modified respect to that previously reported in the literature. This compound has been successfully proven as a photo-Fenton catalyst, for phenol mineralization under ultraviolet radiation (UVA). Using optimal reaction conditions, mineralization degrees up to 90% were attained for phenol as pollutant. XPS and chemical analysis of iron in solution revealed that upon UVA light exposure, the catalyst surface experiences chemical changes both, in the pre-activation stage and during the photocatalytic reaction. Other synthesis conditions have been successfully attempted and they are reported in this work.

On the other hand, **FeHPAA** exhibits also tunable proton conductivity. The bottom line conductivity of the as-synthesized material ($\sigma = 1.1 \times 10^{-5}$ $S \cdot cm^{-1}$) was increased by more than two orders of magnitude upon exposure to vapors from a concentrated NH_3 aqueous solution ($\sigma = 2.5 \times 10^{-3}$ $S \cdot cm^{-1}$, at 80 °C and 95% RH). Activation energy (E_a) values were in the range 0.31-0.36 eV, which is characteristic of a Grotthuss-type proton transfer mechanism.

3. $Ca_2[(HO_3PC_6H_3COOH)_2]_2[(HO_3PC_6H_3(COO)_2H)(H_2O)_2] \cdot 5$ H_2O (**Ca-PiPhtA-I**) shows an open 3D framework containing 1D channels occupied by lattice water. This arrangement creates an extended hydrogen bond network within the structure. Dehydration at 75 °C (**Ca-PiPhtA-II**) destroys partially this H-bond network and diminishes proton conductivity. Conversely, exposure the as-synthesized solid to ammonia vapors gave rise to a third material, **Ca-PiPhtA-NH₃**. The structural and spectroscopy data suggest that a new 2D framework with intercalated water and NH_3 species is obtained. This sample exhibits the highest proton conductivity in this series of compounds ($\sigma = 6.6 \times 10^{-3}$ $S \cdot cm^{-1}$, at 24 °C and 98% RH), and an Ea value (0.4 eV) corresponding to a Grotthuss-type mechanism.

4. Lanthanide derivatives of amino-*tris*-(methylenephosphonic) [$N(CH_2PO_3H_2)_3$, H_6AMP] were obtained by crystallization at room temperature. These materials, with formula: $Ln\{[(HN(CH_2PO_3H)_3(H_2O)_4]Cl\}$, (**Ln-AMP**) (Ln= La^{3+}, Pr^{3+}, Sm^{3+}, Gd^{3+}, Tb^{3+}, Dy^{3+} y Ho^{3+}), are isostructural and their crystal structure were solved/determined from single crystal data and/or by Rietveld refinement from powder diffraction data. These compounds display a 2D framework built up of positively charged sheets, with charge-compensating Cl^- ions and lattice water between layers. Besides showing photoluminescence properties, these compounds also

exhibited proton conductivity, as determined for **Gd-AMP** (σ = 3.96 $\times 10^{-4}$ S·cm^{-1}, at 80 °C and 95% RH) that showed a remarkably low activation energy of only 0.20 eV, once again indicative of a Grotthuss-type proton transfer mechanism.

5. Finally, preliminary results of metal derivatives with sulfophosphonate ligand $[(H_2O_3PCH_2)_2$-N-$(CH_2)_2SO_3H$ have been obtained by systematic synthesis procedures (high-throughput and microwave-assisted methodologies) but the resulting solids were amorphous or showed low crystallinity.

CAPÍTULO 5
CONCLUSIONES

CONCLUSIONES

1. Se ha sintetizado una familia de derivados metálicos del ácido *R,S* 2-hidroxifosfonoacético (HPAA) con elementos alcalinos mediante cristalización a temperatura ambiente. Por un lado, para los derivados alcalinos (Li^+, Na^+, K^+ y Cs^+) se ha investigado la relación directa existente entre el radio iónico y el incremento de la dimensionalidad, siendo 1D para el ($Li_3(OOCCH(OH)PO_3)(H_2O) \cdot H_2O$, *Li-HPAA*), láminas pilareadas para $Na_2(OOCCH(OH)PO_3H)(H_2O)_4$, *Na-HPAA*) y 3D para los sólidos $K_2(OOCCH-(OH)PO_3H)(H_2O)_2$, *K-HPAA* and $Cs(HOOCCH(OH)PO_3H$, *Cs-HPAA*. Todos los compuestos presentan conductividad protónica variable, fuertemente dependiente de la naturaleza estructural de las moléculas de agua (coordinadas o de cristalización) y de las redes de enlaces de hidrógeno establecidas. El *Na-HPAA* contiene tanto moléculas de agua de coordinación como de cristalización junto con un cierto desorden estructural en la disposición del ligando mostrando la más alta conductividad protónica, de 5.6×10^{-3} S·cm^{-1} a 24 °C y 98% de humedad relativa (HR). Adicionalmente para el *Cs-HPAA* se observó un inusual enriquecimiento del enantiómero (S-HPAA) del ligando a partir de una simple cristalización a temperatura ambiente.

2. Se ha reproducido la síntesis del sólido $Fe^{II}[HO_3PCH(OH)COO] \cdot 2H_2O$, (*FeHPAA*), mediante procedimientos alternativos más simples y medioambientalmente más amigables al previamente publicado. El FeHPAA se ha ensayado como un fotocatalizador Fenton eficiente para la mineralización de fenol bajo radiación UVA obteniéndose, en las óptimas condiciones de reacción, un grado de mineralización del 90% a 80 minutos. Los análisis por espectroscopia de fotoelectrones de rayos X (XPS) revelaron importantes

modificaciones químicas que se producen en la superficie del catalizador después de su pre-activación bajo UVA y en ausencia de fenol, así como después de la fotodegradación del fenol. Estas modificaciones aumentan la disponibilidad de especies de Fe(II) en la superficie del catalizador incrementando el grado de conversión de mineralización de fenol.

Por otro lado, se han obtenido algunos resultados preliminares con una familia de fosfonatos metálicos de hierro (II) obtenidos mediante la exposición del compuesto laminar *FeHPAA* a los vapores de NH_3 a diferentes tiempos de exposición. Este proceso tan simple conduce a un incremento de la conductividad de protones a 80 ºC y 95% de HR, pasando de $\sigma = 1.1 \times 10^{-5}$ S·cm^{-1}, para el sólido reciente sintetizado y sin exponer a vapores de amoniaco, a $\sigma = 2.5 \times 10^{-3}$ S·cm^{-1}, para el sólido con el mayor contenido de NH_3/H_2O (24 h de exposición). Los valores de las energías de activación (Ea) oscilan entre 0.31 a 0.36 eV, valores habituales para mecanismos de transferencia protónica tipo Grotthuss.

3. Se ha sintetizado el derivado cálcico del ácido 5-(dihidroxifosforil)isoftálico. $Ca_2[(HO_3PC_6H_3COOH)_2]_2[(HO_3PC_6H_3(COO)_2H)(H_2O)_2]\cdot5H_2O$, (*Ca-PiPhtA-I*), presenta un entramado tridimensional abierto y con canales 1D ocupados por moléculas de agua las cuales interaccionan por enlaces de hidrógeno. La deshidratación parcial del *Ca-PiPhtA-I* a 75 ºC conduce a la formación de una nueva fase, $Ca_2[(HO_3PC_6H_3COOH)_2]_2[(HO_3PC_6H_3(COO)_2H)(H_2O)_2]$, (*Ca-PiPhtA-II*), proceso que destruye parcialmente los enlaces de hidrógeno y disminuye los valores de conductividad del compuesto. Cuando el compuesto *Ca-PiPhtA-I* se expone a vapores de amoniaco concentrado se obteniéndose un nuevo derivado, *Ca-PiPhtA-NH₃*. Los datos estructurales y espectroscópicos sugieren la formación de un nuevo entramado

bidimensional con moléculas de H_2O y NH_3, siendo esta muestra la que presenta los valores de conductividad más altos, σ= 6.6 × 10^{-3} S·cm^{-1}a 24 ºC y 98% de humedad relativa, con una Ea=0,4 eV.

4. Se ha obtenido una familia de derivados del ácido amino-*tris*-(metilenfosfónico) (H$_6$AMP) por cristalización a temperatura ambiente. Estos materiales, con formula general Ln{[(HN(CH$_2$PO$_3$H)$_3$ (H$_2$O)$_4$]Cl}, (***Ln-AMP***) (Ln= La^{3+}, Pr^{3+}, Sm^{3+}, Gd^{3+}, Tb^{3+}, Dy^{3+} y Ho^{3+}) son isoestructurales y sus estructuras cristalinas han sido resueltas a partir de datos de monocristal y/o mediante afinamientos de Rietveld. Estos compuestos se caracterizan por presentan un entramado bidimensional, con láminas cargadas positivamente, y compensadas por la presencia de aniones Cl$^-$ y agua de cristalización entre las mismas. Para los estudios de impedancia se ha tomado como compuesto representativo de la serie el ***Gd-AMP***, obteniéndose unos valores de conductividad de σ= 3.96 × 10^{-4} S·cm^{-1} a 80 ºC y 95% HR. La baja energía de activación determinada, Ea= 0,20 eV, indica un mecanismo de transporte de protones tipo Grotthuss.

5. Finalmente, se han obtenido algunos resultados preliminares para el estudio del ácido sulfofosfónico (H$_2$O$_3$PCH$_2$)$_2$-N-(CH$_2$)$_2$SO$_3$H, (DVb382) con cationes de distinta carga. Estos estudios se han realizado aplicando una metodología de síntesis en paralelo, denominada High-throughput" o mediante síntesis asistida por microondas, si bien, los sólidos obtenidos fueron amorfos o de baja cristalinidad.

RESUMEN
(Spanish version)

RESUMEN

1. INTRODUCCIÓN.

Los materiales con ensamblaje metal-orgánico (metal organic frameworks, MOFs) son una subclase dentro de los denominados polímeros de coordinación (CPs), caracterizados por la unión química entre ligandos orgánicos y centros metálicos, que se puede extender en una, dos o tres dimensiones dependiendo de la coordinación metal-ligando establecida. En general son materiales cristalinos y, en muchos casos, presentar porosidad permanente. Las entidades orgánicas están formadas por ligandos di-, tri- o tetradentados que pueden ser grupos carboxilatos, imidazolatos, denominados genéricamente ZIFs (de sus siglas en inglés "Zeolite-like Imidazol Frameworks") y caracterizados por presentar entramados tipo zeolíticos, fosfonatos, sulfonatos, etc,. La química de estos materiales ha experimentado un crecimiento exponencial en los últimos años debido al gran número de posibles aplicaciones que pueden presentar. Dichas aplicaciones van desde el almacenamiento de gases, catálisis, intercambio iónico, conductividad protónica, magnetismo, fotoluminescencia, etc.

En cuanto a los fosfonatos metálicos, que es el tema objeto de estudio de la presente memoria, su base estructural reside en los enlaces de coordinación de ligandos fosfonatos, por ej. H_2PO_3-R −siendo R un grupo orgánico−, con cationes metálicos de, prácticamente, toda la tabla periódica. Comparativamente con otros grupos quelatos, la química de coordinación de los fosfonatos es menos predecible debido a que pueden coexistir, en un único cristal, varios modos de protonación (R-PO_3H_2, RPO_3H^- y R-PO_3^{2-}) y, por ende, varios modos de coordinación al centro metálico. Además, en muchos casos pueden presentar otros grupos

funcionales adicionales tales como grupos carboxilatos, sulfonaltos, hidroxilo, amino, etc. dando lugar a la familia de fosfonatos metálicos.

El desarrollo de la química de los fosfonatos metálicos ha transcurrido de forma paralela, aunque a un ritmo menos vertiginoso que la de los MOFs basados en carboxilatos, pasándose de una mera caracterización estructural, de los primeros sólidos, al diseño de materiales por selección apropiada de sus componentes para aplicaciones específicas.

Sin lugar a duda, una de las características que hacen de los fosfonatos metálicos un tema de investigación muy atractivo es la gran versatilidad estructural que presentan y que es consecuencia tanto de los constituyentes que los integran como de las condiciones de síntesis empleadas para su preparación. Esta diversidad estructural les confieren propiedades tan interesantes como: capacidad de adsorción de gases, adsorción selectiva de iones, intercambio iónico, propiedades luminiscentes, agentes anticorrosión, conductividad protónica, sólidos ácidos,…

La posibilidad de ajustar el tamaño de poros, en muchos casos, obteniéndose compuestos microporosos, abre nuevas vías para la utilización de estos MOFs de fosfonatos metálicos como adsorbente y para el almacenamiento/separación de gases. Sin embargo, a pesar de los numerosos fosfonatos porosos descritos en la bibliografía, son escasos los estudios de adsorción y posible almacenamiento de gases como H_2, CO_2, CH_4 o NO.

Por otra parte, el uso de fosfonatos metálicos como catalizadores heterogéneos puede ser otra importante aplicación de estos híbridos. Así, por ejemplo, diversos mono- y difosfonatos de Sn(IV) muestran buenas propiedades como ácidos de Brønsted en procesos oxidativos Baeyer-

Villiger, donde se produce la conversión de cetonas en esteres y de aldehídos en fenoles.

En cuanto a las posibles propiedades fotocatalíticas de estos materiales, apenas existen datos, pero a la vez, los que están disponibles en estos momentos resultan bastantes prometedores. Así, polifosfonatos (di-, tetra- y penta-fosfonatos) macroporosos de titanio muestran una alta actividad catalítica para la fotodescomposición de colorantes bajo irradiación con luz UV o visible, además de una elevada afinidad y selectividad hacia determinados cationes metálicos, propiedades que pueden resultar de gran utilidad en el tratamiento de aguas residuales. Por otra parte, estudios preliminares han demostrado que la incorporación de los grupos fosfonatos en TiO_2 contribuye a incrementar la actividad fotocatalítica para la degradación de colorantes, bajo radiación UV y visible, desplazando el umbral de absorción hacia la región del visible.

Además de la potencial aplicabilidad de los fosfonatos metálicos en los diversos campos anteriormente citados, otras características que han despertado el interés en estos materiales son sus propiedades luminiscentes y de conducción protónica, dado su posible uso en PEMFCs (de sus siglas en inglés "Proton Exchange Membrane Fuel Cells"). En relación a las primeras, existe una excelente revisión científica sobre las propiedades luminiscentes de fosfonatos metálicos, tanto de lantánidos como de elementos de transición. En ella se pone de relieve la posibilidad de diseñar nuevos emisores de luz que abarquen desde el azul hasta el IR, en base a la correcta selección del o de los cationes metálicos y del ligando organofosfonato que integren la estructura cristalina. Muchos fosfonatos metálicos, presentan estructuras cristalinas abiertas con moléculas de disolvente ocluidas. La eliminación de estas moléculas puede modificar radicalmente sus propiedades luminiscentes; por ejemplo, la emisión en el IR de muchos fosfonatos lantánidos queda impedida cuando

las moléculas de agua están presentes en la estructura; por otra parte, la intensidad relativa de los picos de emisión o la vida media del estado excitado puede alterarse como consecuencia de cambios en el entorno de coordinación del metal. Estos cambios pueden permitir el uso de estos materiales como sensores en aplicaciones específicas.

La necesidad de encontrar nuevos conductores protónicos que mejoren la eficiencia de las actuales pilas de combustible PEMFC, han incrementado el interés de los MOFs, en general, y de los ácidos fosfónicos y sus derivados metálicos, en particular, para este fin. Los fosfonatos metálicos presentan características inherentes que los convierten en candidatos prometedores. Muchos de estos sólidos tienen entramados robustos, lo que permite su modificación para generar sitios ácidos incrementándose notablemente la conductividad protónica, por ejemplo mediante procesos de sulfonación.

Los conductores protónicos basados en entramados metal-orgánicos se pueden clasificar en dos categorías: anhidros y los conductores protónicos, donde el transportador de protones son las moléculas de agua. En el caso de los materiales anhidros, la conducción de los H^+ se puede lograr por acumulación de moléculas orgánicas protonadas en los poros. Para el caso de los conductores protónicos mediados por moléculas de agua, se han descrito dos tipos de mecanismos: vehicular y Grotthuss. El mecanismo del tipo vehicular implica la difusión de un protón por parte de una especie portadora o grupos que contienen protones como son H_3O^+ o NH_4^+, estos grupos protonados actúan como vehículos para los protones. La especie que actúa como vehículo portador del protón se mueve a través de los canales presentes en la estructura del compuesto, mientras que las especies no protonadas se difunden en sentido contrario, dando como resultado una conducción de protones a través de procesos de difusión. El mecanismo tipo Grotthuss implica el movimiento de los protones a lo largo

de la una red infinita de enlaces de hidrógeno. El salto del protón continúa si tiene lugar una reordenación estructural concomitante. Los sitios aceptores de protones en las estructuras de los polímeros de coordinación no solo se limitan a la existencia de grupos funcionales presentes en la superficie de los compuestos. También pueden implicar la presencia de moléculas de disolvente o de algún tipo de molécula huésped dentro de los poros existentes. La conductividad protónica en el caso de los polímeros de coordinación no se limita a un solo tipo de mecanismo de conducción, sino que puede ser una combinación de los dos tipos de mecanismos. Para poder diferenciar cuál de los dos mecanismos está presente en el material se tiene en cuenta el análisis de las energías de activación (Ea) del proceso. De tal modo que un valor bajo de la energía de activación (0.1 – 0.4 eV) es característico de un mecanismo tipo Grotthuss, mientras que el mecanismo tipo vehicular es más dominante a valores de Ea altos (0.5 – 0.9 eV).

Por otra parte, el hecho de que estos polímeros de coordinación sean sólidos cristalinos puede permitir obtener información sobre el mecanismo de conducción que tiene lugar (Grotthus o transporte protónico), lo cual no es posible para los electrolitos macromoleculares debido a la pérdida del orden cristalino a largo alcance. Es más, estudios recientes en ácidos polifosfónicos revelan que la movilidad protónica está íntimamente relacionada con la cristalinidad y que depende fuertemente del ordenamiento supramolecular del compuesto. Además, muchos fosfonatos metálicos contienen grupos hidrogenofosfonatos coordinados a los centros metálicos, lo que implica la presencia de protones ácidos que pueden participar en el transporte protónico mediante interacciones de enlaces de hidrógeno entre sí o con otras moléculas que actúen como portadores (agua, NH_4^+). No obstante, aunque la presencia de grupos hidrogenofosfonatos aumentan la conducción pueden comprometer la

robustez estructural, por lo que es preferible el desarrollo de entramados 3D, frente estructura 2D y/o 1D, conteniendo estos grupos.

2. OBJETIVOS.

En la presente memoria se investigan las propiedades de conducción protónica, fotocatalíticas y fotoluminiscentes de fosfonatos metálicos multifuncionales, preparados por incorporación de iones metálicos activos y/o funciones orgánicas específicas en diferentes sistemas estructurales. Para estudiar las correlaciones existentes entre estructura y propiedades, los métodos de síntesis se han optimizado, con el propósito de obtener materiales que posean un elevado grado de cristalinidad.

La consecución de este objetivo principal se ha abordado mediante las siguientes etapas de trabajo:

- Síntesis de fosfonatos metálicos cristalinos mediante la combinación adecuada de uno de los tres ácidos fosfónicos empleados: $HO_2CCH(OH)PO_3H_2$ (HPAA), $C_6H_3(H_2PO_3)(CO_2H)_2$ (PiPhtA) o $N(CH_2PO_3H_2)_3$ (H_6AMP) y una sal de un metal, seleccionado según las propiedades que se desean investigar en cada caso (alcalinos: Li^+, Na^+, K^+ y Cs^+, alcalinotérreos: Ca^{2+} ; de transición: Fe^{2+}; o lantánidos: La^{3+}, Pr^{3+}, Sm^{3+}, Gd^{3+}, Tb^{3+}, Dy^{3+} y Ho^{3+}). También, se incluye un estudio preliminar usando otras funcionalidades orgánicas (grupos sulfónicos, por ejemplo, $(H_2O_3PCH_2)_2$-N-$(CH_2)_2SO_3H$) con el objeto de evaluar sus posibles efectos.

- Resolución estructural y caracterización química de los sólidos obtenidos. Para elucidar las estructuras cristalinas se emplea difracción de monocristal, cuando esto sea posible, y

difracción de rayos X de polvo, tanto de laboratorio como radiación sincrotrón. La caracterización química se realizará empleando un amplio abanico de técnicas instrumentales: ATD-TG, espectroscopía IR, UV-Vis, XPS, análisis elemental y microscopía SEM, entre otras.

■ Estudio de la fotodegradación de contaminantes ambientales presentes frecuentemente en las aguas naturales, como fenol, mediante el uso de un fosfonato de Fe(II) como fotocatalizador heterogéneo para procesos avanzados de oxidación. Se pretende determinar los parámetros que influyen en la fotooxidación y las condiciones óptimas de mineralización del contaminante orgánico seleccionado.

■ Estudio de las propiedades de conducción protónica en aquellos materiales cuya estructura presenta potenciales trayectorias de transferencia protónica, a través de redes de enlace de hidrógeno. Se determina la conductividad protónica y la energía de activación del proceso en un intervalo de temperaturas no superior a 100 ºC y diversas condiciones de humedad relativa. Estos datos se analizan estableciendo correlaciones con la estructura cristalina correspondiente. Finalmente, se investiga la reacción de los sólidos sintetizados con amoniaco en fase vapor, con el objeto de comprobar las modificaciones estructurales introducidas y su efecto sobre la conductividad protónica.

3. RESULTADOS Y DISCUSIÓN.

A continuación se resumen los principales resultados obtenidos para los diferentes fosfonatos metálicos estudiados.

3.1. Derivados alcalinos del ácido R,S 2-hidroxifosfonoacético.

Se ha sintetizado una familia de derivados alcalino-metálicos [(Li$_3$(OOCCH(OH)PO$_3$)(H$_2$O)·H$_2$O, **Li-HPAA**), (Na$_2$(OOCCH(OH)PO$_3$H) (H$_2$O)$_4$, **Na-HPAA**), (K$_2$(OOCCH-(OH)PO$_3$H)(H$_2$O)$_2$, **K-HPAA** y Cs(HOOCCH(OH)PO$_3$H, **Cs-HPAA**); **M-HPAA**]. Estos sólidos se han obtenido por combinación del ácido comercial *R,S* 2-hidroxifosfonoacético (HO$_2$CCH(OH)PO$_3$H$_2$, HPAA) con los correspondientes hidróxidos alcalinos (LiOH y KOH) o las sales metálicas (NaCl y CsCl). Todos los compuestos se prepararon a temperatura ambiente en disolución acuosa o en una mezcla H$_2$O/DFM a un pH próximo a 2 y utilizando siempre un ligero exceso de la sal metálica o hidróxido alcalino respecto al ácido fosfónico.

La estructura cristalina de todos los compuestos obtenidos pudo ser resuelta por monocristal, excepto en el caso de **Li-HPAA**, cuya estructura se resolvió *ab initio* mediante difracción de polvo, afinándose la estructura obtenida por aplicación del método de Rietveld. En dicha serie de compuestos **M-HPAA** (M = Li$^+$, Na$^+$, K$^+$ y Cs$^+$) se observa una gradual complejidad estructural, desde monodimensional (1D) hasta tridimensional (3D). Dicho incremento en la complejidad estructural va acompañado de un aumento del tamaño del ion metálico alcalino. Así, el derivado de Li$^+$ ((Li$_3$(OOCCH(OH)PO$_3$)(H$_2$O)·H$_2$O **Li-HPAA**) es 1D, el de Na$^+$ (Na$_2$(OOCCH(OH)PO$_3$H)(H$_2$O)$_4$, **Na-HPAA**) contiene láminas entre pilares y los de K$^+$ y Cs$^+$ (K$_2$(OOCCH(OH)PO$_3$H)(H$_2$O)$_2$, **K-HPAA**) y (Cs(HOOCCH(OH)PO$_3$H, **Cs-HPAA**) son 3D. Un dato a subrayar es el desorden estructural que presenta **Na-HPAA,** atribuido a la existencia de un exceso enantiomérico (~ 20%) del ligando *R,S*-HPAA en la estructura del compuesto.

Destacar también que el compuesto Cs(HOOCCH(OH)PO$_3$H, **Cs-HPAA**, presenta un inusual enriquecimiento del enantiómero *S*-HPAA,

cuando se obtiene el sólido por cristalización lenta a temperatura ambiente. Para poder confirmar la quiralidad del derivado de Cs, se realizó un estudio por espectroscopía de dicroísmo circular electrónico (Electronic Circular Dichroism, ECD) asistido por métodos computacionales. Los resultados del estudio del **Cs-HPAA** en disolución acuosa mostraron una señal negativa a 210 nm, que no se aprecia en las muestras de referencia (disolución de ácido *R,S*-HPAA y el *R,S*-CsHPAA obtenido por precipitación rápida). Adicionalmente, mediante métodos computacionales y tomando como base los datos cristalográficos del **Cs-HPAA** se pudo obtener un espectro simulado de ECD en el cual se aprecia una señal entre 200 y 300 nm, confirmándose la presencia de un exceso del enantiómerico en la muestra de **Cs-HPAA** obtenida por cristalización lenta a temperatura ambiente. Por tanto, **Cs-HPAA** constituye un ejemplo notable de enriquecimiento enantiomérico espontáneo a partir de una mezcla racémica.

Por otro lado, la serie de compuestos **M-HPAA** ha sido estudiada por espectroscopía de impedancia electroquímica (Electrochemical Impedance Spectroscopy, EIS). A partir de la información obtenida de las medidas EIS se pueden conocer propiedades del material, como por ejemplo la conductividad protónica de aquellos materiales cuya estructura presenta potenciales trayectorias de transferencia protónica, a través de redes de enlace de hidrógeno. La impedancia es, por tanto, una magnitud compleja que se puede expresar en su componente real e imaginaría:

$$Z(t) = |Z|(\cos\varphi + j\,\mathrm{sen}\varphi) = Z'(w) + jZ''(w)$$

La representación gráfica de la parte imaginaria de la impedancia Z'' ($\Omega \cdot cm$) frente a la parte real Z'($\Omega \cdot cm$), se conoce como diagramas de Nyquist.

Los compuestos de la serie **M-HPAA** se caracterizan por presentar una conductividad protónica variable, dependiente de la función estructural

de las moléculas de agua y las redes de enlaces de hidrógeno internas. Así, **Na-HPAA**, conteniendo tanto agua coordinada como no coordinada, muestra el valor más alto de conductividad protónica de la serie: 5.6×10^{-3} S·cm⁻¹, a 24 °C y 98% de humedad relativa (HR) frente a 3.5×10^{-5} S·cm⁻¹ observado para el **Cs-HPAA**. Obteniéndose unos valores de Ea para **Na-HPAA** (0.39 eV) y **Cs-HPAA** (0.40 eV) dentro del rango establecido para un mecanismo por transferencia protónica tipo Grothuss (0.1 - 0.4 eV).

Comparando los valores de conductividad de los sólidos **M-HPAA** de mayor dimensionalidad (Na⁺, K⁺ y Cs⁺), los valores obtenidos son consistentes con la presencia de grupos ácidos y un contenido creciente en moléculas de agua, las cuales actúan como portadores de protones. De hecho, la presencia de moléculas de agua de cristalización mejora aún más las vías de transferencia de protones, como se observa para **Na-HPAA**. Además, el desorden estructural que presenta este sólido también podría contribuir a mejorar la conductividad. La presencia de redes extendidas de enlaces de hidrógeno en estos sólidos contribuye a definir diferentes vías de transferencia de protones. A pesar de la naturaleza anhidra de **Cs-HPAA**, éste todavía exhibe una conductividad residual, similar a la mostrada por otros polímeros de coordinación. En este caso, existen trayectorias de corto recorrido de transporte de protones en la estructura debido a los fuertes enlaces de hidrógeno que se establecen entre grupos -P-OH y –COOH vecinos, así como por la presencia de protones situados a distancias equidistantes entre grupos fosfonato y carboxilato. **K-HPAA** tiene sin embargo un comportamiento intermedio entre los derivados de Na y Cs y, por lo tanto, un valor de conductividad intermedia (1.3×10^{-3} S·cm⁻¹). La falta de agua de cristalización en **K-HPAA** hace la conducción de protones más difícil, por lo que se produce por un mecanismo vehicular (Ea> 0.5 eV). De modo diferente, la conducción de protones en los derivados de Na y Cs se produce por un mecanismo tipo

Grotthuss, corroborado por el más bajo valor de la energía de activación encontrado para estos sólidos. La baja conductividad medida para el *Li-HPAA*, 1.1×10^{-4} S·cm^{-1}, en comparación con la de los derivados de K y Na, puede ser debido principalmente a la ausencia de grupos ácidos y la baja movilidad de las moléculas de agua fuertemente coordinado en el *Li-HPAA*. Dicho valor está, sin embargo, muy cerca de los publicados para algunos tetrafosfonatos divalente con entramados monodimensionales (1D) y en los que también está implicado un mecanismo vehicular.

Con objeto de descartar la contribución de iones Na$^+$ a la conductividad iónica medida, se realizó un estudio completo del compuesto utilizando electrodos no polarizantes y bajo diferentes corrientes de H$_2$-Ar al 5% y H$_2$ al 100%. Dicho estudio reveló la ausencia de conducción de iones alcalinos, ya que no se apreció la presencia de fenómenos de electrodo en los espectros de impedancia obtenidos bajo dichas condiciones de trabajo *(Bazaga-García et al., 2015)*.

3.2. *Derivados de Fe(II) del ácido R,S 2-hidroxifosfonoacético: actividad fotocatalítica y conductividad protónica.*

Se han realizados estudios de fotodegradación de contaminantes ambientales presentes frecuentemente en las aguas naturales mediante el uso de fosfonato de Fe(II) como fotocatalizador heterogéneo para procesos avanzados de oxidación (Advanced Oxidation Processes, AOPs).

La actividad fotocatalítica de estos materiales se ha determinado mediante la técnica analítica del Carbono Orgánico Total (TOC). Dicha técnica de análisis se basa en la determinación de la concentración de carbono disuelto en las muestras, obteniéndose el valor correspondiente de la concentración de TOC como una diferencia entre las concentraciones del carbono total disuelto (TC) y el carbono inorgánico disuelto (IC). Para

un correcto seguimiento de la evolución de la concentración de TOC presente en el medio, se han tomado una serie de alícuotas a diferentes tiempos de reacción. También se ha determinado la presencia de compuestos intermedios en el medio de reacción a lo largo de los ensayos fotocatalíticos, mediante cromatografía de líquidos acoplada a espectrometría de masas (HPLC-MS).

Mediante un procedimiento alternativo al publicado previamente en bibliografía, se ha obtenido por reacción hidrotermal la síntesis del compuesto laminar $Fe^{II}[HO_3PCH(OH)COO]\cdot 2H_2O$ (**FeHPAA**). El sólido obtenido (**FeHPAA**) se caracterizó inicialmente por difracción de rayos-X, análisis térmico diferencial y termogravimétrico (ATD-TG), espectroscopia infrarroja con transformada de Fourier (FTIR), con objeto de demostrar la validez del método de síntesis, el cual permite reducir los tiempos de reacción de 4 a 2 días.

Este compuesto se comporta como catalizador foto-Fenton en la mineralización de fenol, bajo radiación ultravioleta (UVA) y en presencia de H_2O_2. Después de investigar las condiciones óptimas de reacción (pH, concentración de catalizador, concentración de H_2O_2, tamaño de partículas, etc.), se alcanzó un grado de mineralización de fenol del 90% a los 80 minutos de ensayo fotocatalítico bajo radiación UVA. Mediante estudios de difracción de rayos-X y espectroscopía Mössbauer se ha demostrado que el compuesto globalmente considerado no experimenta cambios químicos importantes. Sin embargo, la superficie del catalizador sí experimenta cambios químicos en la fase de pre-activación bajo UVA (en presencia de una concentración mínima de H_2O_2) así como al final del proceso de fotodegradación del fenol. Los cambios superficiales mostrados por espectroscopia de fotoelectrones de rayos X (XPS) sugieren una mayor presencia de Fe^{2+} superficial, y por tanto de sitios activos, lo que aumenta la oxidación de fenol. Además, mediante estudios de

cromatografía de líquidos acoplada a espectrometría de masas (HPLC-MS) se ha podido descartar la presencia de productos intermedios de mayor peligrosidad medioambiental como pueden ser los obtenidos por polimerización de los derivados fenólicos a lo largo de los ensayos fotocatalíticos. También se ha podido verificar la presencia de compuestos intermedios ya descritos en bibliografía (hidroquinona, catecol o benzoquinona), los cuales están presentes en los primeros tiempos de los ensayos fotocatalíticos como producto de la degradación de fenol. También se obtuvieron señales de otros compuestos tales como ácido fórmico o ácido oxálico procedentes de la completa o parcial mineralización del fenol *(Bazaga-García et al., 2012)*.

Este mismo compuesto, $Fe^{II}[HO_3PCH(OH)COO]\cdot2H_2O$ (*FeHPAA*), también se ha preparado a reflujo durante 24 h para reducir el coste energético al disminución del tiempo y temperatura de reacción, el consumo de reactivos y eliminando la reactivos nocivos para el medio ambiente como el NaF, utilizado en la síntesis original. El sólido obtenido fue caracterizado por las técnicas habituales confirmándose que se trata del mismo compuesto que el previamente reportado.

La presencia de grupos ácidos y de moléculas de agua en el sólido *Fe-HPAA*, nos condujo a estudiar también sus propiedades como conductor protónico. El valor de conductividad determinado a 80 ºC y 98 % de humedad relativa fue de $\sigma=1.1 \times 10^{-5}$ S·cm^{-1} con una Ea de 0.36 eV. Con objeto de incrementar su valor de conductividad, el sólido obtenido se expuso a vapores de NH_3 a partir de una disolución acuosa concentrada del mismo (28% de NH_3) a diferentes tiempos (1, 5, y 24 horas). Los diferentes derivados, *(NH₃/H₂O)-FeHPAA_xh*, han sido caracterizados mediante difracción de rayos X y se ha determinado el contenido de material amorfo/no difractante, adicionando ZnO (20 % w/w) como estándar interno. Los resultados de los afinamientos indican que la fracción

cristalina correspondiente al **Fe-HPAA** prácticamente permanece constante para tiempos de exposición comprendidos entre 1 y 24 horas, no apreciándose cambios importantes en los parámetros de celda. Ello sugiere que no está teniendo lugar reacciones de intercalación del NH_3/H_2O en el espacio interlaminar sino que estas especies, cuyo contenido se incrementa conforme a los datos de análisis elemental y termogravimétrico, se están incorporando a la fase amorfa del compuesto. Una caracterización completa de esta familia de compuestos está en curso.

Los diferentes derivados **(NH₃/H₂O)-FeHPAA_xh** se han ensayado como conductores protónicos observándose un aumento de más de dos órdenes de magnitud en la conductividad protónica, llegando a ser ésta de 2.5×10^{-3} S·cm^{-1}, a 80 ºC y 95% de humedad relativa, para la muestra expuesta a vapores de amoniaco durante 24 h y de composición $Fe[HO_3PCH(OH)COO]^-(H_2O)_{3.2}(NH_3)_{1.1}$. Los valores de la energía de activación (Ea) para la muestras expuestas a distintos tiempos oscilaron en el rango de 0.32 y 0.36 eV, valores que se corresponden con un mecanismo de transferencia protónica tipo Grotthuss.

3.3. Síntesis, caracterización estructural y propiedades de 5-(dihidroxifosforil)isoftalato de calcio.

Dado que la coexistencia de grupos ácidos y agua en las cavidades del entramado estructural favorece las interacciones de enlace de hidrógeno y, por tanto, las propiedades de conducción protónica, se han investigado sistemas órgano-inorgánicos con cavidades internas donde se cumplan tales condiciones. Un ejemplo lo constituye el compuesto $Ca_2[(HO_3PC_6H_3COOH)_2]_2[(HO_3PC_6H_3(COO)_2H)(H_2O)_2]\cdot5H_2O$ (**Ca-PiPhtA-I**) el cual se aisló en medio acuoso por cristalización a temperatura ambiente,

utilizando una relación molar ligando:Ca^{2+} de 1:1 y un pH~3.0. En este caso, el ligando orgánico usado como precursor, el ácido 5-(dihidroxifosforil)isoftálico $(C_6H_3(H_2PO_3)(CO_2H)_2$, PiPhtA), se preparó previamente, mediante síntesis de laboratorio, a partir del ácido 5-aminoisoftálico. El compuesto **Ca-PiPhtA-I** cristaliza en el sistema ortorrómbico, grupo espacial *Pca2₁*, y con parámetros de celda de a=23.112(4) Å, b=6.9534(13) Å, c=22.638(4) Å y V=3638.1(12) $Å^3$. Su estructura cristalina se resolvió a partir de datos de monocristal y contiene dos átomos de Ca, tres ligandos PiPhtA y siete moléculas de H_2O, en la parte asimétrica de la celda unidad. El entorno de coordinación de los átomos de calcio es una bipirámide pentagonal. Este sólido se caracteriza por presentar un entramado tridimensional abierto y con canales 1D ocupados por moléculas de agua entre las que se establecen interacciones de enlace de hidrógeno.

A partir de este sólido se obtuvieron otros dos nuevos compuestos. El primero de ellos, por deshidratación parcial a 75 ºC, con fórmula: $Ca_2[(HO_3PC_6H_3COOH)_2]_2[(HO_3PC_6H_3(COO)_2H)(H_2O)_2]$, (**Ca-PiPhtA-II**). Su estructura cristalina fue obtenida por afinamiento Rietveld de datos de sincrotrón, utilizando como modelo de partida la estructura cristalina del **Ca-PiPhtA-I** y reduciendo la simetría del grupo espacial ortorrómbico *Pca2₁* al monoclínico *Pa*.

El segundo derivado, con fórmula: $Ca_2[(HO_3PC_6H_3COOH)_2]_2[(HO_3PC_6H_3(COO)_2H)(H_2O)_2]·14H_2O$ $(NH_3)_7$, (**Ca-PiPhtA-NH₃**), se obtuvo por exposición de la muestra inicial (**Ca-PiPhtA-I**) a vapores de amoniaco concentrado y sin deshidratación previa. Este sólido presenta un complejo difractograma de rayos-X con picos de difracción a 15.3 y 13 Å, atribuidos al espaciado basal de una nueva fase laminar obtenida por la ruptura parcial de los enlaces interlaminares fosfonato/Ca^{2+} o carboxilato/Ca^{2+} del compuesto de partida **Ca-PiPhtA-I**. El

estudio por espectroscopia infrarroja con transformada de Fourier (FTIR) de los compuestos *Ca-PiPhtA-I* y *Ca-PiPhtA-NH₃* reveló profundos cambios estructurales en este último, en comparación con el compuesto de partida. Los datos de FTIR indican la existencia de fuertes enlaces de hidrogeno entre las moléculas de agua y NH_3 intercaladas en el compuesto laminar *Ca-PiPhtA-NH₃*.

Un tercer derivado, *Ca-PiPhtA-III*, se obtuvo por tratamiento de la muestra de *Ca-PiPhtA-I* a 40 ºC durante 2 horas, y posterior estabilización a temperatura ambiente y humedad relativa controlada (98% HR) Si bien este tratamiento no implica cambios de composición, sí conlleva variaciones estructurales y texturales con respecto al compuesto de partida, *Ca-PiPhtA-I*.

Los tres derivados cálcicos aislados fueron estudiados por espectroscopía de impedancia para determinar sus propiedades de conductividad protónica. Siendo el compuesto con NH_3 adsorbido, *Ca-PiPhtA-NH₃*, el que mostró la conductividad protónica más alta, $\sigma = 6.6 \times 10^{-3}$ S·cm^{-1}, a 24 ºC y 98% de humedad relativa, con un valor de Ea = 0.4 eV *(Bazaga-García et al., 2014)*. Además, se comprobó que el pretratamiento de la muestra a 40 ºC es efectivo para mejorar el transporte protónico, ya que origina un aumento en la conductividad, que varía desde 5.7×10^{-4} S·cm^{-1}, en **Ca-PiPhtA-I**, a 1.3×10^{-3} S·cm^{-1} en **Ca-PiPhtA-III**, todos los valores determinados a 24 ºC y 98% de humedad relativa. La menor conductividad se observó para el compuesto parcialmente deshidratado a 75 ºC, **Ca-PiPhtA-II**, con un valor de 3.6×10^{-4} S·cm^{-1}.

Estos resultados ponen de manifiesto la importancia de las interacciones de enlace de hidrógeno y su efecto sobre las propiedades de conductividad de los materiales, al menos en el caso de esta serie de compuestos. Por último, resaltar también, a partir de este estudio, que generar nuevas estructuras con cavidades internas, donde sea posible

alojar diversas moléculas huésped de diferente naturaleza química, puede resultar una estrategia general de establecer innumerables trayectorias de transferencia protónica; observándose, en muchos casos, mayor conductividad, en los productos derivados que en los materiales de partida.

3.4. Derivados lantánidos del ácido amino-tris-(metilenfosfónico).

Se ha elegido el ácido amino-*tris*-(metilenfosfónico), $(N(CH_2PO_3H_2)_3$, $H_6AMP)$, uno de los ácidos fosfónicos comerciales más frecuentemente utilizados, especialmente como inhibidor de la corrosión de metales, para la preparación de una familia de derivados lantánidos. Estos compuestos, a diferencia de otros descritos en la bibliografía, se han obtenidos por cristalización a temperatura ambiente, haciendo reaccionar al ácido fosfónico con el nitrato del lantánido correspondiente en una relación molar ligando:metal 5:1 y a pH<1. Los materiales sintetizados responden a la estequiometría general $Ln\{[(HN(CH_2PO_3H)_3(H_2O)_4]Cl\}$, (**Ln-AMP**) (Ln= La^{3+}, Pr^{3+}, Sm^{3+}, Gd^{3+}, Tb^{3+}, Dy^{3+} y Ho^{3+}). Todos los compuestos de la familia **Ln-AMP** son isoestructurales y cristalizan en el grupo espacial *Cc*. De todos ellos, sólo los compuestos **La-AMP**, **Pr-AMP** y **Ho-AMP** se obtuvieron en forma de monocristal, mientras que para los restantes miembros de la serie se obtuvieron únicamente muestras policristalinas. La estructura cristalina de estos últimos se determinó mediante afinamiento de Rietveld y usando como modelo de partida la estructura cristalina del La-AMP. Esta familia de compuestos se caracteriza, desde el punto de vista estructural, por presentar un entramado bidimensional, con láminas cargadas positivamente, y compensadas por la presencia de aniones Cl⁻ y agua de cristalización entre las mismas.

Sus propiedades como conductores prótonicos se han evaluado, de manera preliminar, eligiendo el derivado de Gd como sólido representativo

de la serie. Los resultados de espectroscopía de impedancia dieron como resultado una conductividad de σ= 3.96 × 10^{-4} S·cm^{-1} a 80 ºC y 95% de humedad relativa. La baja energía de activación determinada, Ea= 0.20 eV; indica un mecanismo de transporte de protones tipo Grotthuss.

Además, se estudiaron las propiedades fotoluminiscentes de la serie completa de derivados *Ln-AMP*. Los resultados más relevantes se obtuvieron con los compuestos *Pr-AMP* y *Tb-AMP*. La transiciones observadas asociadas con fuertes bandas de absorción son solo atribuidas al tipo *f-f*, propia de los iones lantánidos, ya que el ligando orgánico trifosfonato no presenta ni propiedades de absorción en el UV-visible ni luminiscencia *(Bazaga-García et al., 2015, resultados no publicados)*.

3.5. Derivados metálicos del ácido (H$_2$O$_3$PCH$_2$)$_2$-N-(CH$_2$)$_2$SO$_3$H.

Un ácido sulfofosfónico no comercial (H$_2$O$_3$PCH$_2$)$_2$-N-(CH$_2$)$_2$SO$_3$H), DVb382, ha sido elegido como ejemplo de ácido fosfónico polifuncional, con grupo sulfónico, para investigar las propiedades resultantes de su combinación con diferentes iones metálicos. Su reactividad con iones metálicos se ha ensayado considerando diferentes variables de síntesis: relación molar ligando:metal, pH, disolventes, temperatura, tiempo de reacción, etc.,. Para ello se han empleado una metodología "high-throughput" y la síntesis por microondas, con la colaboración del grupo del profesor N. Stock del Instituto de Química Inorgánica de la Universidad Christian-Albrechts (CAU) de Kiel (Alemania). La metodología high-throughput permite la optimización de las variables de reacción, ya que se pudieron realizar de forma simultánea y en paralelo entre 24 y 48 síntesis diferentes. Para los realizados se han empleado tanto metales divalentes alcalinos-térreos (Ca, Mg) como de transición (Co, Zn) y elementos lantánidos (La, Sm, Gd y Eu). Para los metales divalentes alcalinos-térreos

y de transición se estudiaron diferentes relaciones molares M^{2+}/DVb382 (1:2, 1:1, 2:1 y 1.5:1), así como diferentes valores de pH inicial (0.5, 1.0, 1.5, 2.0, 2.5 y 3.0) bajo condiciones hidrotermales a 140 ºC y 160 ºC. Similares condiciones se utilizaron también para las síntesis por microondas. Sin embargo, e independientemente del método de síntesis ensayado, sólo se obtuvieron sólidos amorfos o con muy baja cristalinadad. En el caso de los derivados lantánidos, se emplearon las mismas condiciones de reacción indicadas para los metales divalentes alcalinos-térreos y de transición pero con una relación molar M^{3+}/DVb382 =2:1. El valor de pH inicial fue igual o inferior 2 y los ensayos hidrotermales se realizaron a 140 ºC durante 16 horas. Sólo los derivados de Sm, Eu y Gd eran sólidos semicristalinos. Una caracterización más completa de los mismos está todavía en curso.

Si bien los materiales obtenidos son todavía amorfos o de baja cristalinidad, la experiencia adquirida en síntesis de MOFs, mediante la metodología sistemática de "High-throughput", es considerada de gran valor por las posibilidades que ofrece de cara a la síntesis de fosfonatos metálicos cristalinos que requieran una profunda optimización de las condiciones de síntesis en un periodo de tiempo corto, y lo que ello supone de ahorro de costes en procedimientos de síntesis de materiales. Este es un activo que se ha incorporado a los métodos de rutina desarrollados en la Universidad de Málaga.

Me gustaría resaltar que pertenezco a un grupo de trabajo que tiene una amplia experiencia en la síntesis de fosfonatos metálicos y caracterización mediante diversas técnicas de estado sólido, en especial la difracción de rayos X combinada con la metodología Rietveld. Por lo tanto, me gustaría destacar mi contribución en la síntesis de los compuestos estudiados, a excepción de los preparados a partir ligandos orgánicos no

comerciales, así como la caracterización completa de todos los materiales estudiados. Por último, también he realizado todos los experimentos fotocatalíticos y de conductividad protónica de los correspondientes fosfonatos metálicos presentados en este trabajo.

REFERENCES

REFERENCES

A

- Abrahams, B.F.; Hoskins, B.F.; Michail, D.M.; Robson, R., *Nature* **1994**, *369*, 727-729.

- Adán, C.; Carbajos, J.; Bahamonde, A.; Oller, I.; Malato, S.; Martínez-Arias, A. *Appl. Catal., B* **2011**, *108-109*, 168-176.

- Adani, F.; Casciola, M.; Jones, D.J.; Massinelli, L.; Montoneri, E.; Roziere, L.; Vivani, R. *J. Mater. Chem.* **1998**, *8*, 961-964.

- Agmon, N. *Chem. Phys. Lett.* **1995**, *244*, 456-462.

- Ai, L.; Zhang, C.; Jiang, J. *Appl. Catal., B* **2014**, *148-149*, 191-200.

- Alberti, G.; Casciola, M.; Costantino, U.; Peraio, A.; Montoneri, E., *Solid State Ionics* **1992a**, *50*, 315-322.

- Attfield, M.P.; Mendieta-Tan, C.; Telchadder, R.N; Roberts, M.A., *RSC Adv.* **2012**, *2*, 10291-10297.

- Attfield, M.P.; Yuan, Z.; Harvey, H.G.; Clegg, W., *Inorg. Chem.* **2010**, *49*, 2656-2666.

B

- Batten, S. R.; Champness, N. R.; Chen, X.-M.; Garcia-Martinez, J.; Kitagawa, S.; Öhrström, L.; O'Keeffe, M.; Suh, M.P.; Reedijk, J. *CrystEngComm* **2012**, *14*, 3001-3004.

- Batten, S. R.; Champness, N. R.; Chen, X.-M.; Garcia-Martinez, J.; Kitagawa, S.; Öhrström, L.; O'Keeffe, M.; Suh, M.P.; Reedijk, J. *Pure Appl. Chem.* **2013**, *85*, 1715-1724.

- Bauer, S; Stock, N. *Angrew. Chem. Int. Ed.* **2007a**, *46*, 6857-6860.

- Bauer, S; Stock, N. *J. Solid State Chem.* **2007b**, *180*, 3111-3120.

- Beier, M.J.; Kleist, W.; Wharmby, M.T.; Kissner, R.; Kimmerle, b.; Wright, P.A.; Grunwaldt, J.D.; Baiker, A. *Chem. Eur. J.* **2012**, *18*, 887-898.

- Bilal, N.; Ali, S.; Iqbal, M., *Asian J. Chem.* **2014**, *26*, 1882-1886.

- Bozzi, A.; Yuranova, T.; Mielczarski, J.; Kiwi, J.; *New J. Chem.* **2004**, *28*, 519-526.

- Brunet, E.; Colón, J.L.; Clearfield, A., *Tailored Organic-Inorganic Materials*, Eds. John Wiley & Sons, Inc. **2015**.

- Bureekaew, S.; Shimomura, S.; Kitagawa, S., *Sci. Technol. Adv. Mat.* **2008**, *9*, 014108.
- Burwell, D.A.; Thompson, M.E., *Chem. Mat.* **1991**, *3*, 14-17.

C

- Cabeza, A.; Aranda, M.A.G., in *Metal phosphonate chemistry: From synthesis to applications*, Eds. Clearfield, A.; Demadis,

K.D., The Royal Society of Chemistry: London **2012**, Ch. 4, p. 107-132.

- Cabeza, A.; Aranda, M.A.G.; Bruque, S. *J. Mater. Chem.* **1999**, *9*, 571-578.

- Cabeza, A.; Bruque, S.; Guagliardi, A.; Aranda, M.A.G. *J.Solid State Chem.* **2001**, *160*, 278-286.

- Cabeza, A.; Olivera-Pastor, P.; Colodrero, R.M.P., in *Organic-Inorganic Materials*, Eds. Brunet, E.; Colón, J.L.; Clearfield, A., Ed. John Wiley & Sons, Inc. **2015**, DOI: 10.1002/9781118792223, Ch. 4.

- Cabeza, A.; Ouyang, X.; Sharma, C.V.K.; Aranda, M.A.G.; Bruque, S.; Clearfield, A. *Inorg. Chem.* **2002**, *41*, 2325-2333.

- Cao, D.K.; Li, Y.Z.; Song, Y.; Zheng, L.M., *Inorg. Chem.* **2005**, *44*, 3599-3604.

- Chaplais, G.; Le Bideau, J.; Leclercq, D.; Vioux, A. *Chem. Mater.* **2003**, *15*, 1950−1956.

- Clearfield, A., *Metal Phosphonate Chemistry. Progress in Inorganic Chemistry*, Ed. Karlin, K.D., John Wiley & Sons Inc. **1998**, Vol. 47, 371-509.

- Clearfield, A; Demadis, K.D., in *Metal Phsphonate Chemistry: From Synthesis to Applications*, Eds. RSC: Cambridge, U.K., **2012**.

- Colodrero, R.M.P.; Cabeza, A.; Olivera-Pastor, P.; Infantes-Molina, A.; Barouda, E.; Demadis, K.D.; Aranda, M.A.G. *Chem. Eur. J.* **2009**, *15*, 6612-6618.

- Colodrero, R.M.P.; Cabeza, A.; Olivera-Pastor, P.; Papadaki, M.; Rius, J.; Choquesillo-Lazarte, D.; García-Ruiz, J.M.; Demadis, K.D.; Aranda, M.A.G. *Cryst. Growth Des.* **2011**, *11*, 1713-1722.

- Colodrero, R.M.P.; Olivera-Pastor, P.; Cabeza, a.; Papadaki, M.; Demadis, K.D.; Aranda, M.A.G. *Inorg. Chem.* **2010**, *49*, 761-768.

- Colodrero, R.M.P.; Olivera-Pastor, P.; Losilla, E.R.; Aranda, M.A.G.; León-Reina, L.; Papadaki, M.; McKinlay, A.C.; Morris, R.E.; Demadis, K.D.; Cabeza, A. *Dalton Trans.* **2012a**, *41*, 4045-4051.

- Colodrero, R.M.P.; Olivera-Pastor, P.; Losilla, E.R.; Hernández-Alonso, D.; Aranda, M.A.G.; León-Reina, L.; Rius, J.; Demadis, K.D.; Moreau, B.; Villemin, D.; Palomino, M.; Rey, F.; Cabeza, A. *Inorg. Chem*. **2012b**, *51*, 7689-7698.

- Colodrero, R.M.P.; Papathanasiou, K.E.; Stavgianoudaki, N.; Olivera-Pastor, P.; Losilla, E.R.; Aranda, M.A.G.; León-Reina, L.; Sanz, J.; Sobrados, I.; Choquesillo-Lazarte, D.; García-Ruiz, J.M.; Atienzar, P.; Rey, F.; Demadis, K.D.; Cabeza, A. *Chem. Mater.* **2012c**, *24*, 3780-3792.

- Colomban, P., in *Proton conductors: Solids, Membranes and Gels Materials and Derives. Chemistry of Solid State Materials*; Cambridge University Press: Cambridge, U.K., **1992**.

- Colomban, P.; Novak, A. *J. Mol. Struct.* **1988**, *177*, 277-308.

- Costantino, F.; Donnadio, A.; Casciola, M. *Inorg. Chem.* **2012**, *51*, 6992-7000.

- Costantino, F.; Ienco, A; Gentili, P.L.; Presciutti, F. *Cryst. Growth Des.* **2010**, *10*, 4831-4838.

- Cunha-Silva, L.; Mafra, L.; Ananias, D.; Carlos, L.D.; Rocha, J.; Almeida-Paz, F.A. *Chem. Mater.* **2007**, *19*, 3527-3538.

D

- Danilich, M.J.; Burton, D.J.; Marchant, R.E. *Vibr. Spectrosc.* **1995**, *9*, 229−234.

- De La Torre, A.G.; Bruque, S.; Aranda, M.A.G. *J. Appl. Crystallogr.* **2001**, *34*, 196-202.

- Demadis, K.D.; Barouda, E.; Raptis, R.G.; Zhao, H., *Inorg. Chem.* **2009a**, *48*, 819-821.

- Demadis, K.D.; Barouda, E.; Stavgianoudaki, N.; Zhao, H. *Cryst. Growth Des.* **2009b**, *9*, 1250-1253.

- Demadis, K.D.; Barouda, E.; Zhao, H.; Raptis, R.G., *Polyhedron* **2009c**, *28*, 3361-3367.

- Demadis, K.D.; Katarachia, S.D. *Phosphorus, Sulfur, and Silicon* **2004**, *179*, 627-648.

- Demadis, K.D.; Katarachia, S.D.; Koutmos, M. *Inorg. Chem. Commun.* **2005**, *8*, 254-258.

- Demadis, K.D.; Katarachia, S.D.; Raptis, R.G.; Zhao, H.; Baran, P. *Cryst. Growth Des.* **2006a**, *6*, 836-838.

- Demadis, K.D.; Ketsetzi, A. *Sep. Sci. Technol.* **2007**, *42*, 1639-1649.
- Demadis, K.D.; Mantzaridis, C.; Lykoudis, P., *Ind. Eng. Chem. Res.* **2006b**, *45*, 7795-7800.

- Demadis, K.D.; Papadaki, M.; Aranda, M.A.G.; Cabeza, A.; Olivera-Pastor, P.; Sanakis, Y., *Cryst. Growth Des.* **2010a**, *10*, 357-364.

- Demadis, K.D.; Papadaki, M.; Cisarova, I. *ACS Appl. Mater. Interface* **2010b**, *2*, 1814-1816.

- Demadis, K.D.; Papadaki, M.; Raptis, R.G.; Zhao H., *Chem. Mater.* **2008**, *20,* 4835-4846.

- Dines, M.B.; DiGiacomo, P.M., *Inorg. Chem.* **1981**, *20*, 92-97.
- Dong, D.; Li, J.; Sun, Z.; Zheng, X.; Chen, H.; Meng, L.; Zhu, Y.; Zhao, Y.; Zhang, J., *Inorg. Chem. Commun.* **2007**, *10*, 1109-1112.

- Donnadio, A.; Nocchetti, M.; Costantino, F.; Taddei, M.; Casciola, M.; Lisboa, F. da S.; Vivani, R., *Inorg. Chem.* **2014**, *53*, 13220-13226.

- Dutta, A.; Patra, A.K.; Bhaumik, A. *Micropor. Mesopor. Mater.* **2012**, *155*, 208-214.

F

- Farrusseng, D., *Metal-Organic Frameworks. Applications from catalysis to gas storage*, Ed. Wiley-VCH: Weinheim, Germany, **2011**.

- Fenton, H., *J.Chem. Soc. Trans.*, **1894**, *65*, 899-910.

- Férey, G., *Chem. Soc. Rev.* **2008**, *37*, 191-214.

- Feyand, M.; Seidler, C.F.; Deiter C.; Rothkirch, A.; Lieb, A.; Wark, M.; Stock, N., *Dalton Trans.* **2013**, *42*, 8761-8770.

- Fletcher, A.J.; Thomas, K.M.; Rosseinsky, M.J., *J. Solid State Chem.* **2005**, *178*, 2491-2510.

- Forster, P.M.; Cheetham, A.K., *Topics in Catalysis* **2003**, *24*, 79-86.

- Fu, R.; Hu, S.; Wu, X*. J. Solid State Chem.* **2011***, 184*, 945-952.

- Fu, R.; Xiang, S.; Zhang, H.; Zhang, J.; Wu, X., *Cryst. Growth Des.* **2005a**, *5*, 1795-1799.

- Fu, R.; Zhang, H.; Wang, L.; Hu, S.; Li, Y.; Huang, X.; Wu, X., *Eur. J. Inorg. Chem.* **2005b**, 16, 3211-3213.

- Fujishima, A.; Honda, K. *Nature* **1972**, *238*, 37-38.

- Furukawa, H.; Cordova, K.E.; O'keeffe, M.; Yaghi, O.M., *Science* **2013**, *341*, 1230444.

G

- Gagnon, K.J.; Perry, H.P.; Clearfield, A. *Chem. Rev.* **2012**, *112*, 1034-1054.

- Grohol, D.; Subramanian, M.A.; Poojary, D.M.; Clearfield, A. *Inorg. Chem.* **1996**, *35*, 5264-5271.

- Gu, Z.-Y.; Park, J.; Raiff, A.; Wei, Z.; Zhou, H.-C. *ChemCatChem.* **2014**, *6*, 67-75.

H

- Haber, F.; Weiss, J., *J. Proc. Roy. Soc. London A*, **1934**, *147*, 332-351.

- Hasan, Z., Jhung, S.H., *J. Hazard. Mater.* **2015**, 283, 329-339.

- Horike, S.; Shimomura, S.; Kitagawa, S. *Nature Chemistry* **2009**, *1*, 695-704.

- Horike, S.; Umeyama, D.; Kitagawa, S. *Acc. Chem. Res.,* **2013**, *46*, 2376-2384.

- Horiuchi, Y.; Toyao, T.; Takeuchi, M.; Matsuoka, M.; Anpo, M. *Phys. Chem. Chem. Phys.* **2013**, *15*, 13243-13253.

J

- Jang, M.Y.; Park, Y.S.; Yamazaki, Y. *Electrochemistry* **2003**, *8*, 691-694.

- Jiang, H.-L.; Xu, Q. *Chem. Commun.* **2011***, 47*, 3351-3370.

- Jiménez-García, L.; Kaltbeitzel, A.; Enkelmann, V.; Gutmann, J.S.; Klapper, M.; Müllen, K. *Adv. Funct. Mater.* **2011**, *21*, 2216-2224.

K

- Kaempfe, P.; Stock, N., *Z. Anorg. Allg. Chem.* **2008**, *634*, 714-717.

- Kano, T., in *Phosphor Handbook*, Eds. Yen, W. M.; Shionoya, S.; Yamamoto, H., CRC press, Boca Raton, 2nd ed, **2006**.

- Kim, C. S.; Lad, R.J.; Tripp, C. P. *Sens. Actuators B: Chem.* **2001**, *76*, 442−448.

- Kim, S.; Dawson, K.W.; Gelfand, B.S.; Taylor, J.M.; Shimizu, G.K.H. *J. Am. Chem. Soc.* **2013**, *135*, 963-966.

- Kinnibrugh, T.L.; Ayi, A.A.; Bakhmutov, V.I.; Zoń, J.; Clearfield, A. *Cryst. Growth Des.* **2013**, *13*, 2973-2981.

- Kitagawa, S.; Kitaura, R.; Noro, S.I., *Angew. Chem. Inter. Ed.* **2004**, *43*, 2334-2375.

- Kreno, L.E.; Leong, K.; Farha, O.K.; Allendorf, M.; Van Duyne, R.P.; Hupp, J.T. *Chem. Rev.* **2012**, *112*, 1105-1125.

- Kreuer, K.-D.; Rabenau, A.; Weppner, W. *Angew. Chem. Int. Ed.* **1982**, *21*, 208-209.

- Kundu, T.; Sahoo, C.; Banerjee, R. *Chem. Commun.* **2012**, *48*, 4998-5000.

L

- Lago, A. B.; Carballo, R.; Fabelo, O.; Fernández-Hermida, N.; Lloretd, F.; Vázquez-López, E.M. *CrystEngComm.* **2013**, *15*, 10550-10562.

- Larson, A.C.; von Dreele, R.B. *General Structure Analysis System (GSAS)*, Los Alamos National Laboratory Report LAUR 86-748, Los Alamos, NM, USA; **2004**.

- Laurier, K.G.M.; Vermoortele, F.; Ameloot, R.; De Vos, D.E.; Hofkens, J.; Roeffaers, M.B.J. *J. Am. Chem. Soc.* **2013**, *135*, 14488-14491.

- Li, J.R.; Sculley, J.; Zhou, H.C., *Chem. Rev.* **2012**, *112*, 869-932.

- Li, S.-L.; Xu, Q., *Energy Environ. Sci.* **2013**, *6*, 1656-1683.

- Li, J.; Dong, D.; Huang, C.; Sun, Z.; Zhu, Y., *Acta Cryst.* **2007a**, *E63*, 2348-2349.

- Li, J.; Meng, L.; Sun, Z.G.; Cui, L.Y.; Zhang, J.; Zhu, Y.Y.; Dong, D.P.; Chen, H.; You, W.S.; Zhu, Z.M., *Inorg. Chem. Commun.* **2007b**, *10*, 535-537.

- Li, J.; Meng, L.; Sun, Z.G.; Liu, Z.M.; Zhao, Y.; Zhang, J.; Zhu, Y.Y.; Lu, X.; Liu, L.; Zhang, N., *Inorg. Chem. Commun.* **2008**, *11*, 211-214.

- Liao, T.-B.; Ling, Y.; Chen, Z.-X.; Zhou, Y.-M-; Weng, L.-H. *Chem. Commun.* **2010**, *46,* 1100-1102.

- Liang, X.; Zhang, F.; Feng, W.; Zou, Z.; Zhao, C.; Na, H.; Liu, C., Suna, F.; Zhu, G. *Chem. Sci.* **2013**, *4,* 983-992.

- Liu, D.; Lu, K.; Poon, C.; Lin, W. *Inorg. Chem.* **2014**, *53*, 1916-1924.

- Liu, Y.; Zhu, Y.; Xu, J.; Bai, X.; Zong, R.; Zhu, Y., *Appl. Catal., B* **2013**, *142-143*, 561-567.
- Lu, W.; Wei, Z.; Gu, Z.-Y.; Liu, T.-F.; Park, J.; Tian, J.; Zhang, M.; Zhang, Q.; Gentle, T.; Bosch, M.; Zhou, H.-C., *Chem. Soc. Rev.* **2014**, *43*, 5561-5593.

M

- Ma, T.Y.; Lin, X.Z.; Yuan, Z.Y., *Chem. Eur. J.* **2010a**, *16*, 8487-8494.

- Ma, T.Y.; Lin, X.Z.; Yuan, Z.Y., *J. Mater. Chem.* **2010b**, *20*, 7406-7415.

- Ma, T.-Y.; Yuan, Z.-Y., *ChemSusChe.* **2011**, *4*, 1407-1419.

- Ma, T.Y.; Zhang, X.J.; Yuan, Z.Y., *Micropor. Mesopor. Mater.* **2009**, *123*, 234-242.

- Maeda, K., *Microporous and Mesoporous Materials* **2004**, *73*, 47-55.

- Manos, M.J.; Moushi, E.E.; Papaefstathiou, G.S.; Tasiopoulos, A.J. *Cryst. Growth Des.* **2012**, *12*, 5471-5480.

- Mao, J.G.; Wang, Z.; Clearfield, A. *New J. Chem.* **2002b**, *26*, 1010-1014.

- Martínez-Tapia, H.S.; Cabeza, A.; Bruque, S.; Pertierra, P.; García-Granda, S; Aranda, M.A.G. *J. Solid State Chem.* **2000**, *151*, 122-129.

- Mendes, R.F.; Silva, P.; Antunes, M.M.; Valente, A.A.; Almeida Paz, F.A. *Chem. Commun.*, **2015**, *51*, 10807-10810.

- Miller, S.R.; Pearce, G.M.; Wright, P.A.; Bonino, F.; Chavan, S.; Bordiga, S.; Margiolaki, I.; Guillou, N.; Férey, G.; Bourrelly, S.; Llewellyn, P.L. *J. Am. Chem. Soc.*, **2008**, *130*, 15967–15981.

- Mondal, S.S.; Bhunia, A.; Demeshko, S.; Kelling, A.; Schilde,U.; Janiakb, C.; Holdt, H.-J. *CrystEngComm.* **2014**, *16*, 39-42.

- Muneer, M.; Bhatti, I.A.; Iqbal, M.; Ather, M., *Pak. J. Chem. Soc.*, **2012**, *34*, 787-794.

N

- Nasalevich, M.A.; van der Veen, M.; Kapteijn, F.; Gascon, J. *CrystEngComm,* **2014**, *16*, 4919-4926.

- Niu, J.; Zhang, X.; Yang, D.; Zhao, J.; Ma, P.; Kortz, U.; Wang, J. *Chem. Eur. J.* **2012**, *18*, 6759-6762.

O

- Öhrström, L. *Crystals* **2015**, *5*, 154-162.

P

- Paszternak, A.; Felhosi, I.; Paszti, Z.; Kuzmann, E.; Vertes, A.; Kalman, E.; Nyikos, L. *Electrochim. Acta* **2010**, *55*, 804-812.

- Ponomareva, V.G.; Kovalenko, K.A.; Chupakhim, A.P.; Dybtsev, D.N.; Shutova, E.S.; Fedin, V.P. *J. Am. Chem. Soc.* **2012**, *134*, 15640-15643.

- Priya, M.H.; Madras, G. *J. Photochem. Photobiol., A* **2006**, *179*, 256-262.

R

- Ramaswamy, P.; Wong, N.E.; Shimizu, G.K.H. *Chem. Soc. Rev.* **2014**, *43*, 5913-5932.

- Rao, K.P.; Vidyasagar, K., *Eur. J. Inorg. Chem.* **2005**, 4936-4943.

- Rietveld, H. M., *J. Appl. Cryst.* **1969**, 2, 65-71.

- Rosseinsky, M.J., *Microporous and Mesoporous Materials* **2004**, *73*, 15-30.

S

- Sadakiyo, M.; Kasai, H.; Kato, K.; Takata, M.; Yumauchi, M. *J. Am. Chem. Soc.* **2014**, *136*, 1702-1705.

- Sadakiyo, M.; Yamada, T.; Kitagawa, H. *J. Am. Chem. Soc.* **2009**, *131*, 9906-9907.

- Sagawe, G.; Lehnard, A.; Lubber, M.; Bahnemann, D, *Helvetica Chimica Acta.*, **2001**, *84*, 3742-3759.

- Sanchez, C.; Julián, B.; Belleville, P.; Popall, M., *J. Mater. Chem.* **2005**, *15*, 3559-3592.

- Schröder, M., *Functional Metal-Organic frameworks. Gas storage, separation and catalysis*, Ed. Springer: Heidelberg, Germany, **2010**.

- Sharma, C.V.K.; Clearfield, A.; Cabeza, A.; Aranda, M.A.G.; Bruque, S. *J. Am. Chem. Soc.* **2001***, 123*, 2885-2886.

- Silva, P.; Vieira, F.; Gomes, A.C.; Ananias, D., Fernandes, J.A.; Bruno, S.M.; Soares, R.; Valente, A.A., Rocha, J.; Almeida Paz, F.A. *J. Am. Chem. Soc.* **2011**, *133,* 15120-15138.

- Sivalingam, G.; Priya, M.H.; Madras, G. *Appl. Catal., B* **2004**, *51*, 67-76.
- Stock, N. *Microporous Mesoporous Mater.* **2010**, *129*, 287-295.
- Stock, N.; Bein, T. *Angew Chem. Int. Ed.* **2004,** *43,* 749-752.

- Stock, N.; Biswas, S. *Chem. Rev.* **2012**, *112,* 933-969.

- Stock, N.; Guillou, N.; Senker, J., Férey, G.; Bein, T. *Z. Anorg. Allg. Chem.* **2005**, *631*, 575-581.

- Stock, N.; Rauscher, M.; Bein, T. *J. Solid State Chem*. **2004a**, *117*, 642-647.

- Stock, N.; Stoll, A.; Bein, T. *Microporous Mesoporous Mater.* **2004b**, *69*, 65-69.

- Su, M.; Qiu, Y.; Jia, W. *Adv. Ther.* **2005**, *22*, 297-306.

- Suh, M. P.; Park, H. J.; Prasad, T. K.; Lim, D.-W. *Chem. Rev.* **2012**, *112,* 782-835.

- Sumida, K.; Rogow, D.L.; Mason, J.A.; McDonald, T.M.; Bloch, E.D.; Herm, Z.R.; Bae, T.H.; Long, J.R., *Chem. Rev.* **2012**, *112*, 724-781.

- Sun, Z.; Chen, H.; Liu, Z.; Cui, L.; Zhu, Y.; Zhao, Y.; Zhang, J.; You, W.; Zhu, Z., *Inorg. Chem. Commun.* **2007**, *10*, 283-286.

- Sun, Z.; Cui, L.; Liu, Z.; Meng, L.; Chen, H.; Dong, D.; Zhang, L.; Zhu, Z.; You, W., *Inorg. Chem. Commun.* **2006**, *9*, 999-1001.

T

- Taddei, M.; Vivani, R.; Constantino, F. *Dalton Trans.* **2013**, *42*, 9671-9678.

- Taylor, J.M.; Dawson, K.W.; Shimizu, G.K.H. *J. Am. Chem. Soc.* **2013**, *135,* 1193-1196.

- Taylor,J.M.; Mah, R.K.; Moudrakovski, I.L.; Ratcliffe, C.I.; Vaidhyanathan, R.; Shimizu, G.K.H. *J. Am. Chem. Soc.* **2010**, *132*, 14055-14057.

- Toby, B.H. *J. Appl. Crystallogr.* **2001**, *34*, 210-213.

V

- Vilela, S.M.F.; Ananias, D.; Gomes, A.C.; Valente, A.A., Carlos, L.D.; Cavaleiro, J.A.S.; Rocha, J.; Tomé, J.P.C.; Almeida Paz, F.A. *J. Mater. Chem.* **2012***, 22*, 18354-18371.

- Vilela, S.M.F.; Firmino, A.D.G.; Mendes, R.F.; Fernandes, J.A.; Ananias, D.; Valente, A.A.; Ott, H.; Carlos, L.D.; Rocha, J.; Tomé, J.P.C.; Almeida Paz, F.A. *Chem. Commun.* **2013a**, *49*, 6400-6402.

- Vilela, S.M.F.; Mendes, R.F.; Silva, P.; Fernandes, J.a.; Tome, J.P.C.; AlmeidaPaz, F.A. *Cryst. Growth Des.* **2013b**, *13*, 543-560.

- Vivani, R.; Costantino, F.; Costantino, U.; Nocchetti, M. *Inorg. Chem.* **2006**, *45*, 2388-2390.

W

- Wang, C.-C.; Li, J.-R.; Lv, X.-L.; Zhang, Y.-Q.; Guo, G. *Energy Environ. Sci.* **2014a**, *7*, 2831-2867.

- Wang, R.; Dong, X.-Y.; Xu, H.; Pei, R.-B.; Ma, M.-L., Zang, S.-Q.; Hou, H.-W.; Mak, T.C.W., *Chem. Commun.* **2014b**, *50*, 9153-9156.

- Wang, W.N.; Sun, Z.G.; Zhu, Y.Y; Dong, D.P.; Li, J.; Tong, F.; Huang, C.Y.; Chen, K.; Li, C.; Jiao, C.Q.; Wang, C.L., *Cryst. Eng. Comm.* **2011**, *13*, 6099-6106.

- Wharmby, M.T.; Mowat, J.P.S.; Thompson, S.P.; Wright, P.A. *J. Am. Chem. Soc.* **2011**, *133*, 1266-1269.

- Wharmby, M.T.; Wright, P.A. in *Metal phosphonate chemistry: From synthesis to applications*, Clearfiels, A.; Demadis, K.D. Eds. The Royal Society of Chemistry: London **2012**, Ch. 10, p. 317-343.

- Wu, J.; Hou, H.; Han, H.; Fan, Y. *Inorg. Chem*. **2007**, *46*, 7960-7970.

- Wu, Z.Y.; Lee, S.; Moore, J.S., *J. Am. Chem. Soc.* **1992**, *114*, 8730-8732.

Y

- Yaghi, O.M.; Li, G.; Li, H., *Nature* **1995**, *378*, 703-706.

- Ying, S.-M.; Zeng, X.-R.; Fang, X.-N.; Li, X.-F.; Liu, D.-S. *Inorg. Chim. Acta* **2006**, *359*, 1589-1593.

- Yoon, M.; Suh, K.; Natarajan, S.; Kim, K. *Angew. Chem. Int. Ed.* **2013**, *52*, 2688-2700.

Z

- Zenobi, M.C; Luengo, C.V.; Avena, M.J.; Rueda, E.H. *Spectrochim. Acta A* **2008**, *70*, 270−276.

- Zhang, J; Li, J.; Sun, Z.G.; Hua, R.N.; Zhu, Y.Y.; Zhao, Y.; Zhang, N.; Liu, L.; Lu, X.; Wanga, W.N.; Tong, F., *Inorg. Chem. Commun.* **2009**, *12*, 276-279.

- Zhang, J.; Li, J.; Sun, Z.G.; Zhao, Y.; Zhu, Y.Y.; Zhang, N.; Liu, L.; Lu, X., *Z. Anorg. Allg. Chem.* **2008**, *634*, 2629-2633.

- Zhang, T.; Lin, W., *Chem. Soc. Rev.* **2014**, *43*, 5982-5993.

- *Zhang, Y.Y.; Zeng, M.H.; Qi, Y.; Sang, S.Y.; Liu, Z.M., Inorg. Chem. Commun.* **2007***, 10*, 33-36.

- Zhu, Y.Y.; Li, J.; Sun, Z.G.; Zhang, J.; Zhao, Y.; Lu, X.; Liu, L.; Zhang, N.Z., *Anorg. Allg. Chem.* **2009**, *635*, 171-174.

- Zima, V.; Svoboda, J.; Melanova, K.; Benes, L.; Casciola, M.; Sganappa, M.; Brus, J.; Trchova, M. *Solid State Ionics* **2010**, *181*, 705-713.

Rosario M. P. Colodrero, Giasemi K. Angeli, Montse Bazaga-Garcia, Pascual Olivera-Pastor, Didier Villemin, Enrique R. Losilla, Estefania Q. Martos, Gary B. Hix, Miguel A. G. Aranda, Konstantinos D. Demadis, y Aurelio Cabeza.

"Structural Variability in Multifunctional Metal Xylenediaminetetraphosphonate Hybrids"

Abstract:

Two new families of divalent metal hybrid derivatives from the aromatic tetraphosphonic acids 1,4- and 1,3-bis(aminomethyl)benzene-N,N′-bis(methylenephosphonic acid), $(H_2O_3PCH_2)_2-N-CH_2C_6H_4CH_2-N(CH_2PO_3H_2)_2$ (designated herein as p-H_8L and m-H_8L) have been synthesized by crystallization at room temperature and hydrothermal conditions. The crystal structures of $M[(HO_3PCH_2)_2N(H)-CH_2C_6H_4CH_2N(H)(CH_2PO_3H)_2(H_2O)_2]\cdot 2H_2O$ (M = Mg, Co, and Zn), M−(p-H_6L), and $M[(HO_3PCH_2)_2N(H)-CH_2C_6H_4CH_2N(H)(CH_2PO_3H)_2]\cdot nH_2O$ (M = Ca, Mg, Co, and Zn and n = 1−1.5), M−(m-H_6L), were solved ab initio by synchrotron powder diffraction data using the direct methods and subsequently refined using the Rietveld method. The crystal structure of the isostructural M−(p-H_6L) is constituted by organic−inorganic monodimensional chains where the phosphonate moiety acts as a bidentate chelating ligand bridging two metal octahedra. M−(m-H_6L) compounds exhibit a 3D pillared open-framework with small 1D channels filled with water molecules. These channels are formed by the pillaring action of the organic ligand connecting adjacent layers through the phosphonate oxygens. Thermogravimetric and X-ray thermodiffraction analyses of M−(p-H_6L) showed that the integrity of their crystalline structures is maintained up to 470 K, without significant reduction of water content, while thermal decomposition takes place above 580 K. The utility of M−(p-H_6L) (M = Mg and Zn) hybrid materials in corrosion protection was investigated in acidic aqueous solutions. In addition, the impedance data indicate both families of compounds display similar proton conductivities (σ= 9.4 × 10^{-5} S·cm^{-1}, at 98% RH and 297 K), although different proton transfer mechanisms are involved.
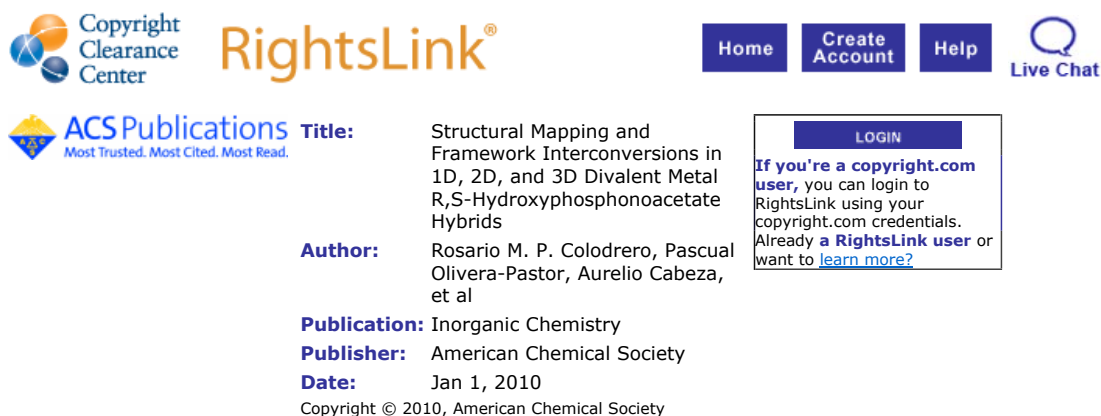
APPENDIX II:
Copyright Permission

Appendix II-A: Copyright Permission from American Chemical Society,
Inorg. Chem. 2010, *49*, 761-768.
Figure 1.2

Copyright Clearance Center   RightsLink®

Home   Create Account   Help   Live Chat

ACS Publications
Most Trusted. Most Cited. Most Read.

Title: Structural Mapping and Framework Interconversions in 1D, 2D, and 3D Divalent Metal R,S-Hydroxyphosphonoacetate Hybrids

Author: Rosario M. P. Colodrero, Pascual Olivera-Pastor, Aurelio Cabeza, et al

Publication: Inorganic Chemistry

Publisher: American Chemical Society

Date: Jan 1, 2010

Copyright © 2010, American Chemical Society

LOGIN

If you're a copyright.com user, you can login to RightsLink using your copyright.com credentials. Already **a RightsLink user** or want to learn more?

PERMISSION/LICENSE IS GRANTED FOR YOUR ORDER AT NO CHARGE

This type of permission/license, instead of the standard Terms & Conditions, is sent to you because no fee is being charged for your order. Please note the following:

- Permission is granted for your request in both print and electronic formats, and translations.
- If figures and/or tables were requested, they may be adapted or used in part.
- Please print this page for your records and send a copy of it to your publisher/graduate school.
- Appropriate credit for the requested material should be given as follows: "Reprinted (adapted) with permission from (COMPLETE REFERENCE CITATION). Copyright (YEAR) American Chemical Society." Insert appropriate information in place of the capitalized words.
- One-time permission is granted only for the use specified in your request. No additional uses are granted (such as derivative works or other editions). For any other uses, please submit a new request.
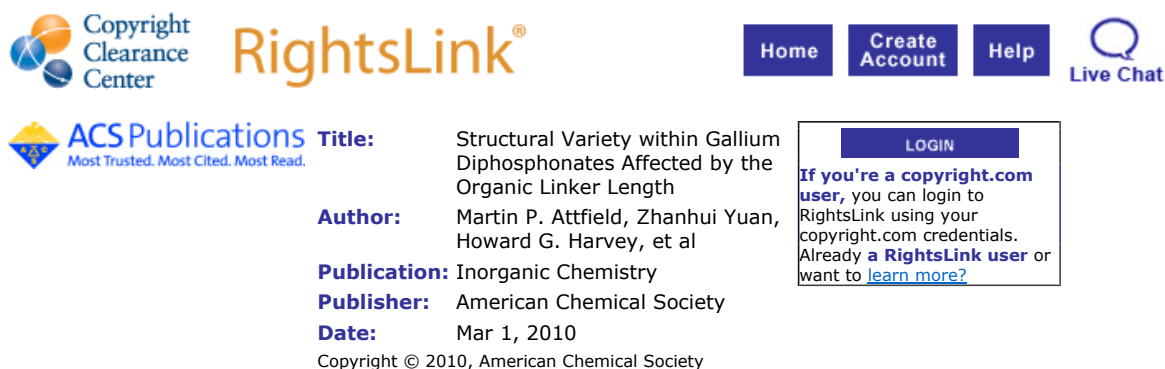
If credit is given to another source for the material you requested, permission must be obtained from that source.

BACK   CLOSE WINDOW

Publicaciones y Divulgación Científica

ma

UNIVERSIDAD DE MÁLAGA

COPYRIGHT PERMISSION

Appendix II-A: Copyright Permission from American Chemical Society,
Cryst. Growth Des. **2005**, *5*, 1795-17499.
Figure 1.3

Publicaciones y Divulgación Científica

ma
UNIVERSIDAD DE MÁLAGA

Appendix II-A: Copyright Permission from American Chemical Society,
Cryst. Growth Des. **2011**, *11,* 1713-1722.
Figure 1.4

Copyright
Clearance
Center

RightsLink®

Home | Create Account | Help | Live Chat

ACS Publications
Most Trusted. Most Cited. Most Read.

Title: Common Structural Features in Calcium Hydroxyphosphonoacetates. A High-Throughput Screening

Author: Rosario M. P. Colodrero, Aurelio Cabeza, Pascual Olivera-Pastor, et al

Publication: Crystal Growth and Design

Publisher: American Chemical Society

Date: May 1, 2011

Copyright © 2011, American Chemical Society

LOGIN

If you're a copyright.com user, you can login to RightsLink using your copyright.com credentials. Already **a RightsLink user** or want to learn more?

PERMISSION/LICENSE IS GRANTED FOR YOUR ORDER AT NO CHARGE

This type of permission/license, instead of the standard Terms & Conditions, is sent to you because no fee is being charged for your order. Please note the following:

- Permission is granted for your request in both print and electronic formats, and translations.
- If figures and/or tables were requested, they may be adapted or used in part.
- Please print this page for your records and send a copy of it to your publisher/graduate school.
- Appropriate credit for the requested material should be given as follows: "Reprinted (adapted) with permission from (COMPLETE REFERENCE CITATION). Copyright (YEAR) American Chemical Society." Insert appropriate information in place of the capitalized words.
- One-time permission is granted only for the use specified in your request. No additional uses are granted (such as derivative works or other editions). For any other uses, please submit a new request.

If credit is given to another source for the material you requested, permission must be obtained from that source.

BACK | CLOSE WINDOW

Publicaciones y Divulgación Científica

ma

UNIVERSIDAD DE MÁLAGA

COPYRIGHT PERMISSION

Appendix II-A: *Copyright Permission from American Chemical Society,*
Chem. Mater. **2012**, *24*, 3780-3792.
Figure 1.5

Copyright Clearance Center — RightsLink®

Home | Create Account | Help | Live Chat

ACS Publications
Most Trusted. Most Cited. Most Read.

Title: Multifunctional Luminescent and Proton-Conducting Lanthanide Carboxyphosphonate Open-Framework Hybrids Exhibiting Crystalline-to-Amorphous-to-Crystalline Transformations

Author: Rosario M. P. Colodrero, Konstantinos E. Papathanasiou, Nikoleta Stavgianoudaki, et al

Publication: Chemistry of Materials

Publisher: American Chemical Society

Date: Oct 1, 2012

Copyright © 2012, American Chemical Society

LOGIN

If you're a copyright.com user, you can login to RightsLink using your copyright.com credentials. Already **a RightsLink user** or want to learn more?

PERMISSION/LICENSE IS GRANTED FOR YOUR ORDER AT NO CHARGE

This type of permission/license, instead of the standard Terms & Conditions, is sent to you because no fee is being charged for your order. Please note the following:
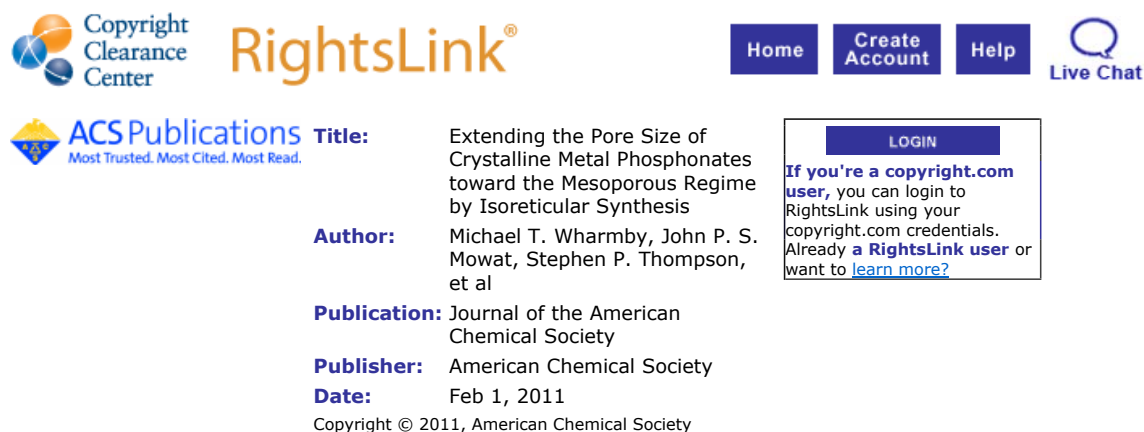
- Permission is granted for your request in both print and electronic formats, and translations.
- If figures and/or tables were requested, they may be adapted or used in part.
- Please print this page for your records and send a copy of it to your publisher/graduate school.
- Appropriate credit for the requested material should be given as follows: "Reprinted (adapted) with permission from (COMPLETE REFERENCE CITATION). Copyright (YEAR) American Chemical Society." Insert appropriate information in place of the capitalized words.
- One-time permission is granted only for the use specified in your request. No additional uses are granted (such as derivative works or other editions). For any other uses, please submit a new request.

If credit is given to another source for the material you requested, permission must be obtained from that source.

BACK | CLOSE WINDOW

Appendix II-A: Copyright Permission from American Chemical Society,
Inorg. Chem. **2010**, *49*, 2656-2666.
Figure 1.7

Copyright Clearance Center   RightsLink®

Home   Create Account   Help   Live Chat

ACS Publications
Most Trusted. Most Cited. Most Read.

Title: Structural Variety within Gallium Diphosphonates Affected by the Organic Linker Length

Author: Martin P. Attfield, Zhanhui Yuan, Howard G. Harvey, et al

Publication: Inorganic Chemistry

Publisher: American Chemical Society

Date: Mar 1, 2010

Copyright © 2010, American Chemical Society

LOGIN

If you're a copyright.com user, you can login to RightsLink using your copyright.com credentials. Already **a RightsLink user** or want to learn more?

PERMISSION/LICENSE IS GRANTED FOR YOUR ORDER AT NO CHARGE

This type of permission/license, instead of the standard Terms & Conditions, is sent to you because no fee is being charged for your order. Please note the following:

- Permission is granted for your request in both print and electronic formats, and translations.
- If figures and/or tables were requested, they may be adapted or used in part.
- Please print this page for your records and send a copy of it to your publisher/graduate school.
- Appropriate credit for the requested material should be given as follows: "Reprinted (adapted) with permission from (COMPLETE REFERENCE CITATION). Copyright (YEAR) American Chemical Society." Insert appropriate information in place of the capitalized words.
- One-time permission is granted only for the use specified in your request. No additional uses are granted (such as derivative works or other editions). For any other uses, please submit a new request.

If credit is given to another source for the material you requested, permission must be obtained from that source.

BACK   CLOSE WINDOW

Publicaciones y Divulgación Científica

ma
UNIVERSIDAD DE MÁLAGA

COPYRIGHT PERMISSION

Appendix II-A: Copyright Permission from American Chemical Society,
J. Am. Chem. Soc. **2008**, *130*, 15967-15981.
Figure 1.8

Copyright Clearance Center

RightsLink®

Home | Create Account | Help | Live Chat

ACS Publications
Most Trusted. Most Cited. Most Read.

Title:	Structural Transformations and Adsorption of Fuel-Related Gases of a Structurally Responsive Nickel Phosphonate Metal−Organic Framework, Ni-STA-12
Author:	Stuart R. Miller, Gordon M. Pearce, Paul A. Wright, et al
Publication:	Journal of the American Chemical Society
Publisher:	American Chemical Society
Date:	Nov 1, 2008

Copyright © 2008, American Chemical Society

LOGIN

If you're a copyright.com user, you can login to RightsLink using your copyright.com credentials. Already **a RightsLink user** or want to learn more?

Appendix II-A: Copyright Permission from American Chemical Society,
J. Am. Chem. Soc. **2011**, *133*, 1266-1269.
Figure 1.9

Copyright Clearance Center

RightsLink®

Home | Create Account | Help | Live Chat

ACS Publications
Most Trusted. Most Cited. Most Read.

Title: Extending the Pore Size of Crystalline Metal Phosphonates toward the Mesoporous Regime by Isoreticular Synthesis

Author: Michael T. Wharmby, John P. S. Mowat, Stephen P. Thompson, et al

Publication: Journal of the American Chemical Society

Publisher: American Chemical Society

Date: Feb 1, 2011

Copyright © 2011, American Chemical Society

LOGIN

If you're a copyright.com user, you can login to RightsLink using your copyright.com credentials. Already **a RightsLink user** or want to learn more?

PERMISSION/LICENSE IS GRANTED FOR YOUR ORDER AT NO CHARGE

This type of permission/license, instead of the standard Terms & Conditions, is sent to you because no fee is being charged for your order. Please note the following:

- Permission is granted for your request in both print and electronic formats, and translations.
- If figures and/or tables were requested, they may be adapted or used in part.
- Please print this page for your records and send a copy of it to your publisher/graduate school.
- Appropriate credit for the requested material should be given as follows: "Reprinted (adapted) with permission from (COMPLETE REFERENCE CITATION). Copyright (YEAR) American Chemical Society." Insert appropriate information in place of the capitalized words.
- One-time permission is granted only for the use specified in your request. No additional uses are granted (such as derivative works or other editions). For any other uses, please submit a new request.

If credit is given to another source for the material you requested, permission must be obtained from that source.

BACK | CLOSE WINDOW

Publicaciones y Divulgación Científica
UNIVERSIDAD DE MÁLAGA

COPYRIGHT PERMISSION

Appendix II-A: Copyright Permission from American Chemical Society,
Inorg. Chem. **2012**, *51*, 7689-7698.
Figure 1.12

Publicaciones y Divulgación Científica

UNIVERSIDAD DE MÁLAGA

Appendix II-B: Copyright Permission from American Chemical Society,

[**a#1**, Bazaga-García et al., *J. Phys. Chem. C* 2012, *116*, 14526-14533]

COPYRIGHT PERMISSION

Appendix II-B: Copyright Permission from American Chemical Society,

[**a#2**, Bazaga-García et al., *J. Am. Chem. Soc.* **2014**, *136*, 5731-5739]

Copyright Clearance Center   RightsLink®

Home   Create Account   Help   Live Chat

ACS Publications
Most Trusted. Most Cited. Most Read.

Title: Guest Molecule-Responsive Functional Calcium Phosphonate Frameworks for Tuned Proton Conductivity

Author: Montse Bazaga-García, Rosario M. P. Colodrero, Maria Papadaki, et al

Publication: Journal of the American Chemical Society

Publisher: American Chemical Society

Date: Apr 1, 2014

Copyright © 2014, American Chemical Society

PERMISSION/LICENSE IS GRANTED FOR YOUR ORDER AT NO CHARGE

This type of permission/license, instead of the standard Terms & Conditions, is sent to you because no fee is being charged for your order. Please note the following:

- Permission is granted for your request in both print and electronic formats, and translations.
- If figures and/or tables were requested, they may be adapted or used in part.
- Please print this page for your records and send a copy of it to your publisher/graduate school.
- Appropriate credit for the requested material should be given as follows: "Reprinted (adapted) with permission from (COMPLETE REFERENCE CITATION). Copyright (YEAR) American Chemical Society." Insert appropriate information in place of the capitalized words.
- One-time permission is granted only for the use specified in your request. No additional uses are granted (such as derivative works or other editions). For any other uses, please submit a new request.
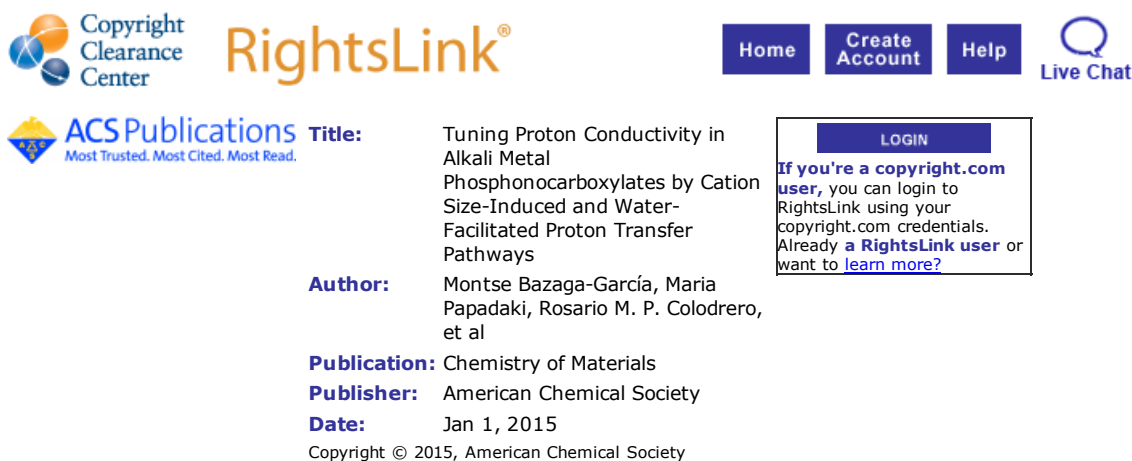
BACK   CLOSE WINDOW

Publicaciones y Divulgación Científica

UNIVERSIDAD DE MÁLAGA

Appendix II-B: Copyright Permission from American Chemical Society,

[**a#3**, Bazaga-García et al., *Chem. Mater.* **2015**, *27*, 424-435]

Copyright
Clearance
Center

RightsLink®

Home | Create Account | Help | Live Chat

ACS Publications
Most Trusted. Most Cited. Most Read.

Title: Tuning Proton Conductivity in Alkali Metal Phosphonocarboxylates by Cation Size-Induced and Water-Facilitated Proton Transfer Pathways

Author: Montse Bazaga-García, Maria Papadaki, Rosario M. P. Colodrero, et al

Publication: Chemistry of Materials

Publisher: American Chemical Society

Date: Jan 1, 2015

Copyright © 2015, American Chemical Society

LOGIN

If you're a copyright.com user, you can login to RightsLink using your copyright.com credentials. Already **a RightsLink user** or want to learn more?

PERMISSION/LICENSE IS GRANTED FOR YOUR ORDER AT NO CHARGE

This type of permission/license, instead of the standard Terms & Conditions, is sent to you because no fee is being charged for your order. Please note the following:

- Permission is granted for your request in both print and electronic formats, and translations.
- If figures and/or tables were requested, they may be adapted or used in part.
- Please print this page for your records and send a copy of it to your publisher/graduate school.
- Appropriate credit for the requested material should be given as follows: "Reprinted (adapted) with permission from (COMPLETE REFERENCE CITATION). Copyright (YEAR) American Chemical Society." Insert appropriate information in place of the capitalized words.
- One-time permission is granted only for the use specified in your request. No additional uses are granted (such as derivative works or other editions). For any other uses, please submit a new request.

BACK | CLOSE WINDOW

Publicaciones y
Divulgación Científica

ma

UNIVERSIDAD
DE MÁLAGA

COPYRIGHT PERMISSION

Appendix II-B: Copyright Permission from American Chemical Society,

[*c#1*, Colodrero et al., *Inorg.Chem.* **2013**, *52*, 8770-8783]

Copyright Clearance Center

RightsLink®

Home | Create Account | Help | Live Chat

ACS Publications
Most Trusted. Most Cited. Most Read.

Title: Structural Variability in Multifunctional Metal Xylenediaminetetraphosphonate Hybrids

Author: Rosario M. P. Colodrero, Giasemi K. Angeli, Montse Bazaga-Garcia, et al

Publication: Inorganic Chemistry

Publisher: American Chemical Society

Date: Aug 1, 2013

Copyright © 2013, American Chemical Society

PERMISSION/LICENSE IS GRANTED FOR YOUR ORDER AT NO CHARGE

This type of permission/license, instead of the standard Terms & Conditions, is sent to you because no fee is being charged for your order. Please note the following:

- Permission is granted for your request in both print and electronic formats, and translations.
- If figures and/or tables were requested, they may be adapted or used in part.
- Please print this page for your records and send a copy of it to your publisher/graduate school.
- Appropriate credit for the requested material should be given as follows: "Reprinted (adapted) with permission from (COMPLETE REFERENCE CITATION). Copyright (YEAR) American Chemical Society." Insert appropriate information in place of the capitalized words.
- One-time permission is granted only for the use specified in your request. No additional uses are granted (such as derivative works or other editions). For any other uses, please submit a new request.

BACK | CLOSE WINDOW

Publicaciones y Divulgación Científica

uma UNIVERSIDAD DE MÁLAGA